Earth and Environmental Science Transactions of the Royal Society of Edinburgh, **113**, 175–226, 2022

Spontaneous Article

Reconstruction of a Ross lost Cambrian *Series 2* mixed siliciclastic–carbonate platform from carbonate clasts of the Shackleton Range, Antarctica

Marta RODRÍGUEZ-MARTÍNEZ[1]*, Werner BUGGISCH[2], Silvia MENÉNDEZ[3], Elena MORENO-EIRIS[1] and Antonio PEREJÓN[1]

[1] Departamento de Geodinámica, Estratigrafía y Paleontología, Facultad de Ciencias Geológicas, Universidad Complutense, C/ José Antonio Novais 12, 28040 Madrid, Spain.
[2] GeoZentrum Nordbayern, Friedrich-Alexander-Universität of Erlangen-Nürnberg (FAU), Schlossgarten 5, 91054 Erlangen, Germany.
[3] Museo Geominero, Instituto Geológico y Minero de España (IGME-CSIC), C/ Ríos Rosas 23, 28003 Madrid, Spain.
*Corresponding author. Email: martarm@geo.ucm.es

ABSTRACT: The presence of archaeocyath-bearing clasts from Cenozoic tills and Cambrian Mount Wegener Formation reveal erosion of a hidden Cambrian carbonate platform in Shackleton Range, Antarctica. We provide microfacies, paleontological, diagenetic and tectonically induced fabric data from carbonate clasts which, in addition to available geochemical and geochronological data from Shackleton Range, allow the paleoenvironmental reconstruction of a lost Cambrian *Series 2* mixed siliciclastic–carbonate platform that was developed and eroded during the Ross orogeny. Carbonate production was dominated by non-skeletal grains in possibly restricted platform-interior and oolitic shoal complex settings, while open subtidal sub-environments (calcimicrobe carpets, calcimicrobe–archaeocyath patch reefs, muddy bottoms) were dominated by a diverse calcimicrobe assemblage and/or by secondary to accessory heterozoan assemblage (archaeocyaths and other sponges, chancelloriids, hyoliths, coralomorphs, trilobites, echinoderms). We describe a Botoman assemblage with 34 archaeocyathan species among 12 existing archaeocyathan genera. A new archaeocyath family Shackletoncyathidae is proposed. New species (*Rotundocyathus glacius* sp. nov., *Buggischicyathus microporus* gen. et sp. nov., *Paragnaltacyathus hoeflei*, *Shackletoncyathus buggischi* gen. et. sp. nov., *Santelmocyathus santelmoi* gen. et sp. nov., *Wegenercyathus sexangulae* gen. et sp. nov.) and *Tabulaconus kordae* coralomorph are reported from Antarctica for the first time. Archaeocyathan fauna share few species with contemporary fauna of South Australia (9) and even fewer with the Antarctic platforms of the Shackleton Limestone (2) or the Schneider Hills limestone (1). Similarity is greater with Antarctic allochthonous assemblages of Permo-Carboniferous tillites from Ellsworth Mountains (2), Cenozoic deposits from King George Island (4) or Weddell Sea (1). The Shackleton Range lost/hidden platform shows a distinct entity related with its tectonosedimentary evolution, in a possible back-arc basin on the Mozambique seaway during the E and W Gondwana amalgamation, which distinguishes it from those developed on the palaeo-Pacific margin of the E Antarctic craton.

KEY WORDS: archaeocyaths, back-arc basin sedimentation, Botoman, calcimicrobes, giant ooids, microfacies, southern Gondwana.

The majority of the Antarctic land surface is covered by ice and snow, resulting in only partial and scattered exposures of Cambrian carbonate platform deposits. Allochthonous archaeocyath-bearing clasts have, therefore, been crucial to establish both a regional biostratigraphic framework and to inform the palaeogeography between localities in Antarctica and southern Gondwana from the Cambrian through to the Late Palaeozoic glaciation records (Fig. 1). Nevertheless, at times, interpretations have been based solely on the presence of archaeocyaths. Meanwhile, the microfacies and diagenetic evolution of the Antarctic Cambrian carbonate platforms have been poorly studied.

Often in Antarctica, the finding of allochthonous archaeocyaths has preceded the location of the Cambrian carbonate successions they came from (Hill 1965; Cooper & Shergold 1991 and references therein). In fact, archaeocyaths were the first Cambrian fossils collected in Antarctica by the Bruce's Scottish National Antarctic Expedition (1902–1904) from deep sea gravels at the Weddel Sea (station 313; see Pirie 1913) and by the Shackleton's British Antarctic Expedition (1907–1909) from moraine deposits of the Beardmore Glacier at the Transantarctic Mountains (TAM) (David & Priestley 1914). However, thick successions of Cambrian carbonate platforms only crop out along

 doi:10.1017/S1755691022000111

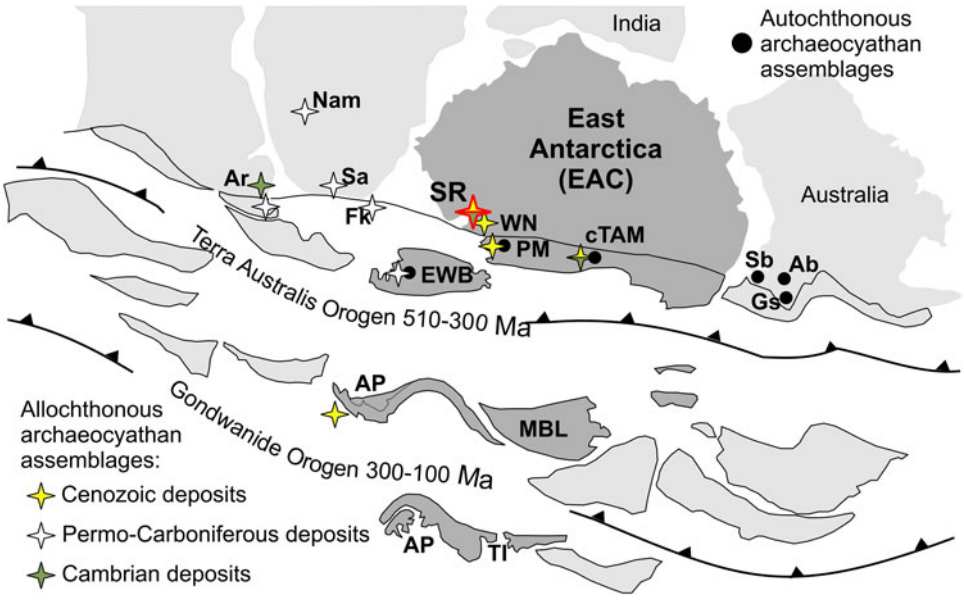

Figure 1 Paleogeography of southern Gondwana during mid-Cambrian–late Carboniferous (modified from Boger 2011) with the distribution of the archaeocyathan assemblages. Star outlined in red: record analysed in this study. E Antarctica region and WAntarctica terranes in dark grey colour. Abbreviations: EAC = East Antarctic Craton; SR = Shackleton Range; PM = Pensacola Mountains; WN = Whichaway Nunataks; cTAM = central Transantarctic Mountains; EWB = Ellsworth–Whitmore Block; AP = Antarctic Peninsula domains; MBL = Marie Byrd Land; TI = Thurston Island; Ar = Argentina; Nam = Namibia; Sa = South Africa; Fk = Falkland Islands; Sb = Stansbury Basin; Gs = Gnalta Shelf; Ab = Arrowie Basin.

the TAM and in the Ellsworth Mountains (EW) at the WAntarctica region.

The intraplate TAM belt separates the E from W Antarctica regions (Fig. 2a) that present clear differences in their geological evolution. The E Antarctic Craton (EAC) is formed by the amalgamation of Precambrian terranes during different Precambrian–Cambrian orogenies (e.g., Boger 2011). The geologic record of the TAM belt (see Goodge 2020) includes a Mesoarchaean and Paleoproterozoic basement (part of the EAC). This basement was rifted and developed an Andean-style Gondwana convergent margin with carbonate deposition (PM and cTAM in Fig. 1), basin inversion and clastic molasse-type sedimentation during the late Neoproterozoic to early Palaeozoic Ross orogenic cycle. Intra-cratonic and foreland basin sedimentation and mantle upwelling (Gondwana breakup) continued during Late Palaeozoic and Early Mesozoic times, and experimented rift-shoulder uplift

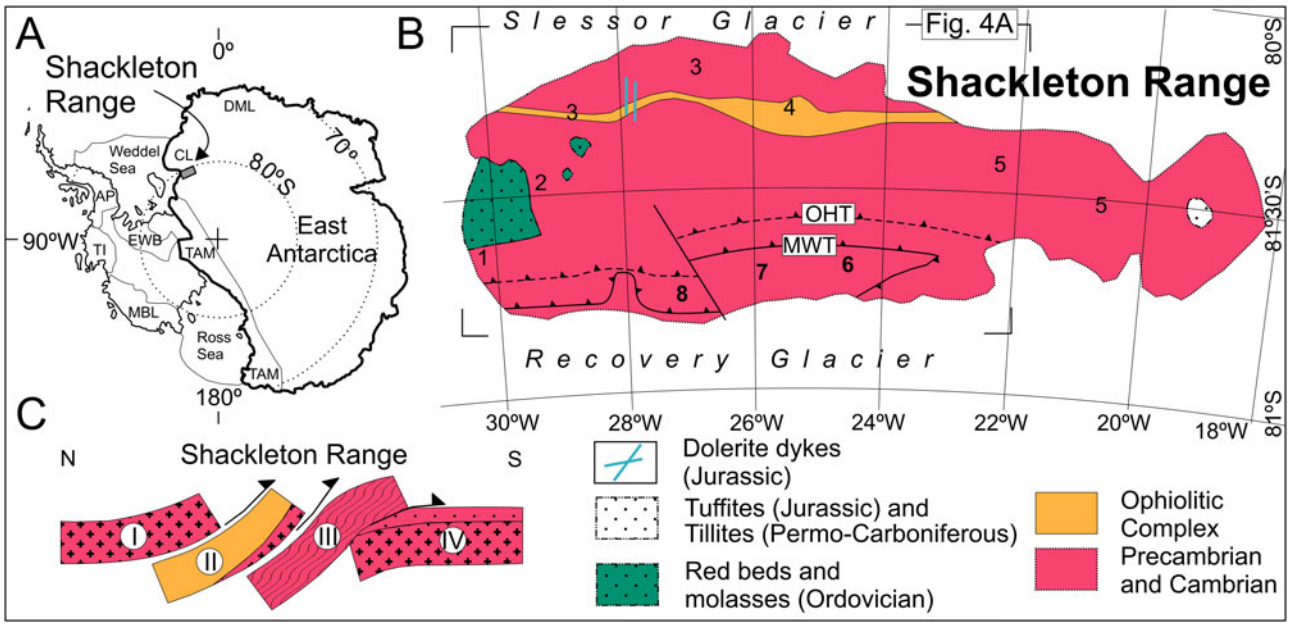

Figure 2 (A) Location of the Shackleton Range on the Antarctica continent. The E Antarctic plate is outlined by a thick black line to distinguish it from the WAntarctic region, which is formed by the amalgamation of several terranes. Abbreviations: AP = Antarctic Peninsula; EWB = Ellsworth–Whitmore Block; TI = Thurston Island; MBL = Marie Byrd Land; TAM = Transantarctic Mountains; CL = Coats Land; DML = Dronning Maud Land. (B) Simplified geologic map of the Shackleton Range. The inferred geology under the permanent snow and ice cover is based on the geology of scattered rock outcrops (1–8). Modified from Krohne *et al.* (2016) after Tessensohn *et al.* (1999a) and Kleinschmidt *et al.* (2002). Rock outcrop localities with archaeocyaths are indicated with numbers in bold: 1 = Otter Highlands; 2 = Haskard Highlands, 3 = La Grange Nunataks; 4 = Herbert Mountains; 5 = Pioneers Escarpment; 6 = Read Mountains; 7 = Du Toit Nunataks; 8 = Stephenson Bastion. Abbreviations: OHT = Otter Highlands Thrust; MWT = Mount Wegener Thrust. (C) Schematic n–S cross-section through the centre of the Shackleton Range. Tectonic units I–IV according to Tessensohn *et al.* (1999a), who interpreted the Shackleton collisional orogen as a result of the final amalgamation between E and W Gondwana during Late Precambrian–Cambrian time. I = Proterozoic basement; II = Ophiolitic complex; III = low-grade metasedimentary units with Cambrian fossils (including archaeocyaths) and Ross deformation ages; IV = Proterozoic basement (East Antarctic Craton) and autochthonous sedimentary cover.

https://doi.org/10.1017/S1755691022000111 Published online by Cambridge University Press

related to Cenozoic extension (Goodge 2020). On the other hand, the W Antarctica extensional province is formed by Palaeozoic–Mesozoic microcontinental blocks (outboard terranes) as the Ellsworth–Whitmore Block (EWB), Thurston Island, Marie Byrd Land and the Antarctic Peninsula (Dalziel & Elliot 1982; EWB, TI, MBL, AP in Fig. 1) and both the Weddell Sea and WAntarctic rift systems (Fig. 2a). From ~500 Ma, the WAntarctica region is a tectonically active margin between the subducting paleo-Pacific oceanic plate and the EAC (Jordan *et al.* 2020 and references therein) (Fig. 1). Thus, the best known Cambrian carbonate successions in Antarctica (TAM and EW) were not part of the same carbonate platform, nor they did share a common tectonosedimentary evolution during the Cambrian – something that is key when establishing the origin of allochthonous archaeocyath-bearing clasts in the neighbouring regions of southern Gondwana (Fig. 1)

On the other hand, the record of Antarctic allochthonous archaeocyathan assemblages is abundant, scattered and, at times, very far from the hypothetical source areas, and some of them have not yet been studied. However, because less than 2 % of the bedrock is exposed in Antarctica, archaeocyath-bearing clasts are key records that give us a chance to solve many geological problems. For instance, in the TAM, the presence of archaeocyath-bearing clasts in Cambrian conglomerates (e.g., Starshot Formation, Douglas Conglomerate) was useful to establish maximum depositional ages, lithostratigraphic relationships and relative timing of deformation, uplift and erosion of the Cambrian *Series 2* carbonate platform (Rowell *et al.* 1986, 1988; Myrow *et al.* 2002a). In recent tills, the presence of archaeocyath-bearing clasts derived from Cambrian polymictic conglomerates would indicate that the Douglas Conglomerate could be hidden under the ice at least as far S as the Beardmore Glacier (Rowell & Rees 1989).

In the EW (EWB in Fig. 1), the Heritage Group contains thick carbonate successions such as the middle Cambrian Drake Icefall Formation and the middle-upper Cambrian Minaret Formation (Webers *et al.* 1992). However, the only record of lower Cambrian carbonate sedimentation occurs as reworked carbonate clasts in the lower Cambrian conglomerates of the Kosco Peak Member (Castillo *et al.* 2017) from the Heritage Group and in Permo-Carboniferous tillites of the Whiteout Conglomerate (Buggisch & Webers 1992). In fact, the Whiteout Conglomerate represents the Late Palaeozoic Gondwana glaciation sedimentation in W Antarctica (Matsch & Ojakangas 1992). But the source area of the carbonate clasts is unknown in the EW; specifically, the archaeocyath-bearing clasts give a lower Cambrian age (Debrenne 1992) and no clasts believed to be from the Minaret Formation are found (Buggisch & Webers 1992).

In Late Palaeozoic Gondwana glaciation deposits outside Antarctica, the presence of archaeocyath-bearing clasts (Fig. 1) allows paleobiogeographic correlations between Antarctica and other erratic assemblages in S Gondwana where the record of Cambrian carbonate successions is unknown, as in the Falkland Islands (Stone *et al.* 2012), South Africa (Debrenne 1975), Namibia (Perejón *et al.* 2019) and Argentina (González *et al.* 2013). In this regard, the autochthonous archaeocyathan assemblages from the lower Cambrian Shackleton Limestone (TAM; Hill 1964b; Debrenne & Kruse 1986, 1989), the Schneider Hills limestone (Pensacola Mountains (PM), TAM; Konyushkov & Shulyatin 1980; Debrenne & Kruse 1989), the middle Cambrian Nelson Limestone (PM; Wood *et al.* 1992) or the upper Cambrian Minaret Formation (EWB; Debrenne *et al.* 1984; Henderson *et al.* 1992) are, so far, essential to establish the likely source areas of allochthonous records. But, are these the only Cambrian carbonate successions, or are there other records hidden under the ice? And, if so, how can we infer and differentiate them?

The Shackleton Range (SR in Fig. 1) is interpreted as a collisional orogen due to the final amalgamation between E and W Gondwana during Late Precambrian–Cambrian times (Tessensohn *et al.* 1999a), but the presence of shallow-water marine successions from the Cambrian is unknown in this sector. However, glacial erratics with Cambrian brachiopods from a locally sourced area were the first fossils collected by the Shackleton Range geological expedition in recent moraine deposits (1970–1971; Clarkson 1971; Thomson 1972). And later, during the German geological expedition GEISHA (1987–1988), Cenozoic glacial erratic archaeocyath-bearing clasts were discovered. Höfle & Buggisch (1995) suggested that a major expansion of the Antarctic Ice Sheet carried these erratic carbonate clasts from their hypothetical source area: the Nelson Limestone in the PM, the southernmost part of the TAM (PM in Fig. 1). Some years later, during the EUROSHACK expedition (1993–1994), a sampling of new archaeocyath-bearing clasts from the Mount Wegener Formation was carried out. Buggisch & Henjes-Kunst (1999) suggested an early Cambrian Atdabanian age for the synorogenic upper slope to basinal deposits of the Mount Wegener Formation on the basis of the potassium–argon (K–Ar) ages of detrital muscovites and the presence of the trace fossil *Oldhamia*, calcimicrobes and archaeocyaths. Therefore, the carbonate clasts from the Mount Wegener Formation come from the erosion of shallow marine deposits; although geochemical and paleocurrent data suggest a northern source area, its final provenance is not yet determined (Buggisch & Henjes-Kunst 1999).

The aims of this paper are: (a) to analyse the microfacies of the Cambrian carbonate clasts from the Shackleton Range (Cenozoic tills and Cambrian Mount Wegener Formation); (b) to identify the diagenetic processes that carbonate clasts and host rock conglomerates have undergone, from the shallow marine platform stage up to the very low-grade metamorphic overprint and nappe-tectonic stage; (c) to analyse the taxonomic relationships of the archaeocyath specimens; (d) to determine the age of archaeocyathan assemblage to set the minimum age of the carbonate platform they derived from; (e) to establish possible palaeobiogeographic correlations between the archaeocyathan assemblage from the Shackleton Range sector and other coeval assemblages; (f) to give new age constraints of the Mount Wegener Formation; (g) to figure out the different depositional subenvironments of the lost carbonate platform in the Shackleton Range sector; and (f) to compare this lost carbonate platform and its tectonosedimentary evolution with other contemporary Antarctic platforms.

1. Geological setting

The Shackleton Range (lat. 80°–81°S, long. 19°–31°W) is the most prominent massif at the Coats Land region of Antarctica, extending for about 200 km in an E–W direction. The range is bounded by the Slessor and Recovery glaciers that drain the E Antarctic Ice Sheet into the Filchner Ice Shelf (Weddell Sea) (Fig. 2a, b). Above permanent snow and ice, the closest outcrops/blocks are the Whichaway Nunataks to the S (130 km), the Argentina Range at the PM to the SW (240 km) and the Theron Mountains to the N (150 km). The first geological survey of the western part of the Shackleton Range was carried out by Stephenson (1966) during the Trans-Antarctic Expedition (1955–1958). Later, the geology of the range was successively studied by numerous field parties from the UK, USSR, Germany, Italy and the USA (see Clarkson 1995; Kleinschmidt 2007; Fig. 3 and references therein).

The geology of the range consists mainly of medium–high-grade amphibolite facies of the Proterozoic Shackleton Range Metamorphic Complex (SRMC) (Clarkson 1972), which is

https://doi.org/10.1017/S1755691022000111 Published online by Cambridge University Press

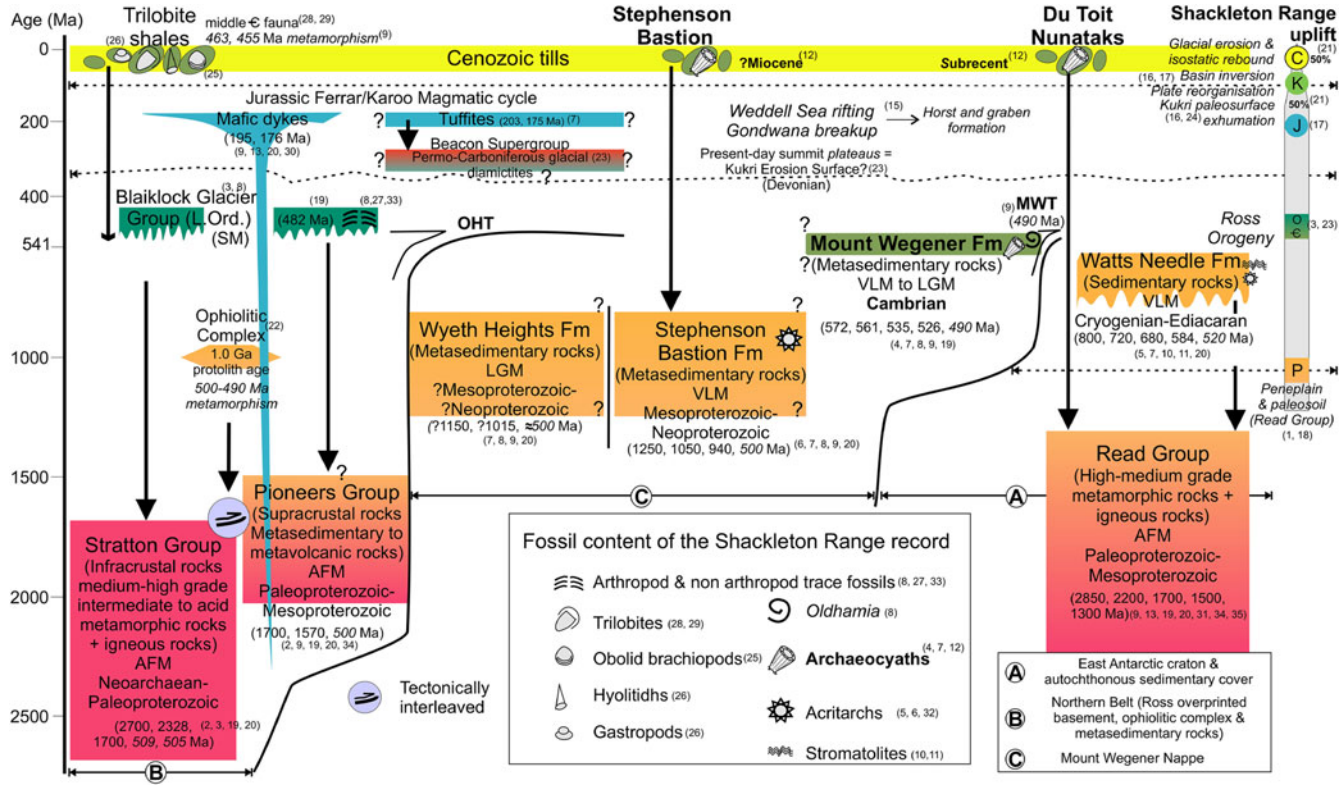

Figure 3 Chronostratigraphic chart of the Shackleton Range showing the main lithostratigraphic units and their fossil content. The Shackleton Range can be subdivided in three tectonic units (Ⓐ, Ⓑ, Ⓒ). The major uplift phases of the Shackleton Range are summarised on the right. Abbreviations: OHT = Otter Highlands Thrust; MWT = Mount Wegener Thrust; AFM = Amphibolite facies metamorphism; LGM = low-grade metamorphism; VLGM = very low-grade metamorphism; SM = sedimentary molasse deposits; ? = relationships between lithostratigraphic units are not always observed due to permanent snow and ice cover and hence are uncertain. The Cambrian record corresponds to the Mount Wegener Formation and the Cenozoic tills. The analysed Cambrian carbonate clasts belong to the Mount Wegener Formation and to the Cenozoic tills from the Stephenson Bastion and Du Toit Nunataks. Ages, lithology, fossil content and uplift data are based on the following publications: 1 = Clarkson (1982); 2 = Brommer *et al.* (1999); 3 = Buggisch *et al.* (1999); 4 = Buggisch & Henjes-Kunst (1999); 5 = Buggisch *et al.* (1995a); 6 = Buggisch *et al.* (1995b); 7 = Buggisch *et al.* (1994a); 8 = Buggisch *et al.* (1990); 9 = Buggisch *et al.* (1994b); 10 = Golovanov *et al.* (1979); 11 = Golovanov *et al.* (1980); 12 = Höfle & Buggisch (1995); 13 = Hofmann *et al.* (1980); 14 = Hotten (1993); 15 = Jordan *et al.* (2017); 16 = Krohne *et al.* (2016); 17 = Lisker *et al.* (1999); 18 = Paech (1982); 19 = Pankhurst *et al.* (1983); 20 = Pankhurst *et al.* (1985); 21 = Paxman *et al.* (2017); 22 = Talarico *et al.* (1999); 23 = Tessensohn (1997); 24 = Tessensohn *et al.* (1999b); 25 = Thomson (1972); 26 = Thomson *et al.* (1995); 27 = Thomson & Weber (1999); 28 = Solov'ev & Grikurov (1979); 29 = Cooper & Shergold (1991); 30 = Spaeth *et al.* (1995); 31 = Rex (1972); 32 = Weber (1991); 33 = Weber & Brady (2004); 34 = Zeh *et al.* (2004); 35 = Will *et al.* (2009).

made of infracrustral rocks from the Neoarchaean–Paleoproterozoic Stratton Group (Tessensohn & Thomson 1990) and the Paleoproterozoic–Mesoproterozoic Read Group (Pankhurst *et al.* 1983, 1985; Fig. 3). The snow and ice cover made it difficult to establish lithostratigraphic relationships between the scattered rock outcrops; in fact, only two sedimentary contacts have been observed between the Proterozoic SRMC and the younger sedimentary successions, disregarding the Cenozoic deposits (Fig. 3). However, the nappe- and thrust-tectonic soon became apparent and finally well established (Marsh 1983; Buggisch *et al.* 1990; Brommer 1998; Kleinschmidt *et al.* 2001). Therefore, the Shackleton Range is subdivided into different tectonostratigraphic units developed during the Ross orogeny (Buggisch *et al.* 1994b; Buggisch & Kleinschmidt 1999; Tessensohn *et al.* 1999a; Fig. 2c, A–C in Fig. 3).

The metasedimentary to metavolcanic supracrustal rocks of the Pioneers Group (Tessensohn & Thomson 1990; Roland *et al.* 1995) and the rocks of the Ophiolitic Complex (Talarico *et al.* 1999) with eclogite facies metamorphism (Schmädicke & Will 2006) occur in the northern part of the range. Both appear tectonically interleaved with the Stratton Group (Fig. 3; Schubert *et al.* 1995), forming the Northern Belt (B in Fig. 3). In the southern part of the range, the Read Group (Tessensohn & Thomson 1990; Olesch *et al.* 1995), which is part of the EAC, is unconformably overlaid by the Watts Needle Formation (Marsh 1983), interpreted as Criogenian–Ediacaran marine mixed platform sedimentation (A in Fig. 3). The boundaries between the northern and southern belts are thrusts (OHT and MWT in Figs 2b, 3), which bound the Mount Wegener Nappe (Kleinschmidt & Buggisch 1994; Buggisch & Kleinschmidt 2007 and references therein). This allochthonous tectonic unit comprises very-low- to low-grade metasedimentary rocks (Clarkson 1972; C in Fig. 3) as the ?Mesoproterozoic to Neoproterozoic Wyeth Heights and Stephenson Bastion Formations, and the Cambrian Mount Wegener Formation, which hosts allochthonous archaeocyath-bearing clasts in conglomerates and olistoliths (Buggisch *et al.* 1999; Buggisch & Henjes-Kunst 1999). The Shackleton Range is a collisional orogen related to the sinistral collision between the E Antarctic and Kalahari Cratons with the closure of the Mozambique Ocean during the final amalgamation of the E and W Gondwana (Talarico *et al.* 1999; Tessensohn *et al.* 1999a; Kleinschmidt *et al.* 2001). This late Pan-African event produced the westward overthrusting of the Northern Belt and the southward overthrusting of the Mount Wegener Nappe over their foreland, the EAC (Read Group) and its sedimentary cover (Watts Needle Formation) according to Buggisch & Kleinschmidt (2007).

The subsequent Blaiklock Glacier Group (Clarkson 1972; Clarkson & Wyeth 1983) consists of post-orogenic Ordovician red beds and molasses (Figs 2b, 3 and references therein), interpreted as alluvial, fluvial to coastal deposits (Buggisch *et al.* 1999). This group unconformably overlies a Pan-African overprinted basement (Stratton Group) in the northwestern and

https://doi.org/10.1017/S1755691022000111 Published online by Cambridge University Press

western part of the Northern Belt. In the easternmost area of the range (Fig. 2b), a small outcrop of non-fossiliferous Permian tillites, considered the basal part of the Beacon Supergroup (Tessensohn *et al*. 1999b), are unconformably overlaid by Upper Triassic–Lower Jurassic volcano-sedimentary deposits (Buggisch *et al*. 1994b; Krohne *et al*. 2016). These volcano-sedimentary rocks have similar geochemistry and/or ages than those observed in dolerite/mafic dykes of the nearby La Grange Nunataks (3 in Fig. 2B), the Whichaway Nunataks and the Theron Mountains. Thus, they are considered part of the Ferrar/Karoo magmatic cycle (Buggisch *et al*. 1994a; Krohne *et al*. 2016). The geochemistry of the N–S strike Jurassic dolerite dykes from La Grange Nunataks corresponds to the initial rifting tholeiites linked with the mafic rocks of the Ferrar Group during the break-up of the Gondwana supercontinent (Spaeth *et al*. 1995). Thus, the younger record of the Shackleton Range is formed by Jurassic dikes and tuffites and Cenozoic tills (Figs 2b, 3 and references therein). The occurrence of Cenozoic tills with Cambrian fauna-bearing clasts has been described in three different locations. At the first locality, the Haskard Highlands (2 in Fig. 2b), shale boulders in moraine contain middle Cambrian fauna (Trilobite shales in Fig. 3). The second and third localities are in the southern part of the range, where the archaeocyaths occur as part of Cenozoic tills at the Du Toit Nunataks and the Stephenson Bastion (7 and 8 in Figs 2b, 3).

2. Stratigraphic record of the allochthonous archaeocyaths in the Shackleton Range

In the Shackleton Range, the ice divide separates tributary glaciers that flow northwards to the Slessor Glacier from those that flow southwards to the Recovery Glacier. The archaeocyath-bearing clasts are found at the S of the Fuchs Dome (central ice cap) and the Shotton Snowfield as glacial erratics in Cenozoic tills and conglomerates hosted by the Cambrian Mount Wegener Formation (Fig. 4a, b).

The glacial erratic archaeocyath-bearing clasts (Fig. 4a–c) were discovered in the Shackleton Range during the German geological expedition GEISHA (1987–1988). At that time, the presence of archaeocyath-bearing clasts in the conglomerates of the Cambrian Mount Wegener Formation was unknown (Fig. 4b, d) and knowledge about the uplift of the Shackleton Range and the glaciology of the region was limited. Höfle & Buggisch (1995) analysed the glacial morphology and till deposits from the Shackleton Range. Some of the data and conclusions are summarised below. The glacial erratic archaeocyath-bearing clasts occur in two different situations (Fig. 3): as Cenozoic tills on top of the Stephenson Bastion table mountain (Fig. 4c) and as part of a subrecent moraine near Du Toit Nunataks (Fig. 4b). The archaeocyath-bearing clasts consist of wackestone, floatstone and boundstone with *Epiphyton, Renalcis*, *Batenevia ramosa* Korde and trilobites. Many of the outcrops at the Shackleton Range are table mountains, relics of an exhumed peneplain (Stephenson 1966; Skidmore & Clarkson 1972; Marsh 1985). The scarce till deposits on the table mountains occur in places protected from erosion. In fact, easily weathered fossiliferous limestone clasts appear in hollows and depressions. On the relict till deposits on top of the Stephenson Bastion table mountain (Fig. 4c), the archaeocyath-bearing clasts are subsidiary clasts while the reddish-brown ?Beacon Supergroup-sandstone derived clasts and local bed rock fragments (greenish-grey quartzite derived from the Stephenson Bastion Formation) are dominant. Subglacial erosional forms on the Stephenson Bastion table mountain (Fig. 4c) suggest that overriding ice covered the western part of Shackleton Range and flowed NW (Höfle & Buggisch 1995; Kerr & Hermichen 1999; Sugden *et al*. 2014). Höfle & Buggisch (1995) hypothesised that the Cambrian exotic erratics on the Stephenson Bastion were generated during a major expansion of the Antarctic Ice Sheet at the end of Miocene. They suggested the Whichaway Nunataks as source area for the exotic ?Beacon Supergroup erratics. For Cambrian archaeocyath-bearing clasts, they suggested the Whichaway Nunataks and the PM, which have early to middle Cambrian limestones. Kerr & Hermichen (1999) interpreted the south-eastern flows as an expansion of the Recovery Glacier and those from the SW as an expansion of the Filchner-Ronne Ice Shelf. They concluded that there is no evidence for extensive glacial modification of the Shackleton Range plateau by the E Antarctic Ice Sheet or by Quaternary ice. Cosmogenic nuclide data indicate that the glacial overriding of the higher summits of the Shackleton Range and deepening of the Slessor and Recovery glaciers troughs was earlier than 2.5 Ma, and significant erosion occurred in the mid-Miocene maximum (Sugden *et al*. 2014).

The archaeocyath-bearing clasts occur in conglomerates and boulders of the Mount Wegener Formation, which is part of the Mount Wegener Nappe. Buggisch & Henjes-Kunst (1999) reported archaeocyaths from E of the Read Mountain at the Oldhamia, Trueman Terraces and the Swinnerton Ledge (Fig. 4d). They described bioclastic rudstone and grainstone, archaeocyath/calcimicrobe boundstone microfacies with diverse biota such as archaeocyaths, trilobites, mollusc, echinoderms and calcimicrobes (*Epyphyton*, *Korilophyton*, *Renalcis granosus* Vologdin, *Renalcis seriata* Korde, *Girvanella*, *Batenevia* and *Subtifloria*) and concluded that the carbonate clasts represent the breakup and destruction of shallow-water carbonate deposits.

3. Mount Wegener Formation

Broadly, the Mount Wegener Formation comprises shales/slates, greywackes and conglomerates, and shows folding and metamorphic overprint that increases from SE to NW (Buggisch *et al*. 1994b). The total thickness of the Mount Wegener Formation probably exceeds 1000 m, and stratigraphy (see Fig. 5), facies, geochemistry and provenance analysis was carried out by Buggisch & Henjes-Kunst (1999) with data obtained during the EUROSHACK expedition (1993–1994). The main results and conclusions are summarised below. The facies of the Mount Wegener Formation are interpreted as marine clastic deposits from upper slope to deep basin set up in synorogenic conditions, the presence of plagioclase and volcaniclastics support an intracontinental back-arc environment (Buggisch *et al*. 1994a). The clast composition of the conglomerates shows evidence of repeated erosion and redeposition in shallow-water conditions before their final sedimentation as marine slope deposits. Reworked sedimentary rocks are dominant, while basement-derived rocks are rare. The most abundant clasts are sandstone, carbonate and conglomerate. The sandstones (greywackes) from the Mount Wegener Formation present intermediate proportions of silicon dioxide/aluminium oxide and low potassium oxide/sodium oxide ratios like those observed in the passive continental margins. Indeed, isotope geochemistry ($\varepsilon_{Nd,530Ma}$ values) suggests that the supracrustal rocks of the Pioneers Group (the Northern Belt, a Ross/Pan-African overprinted basement; Fig. 3) could be a potential source of sediments from the Mount Wegener Formation. The K–Ar dating ages of detrital muscovites between 572 and 534 Ma also suggest basement rocks with Pan-African cooling histories as the main source.

The age of the Mount Wegener Formation was interpreted by Buggisch *et al*. (1994b) as early Cambrian based on the presence of fossils (*Oldhamia* cf. *antiqua* and *Oldhamia* cf. *radiata*, *Epiphyton* sp. and ?*Botomaella* sp.) and on the rubidium–strontium (Rb–Sr) analysis (561 ± 18 Ma and 539 ± 9 Ma

https://doi.org/10.1017/S1755691022000111 Published online by Cambridge University Press

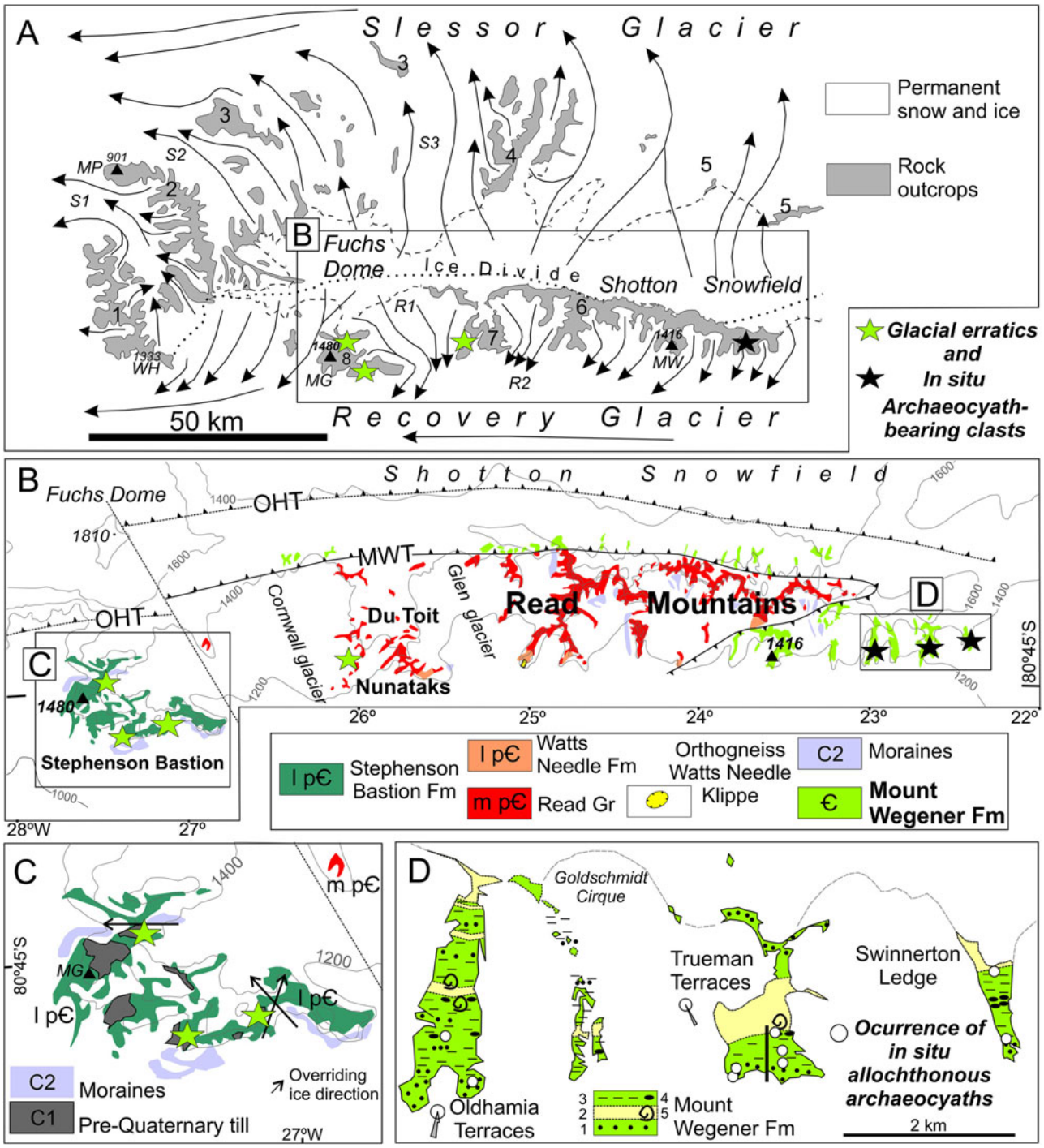

Figure 4 (A) Location of glacial erratics and *in situ* archaeocyath-bearing clasts in the Shackleton Range. The main rock outcrops (1–8), some tributary glaciers (S1–3, R1–2) and the current direction of ice flows are shown (modified from Höfle & Buggisch 1995). Box outlines area of (B). Abbreviations: 1 = Otter Highlands; 2 = Haskard Highlands; 3 = La Grange Nunataks; 4 = Herbert Mountains; 5 = Pioneers Escarpment; 6 = Read Mountains; 7 = Du Toit Nunataks; 8 = Stephenson Bastion; S1 = Blaiklock Glacier; S2 = Straton Glacier; S3 = Gordon Glacier; R1 = Cornwall Glacier; R2 = Glen Glacier. (B) Partial geological map of the southern Shackleton Range (modified from Clarkson *et al.* 1995). Black stars: *in situ* archaeocyath-bearing clasts are found in Cambrian marine slope deposits of the Mount Wegener Formation (Buggisch *et al.* 1994a; Buggisch & Henjes-Kunst 1999). Green stars: glacial erratic archaeocyath-bearing clasts occur as part of pre-Quaternary till deposits (Stephenson Bastion) and recent frontal moraines (Du Toit Nunataks). Boxes outline areas of (C) and (D). Abbreviations: OHT = Otter Highlands Thrust; MWT = Mount Wegener Thrust. (C) Detail from (B) showing the location of glacial erratic archaeocyath-bearing clasts according to Höfle & Buggisch (1995). The late Precambrian Stephenson Bastion Formation emerges in a plateau landform. Archaeocyaths occur as part of pre-Quaternary till deposits on the plateau. The pre-Quaternary till deposits on the Stephenson Bastion plateau, erosive structures and forms (striated rock surfaces, roches moutonnées, etc.) suggest that the overriding ice flowed northwestward (see the text). The overriding ice directions are shown according to Kerr & Hermichen (1999) and Sugden *et al.* (2014). (D) Detail from (B) showing the location of the sampling sites with archaeocyaths within the Mount Wegener Formation. The exact location of the samples with archaeocyaths from Oldhamia Terraces is unknown. Key: 1 = conglomerates; 2 = greywackes; 3 = shales; 4 = olistoliths; 5 = *Oldhamia* ichnotaxon. Geological map and sedimentary palaeocurrents of the Mount Wegener Formation according to Buggisch & Henjes-Kunst (1999). The black bar represents the stratigraphic section (see Fig. 5). Abbreviations for (A) and (C): MP = Mount Provender; WH = Wyeth Heights; MG = Mount Greenfield; MW = Mount Wegener.

https://doi.org/10.1017/S1755691022000111 Published online by Cambridge University Press

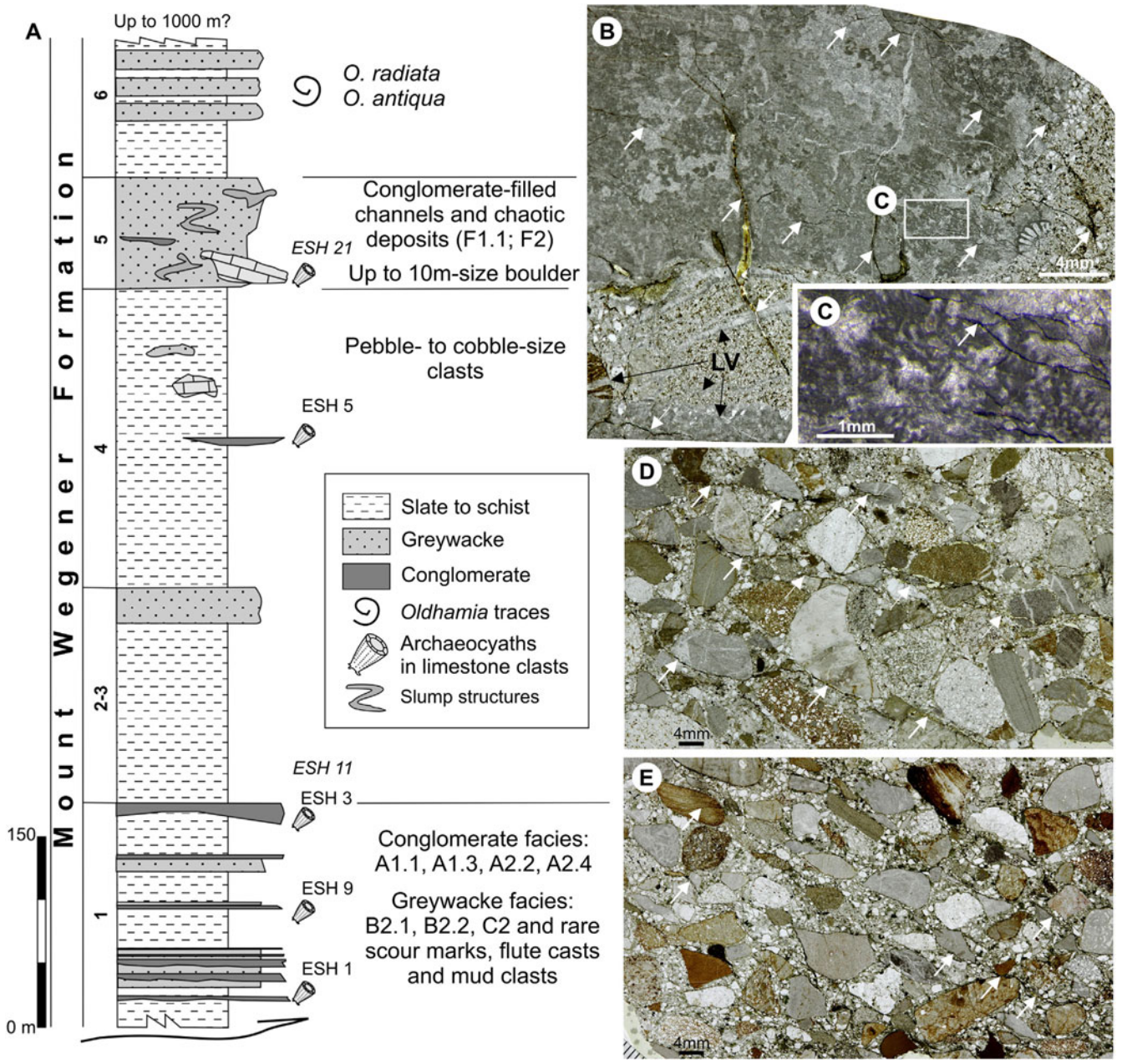

Figure 5 (A) Stratigraphic section of the lower part of the Mount Wegener Formation in Trueman Terraces (total thickness probably exceeds 1000 m) and distribution of facies codes (modified from Buggisch & Henjes-Kunst 1999). Facies codes according to Pickering *et al.* (1986): A1.1 = stratified gravels; B2.1 = parallel-stratified sands; B2.2 = cross-stratified sands; C2 = organised sand-mud couplets; F1.1 = rubble; F2 = contorted/disturbed strata. Only the stratigraphic position of the samples with archaeocyaths (ESH Trueman Terraces) and those with probable lateral equivalence (ESH Swinnerton Ledge) is shown. (B–E) Thin-section photomicrographs (plane-polarised light) of polymictic conglomerates of the Cambrian Mount Wegener Formation in Oldhamia Terraces (B) and Trueman Terraces (D) and conglomerate clast of the Cenozoic tills on the Stephenson Bastion (E) (see Fig. 4). (B) Calcimicrobe-rich limestone pebble floating in a sandy matrix. Clasts and sandy matrix are cut by a late vein fracture system (LV) that is cut by an incipient rough cleavage fabric (white arrows). (C) Detail *Epiphyton* and cements crossed by a late cleavage fabric (white arrow). (D–E) Note the similarities in clast composition and tectonic deformation (white arrows: cleavage, irregular sutured grain boundaries) in both conglomerates. In these examples, conglomerate clast from the Cenozoic tills (E) show more continuous cleavage traces around strongly tectonically oriented grains.

isochrones; Fig. 3 and references therein). The structural data and K–Ar analysis on phyllosilicates (2–6 μm whole rock fraction) indicate that the low-grade metamorphic overprint and the southwards transport of the Mount Wegener Nappe occurred around 490 Ma as a result of the Ross (Pan-African) orogeny (Buggisch *et al.* 1994b).

4. Materials and methods

The carbonate clasts and archaeocyath-bearing limestone clasts samples described here were collected during the GEISHA (First German geological expedition to the Shackleton Range) and EUROSHACK (European Antarctic Geological Expedition) expeditions. These geoscientific land expeditions took place in the Shackleton Range during 1987/1988 and 1994/1995, respectively. GEISHA was jointly supported by the Alfred Wegener Institute for Polar and Marine Research (AWI) and Federal Institute for Geosciences and Natural Resources (BGR), whereas EUROSHACK was under the leadership of the BGR and British Antarctic Survey (BAS).

In the GEISHA expedition, about 300 samples were collected to assess the degree of metamorphism, and approximately 200 thin sections were studied with this purpose (Buggisch *et al.* 1994b). In the EUROSHACK expedition, about 150 samples

https://doi.org/10.1017/S1755691022000111 Published online by Cambridge University Press

were taken from 43 different stratigraphic levels and/or localities from the Mount Wegener Formation. They were used to analyse facies, provenance, geochemistry and K–Ar dating. Most of these samples come from conglomerates or limestone clasts within the conglomerates (Buggisch & Henjes-Kunst 1999).

A total of 237 petrographic thin sections have been reviewed in this study (GEISHA and EUROSHACK samples): 45 from the Stephenson Bastion and Du Toit Nunataks and 188 from the Read Mountains (Fig. 4b). GEISHA thin sections are from the Stephenson Bastion (9) and Du Toit Nunataks (2). EUROSHACK thin sections are from the Stephenson Bastion (34) and the Mount Wegener Formation (189) in the eastern part of the Read Mountains: Oldhamia (91) and Trueman (50) terraces, Swinnerton Ledge (47). In addition, four thin sections of indeterminate origin from EUROSHACK have been reviewed.

Out of 237 petrographic thin sections, 223 were medium in size ($5 \times 5\ cm^2$) and 14 were small ($2.7 \times 4.8\ cm^2$). The microfacies and palaeontological analyses were performed with petrographic and binocular microscopes. The samples were classified according to the schemes of Dunham (1962), Embry & Klovan (1971) and Wright (1992). The peloid subcategories are according Flügel (2004) and the sediment grain sizes according Wentworth (1922) size classes. The percentage of allochems was semi-quantitatively analysed by visual estimation charts (several authors in Flügel 2004). The basic types of porosity and pore-size classes were described following the classification of Choquette & Pray (1970). Selected thin sections were stained with alizarin red sulphur and potassium ferricyanide to analyse their staining response (calcite/dolomite and iron content, respectively) according to Dickson (1965, 1966). The classification of dolomite crystal fabrics follows the Sibley & Gregg (1987) scheme and the crystal-size scale for carbonate rocks is according to Folk (1962). A total of 367 archaeocyath specimens and one coralomorph have been recognised from 46 thin sections. Among archaeocyathan specimens, 189 were classified following the systematics of the *Treatise on invertebrate paleontology* (Debrenne *et al*. 2015).

The studied material is housed in the Museo Geominero (MGM), Instituto Geológico y Minero de España (IGME, Spanish Geological Survey, Madrid) under the code numbers MGM-7202X–MGM-7438X.

5. Carbonate clasts record from the Cambrian Mount Wegener Formation and the Cenozoic tills

The analysed carbonate clasts from the Cambrian Mount Wegener Formation and the Cenozoic tills (Stephenson Bastion and Du Toit Nunataks) show equivalent components and microfacies. The analysed carbonate clasts are accessory to primary components in the sandy polymictic conglomerates and breccias from the lower Cambrian Mount Wegener Formation and from the Cenozoic tills. The carbonate clasts correspond to limestones and dolostones (see sections 5.1 and 5.2) where the main allochems are non-skeletal grains, skeletal grains and calcimicrobes. The non-skeletal grains include aggregate grains, mud peloids (micritic intraclasts), bahamite peloids (round micritic grains), algal peloids (calcimicrobe-derived micritic grains) and different types of ooids (types 1–3). Very fine to fine-grained size superficial ooids with quartz nuclei are type 1 ooids. Medium-sized and very coarse to granule-sized ooids are type 2 and type 3, respectively. The carbonate clasts from the Mount Wegener Formation and Cenozoic tills also show equivalent early to late diagenetic phases and tectonic-induced fabrics (Fig. 5). The main diagenetic processes recorded in carbonate clasts and their host rocks (conglomerates) are described in section 6.

In addition to the similarities observed in the microfacies, diagenetic and tectonic processes, the size distribution of the archaeocyathan cups has been analysed to assess whether or not the allochthonous archaeocyaths from the Cenozoic tills (Stephenson Bastion and Du Toit Nunataks) are derived or not from the Mount Wegener Formation (Fig. 6). The diameter of the archaeocyathan cups is measured in transverse section from the thin sections. A total number of 189 specimens have been analysed (see section 7) and 181 specimens have been measured from the Stephenson Bastion/Du Toit Nunataks (70) and the Mount Wegener Formation (111). Some archaeocyaths cups are distorted by tectonic stresses (see section 6). In these cases, the minimum diameter has been selected to reduce bias due to tectonically strained archaeocyath cups and characterise the size distribution of archaeocyaths. The archaeocyathan fauna from the Cenozoic tills shows the same average diameter as those observed in the Mount Wegener Formation (3.25 mm), as well as equivalent median values (2.65 and 2.85 mm, respectively; see Fig. 6a, b). Therefore, the analysis of cup sizes supports a single source for the archaeocyaths from the Cenozoic tills and the Mount Wegener Formation. In addition, we have grouped all the measured archaeocyaths into a single set to analyse how the cup sizes are distributed. We have selected three diameter size ranges: small (0.2–2.9 mm), medium (3.0–5.9 mm) and large (6.0–14 mm). In the Shackleton Range, more than half of the specimens are small in size (53 %), and the rest are mainly medium in size (34 %), while the largest sizes are minority (13 %) (Fig. 6c). Most archaeocyaths have a size diameter ranging from 10 to 50 mm (Rowland 2001). Furthermore, typical conical cups of Ajacicyathidae are around 5–15 mm (Debrenne *et al*. 2012). Cordie & Dornbos (2019) have measured the traditional morphometric characters of more than 1000 archaeocyaths, mainly from the orders Ajacicyathida and Archaeocyathida. They have reported an average diameter of 10.6 mm and a median value of 8.67 mm (0.78 mm minimum to 74 mm maximum). Cordie & Dornbos (2019) reported an average diameter of 10.6 mm from more than 1000 measured archaeocyaths. Therefore, the archaeocyaths from the Shackleton Range record are small compared to published data. This trend in a smaller sized fauna for Antarctic record has also been observed in Cambrian helcionelloids from the Shackleton Limestone (central TAM) that were compared with helcionelloid mollusc assemblages from the Ajax Limestone (Australia) and the Bastion Formation (Greenland) (Jackson & Claybourn 2018).

All these data from the analysis of microfacies, diagenetic processes and archaeocyathan diameter sizes confirm that Cenozoic carbonate erratics from the Stephenson Bastion and Du Toit Nunataks are derived from the Cambrian Mount Wegener Formation. Thus, the analysis of carbonate clasts from the Shackleton Range provides crucial information about the history of a hidden Cambrian carbonate platform from which they were derived.

5.1. Dolostone clasts microfacies (DM)

The analysed dolostone clasts (Figs 7, 8a) have been arranged in three main categories according to the percentage of quartz grains, the proportion of non-skeletal grains or the predominance of a dolomite crystal fabric as: (DMa) dolomitic sandstones to sandy dolostones (two and four subcategories, respectively); (DMb) aggregate-grain- to ooid-rich dolostones (three subcategories); and (DMc) dolostones.

The presence of very well-rounded quartz sand grains is characteristic in the dolomitic sandstones to sandy dolostones. Dolomitic sandstones range from fine to medium very well-sorted dolomitic sandstone (DMa1) to coarse, poorly sorted intraclastic dolomitic sandstone (DMa2) (Fig. 7a). In the first one, quartz grains reach up to 65 % of the rock volume. In the second one,

https://doi.org/10.1017/S1755691022000111 Published online by Cambridge University Press

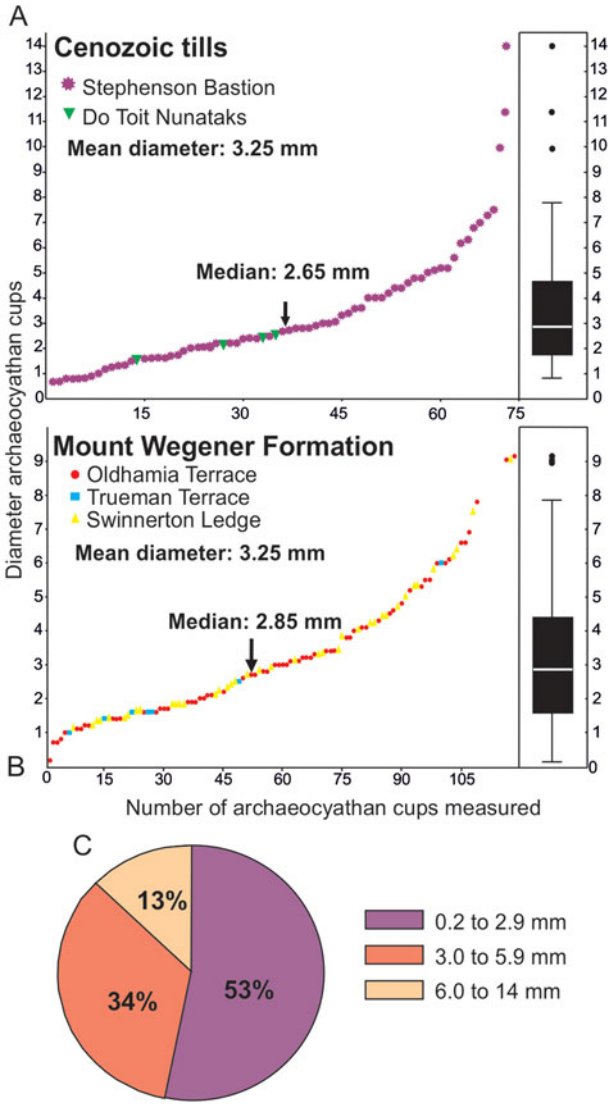

Figure 6 Distribution of the archaeocyath diameters from the Shackleton Range. (A) Diameter sizes graph of the archaeocyathan cups from Cenozoic tills located at the Stephenson Bastion and Du Toit Nunataks. (B) Diameter sizes graph of the archaeocyathan cups from the Mount Wegener Formation (Oldhamia and Trueman Terraces and Swinnerton Ledge). (C) Pie chart showing the three stablished ranges of measurements of archaeocyathan cup diameters.

they represent 40–50 %, while subrounded dolomicrite and dolospar intraclasts reach 30 % of the rock volume.

The sandy dolostones are coarse intraclastic dolorudites (DMa3), medium oolitic-intraclastic dolorudites (DMa4) and dolomicrites (DMa5–6), and their quartz grain content is in the range 1–30 % of the rock volume. In the sandy, coarse, very poorly sorted massive clast-supported intraclastic dolorudites (DMa3) (Fig. 7b), subangular to well-rounded intraclasts (up to 1.7 cm) are polygenic. Dolomicrites and silty dolomicrites are dominant intraclasts (up to 60 % of the rock volume), while dolograinstones rich in ooids, aggregate-grains or algal peloids are minor intraclasts. Oolitic dolograinstone intraclasts are made up of different types of ooids (types 1–3). In addition, fragments of type 3 oolitic cortices, abraded micritic-coated clasts and orange fibrous cement crusts also occur. Dominant coarse, very well-rounded quartz (up to 1 mm) and minor fine to medium subangular quartz sand grains are up to 25 % of the rock volume. Calcimicrobe intraclasts with *Proaulopora* and ?*Renalcis* are accessories.

In the sandy, medium poorly to moderately sorted oolitic-intraclastic dolorudites (DMa4) (Fig. 7c), elongated intraclasts are imbricated. Sandy oolitic (type 2) compound granule-size intraclasts account for about 35 % of the rock volume, while silty dolomicrite intraclasts are around 15 %. Superficial ooids (type 1) are 15 % of the rock volume. Quartz content corresponds to coarse very well-rounded grains (10 %) and fine to medium subangular grains (20 %).

The most common sandy dolomicrites (DMa5) are massive, with very accessory dispersed silt to very fine quartz grains (1 %). However, there are others (DMa6) with rare scattered pelletoids, superficial ooids (5 %) and accessory silt-sized quartz grains (10–15 %) that show the characteristic non-fabric-selective porosity (20 % of the rock volume). These large megapores (>1 cm) configure a network of irregular vuggy to channelised cavities with clastic fillings (Fig. 7d). The sedimentary fillings are primarily angular to subangular silt-size quartz grains, very fine- to medium sand-sized superficial ooids and minor well-rounded medium sand-sized quartz grains.

Aggregate grain- to ooid-rich dolostones (DMb) are dominated by aggregate grains or ooids or a mixture of non-skeletal grains. Different cements and replacements of dolomite and silica occur in primary interparticle porosity and secondary selective leaching of the cortex and nuclei of non-skeletal grains, resulting in varying degrees of preservation of the original fabrics (see section 6). Compound grains, 200 µm to 1 mm in size, with grape-like to lobate shapes and irregular dark micritic envelopes, are forming aggregate grain dolowackestones to dolopackstones (DMb1) (Fig. 7e) with very accessory small superficial ooids (type 1). Laminar micritic concentric type 3 ooids (up to 5 mm, 'giant ooids' *sensu* Sumner & Grotzinger 1993 rather than pisoids) can form loosely packed oolitic dolowackestones to packed dolograinstones (DMb2) (Fig. 7f). These microfacies show moderately sorted to well-sorted simple ooids, with both spherical and ellipsoidal shapes. Symmetrical cortices predominate and broken cortices that act as nuclei are very common. Very well-rounded quartz grains (650 µm) are accessory in matrix and within compound ooids. Oolitic dolograinstones with very well-sorted silicified type 2 ooids (medium-grained sand size) also occur. The very poorly sorted aggregate grain-oolitic dolograinstone (DMb3) (Fig. 7g) shows a distinctive regular to irregular fenestral fabric (up to 1.5 cm wide) that is filled with geopetal infills and cements. In this microfacies, ooids are mixture of 1–2–3 types with different preservations. In the fenestral aggregate grain-oolitic dolograinstone are found large compound intraclasts, up to 5 mm wide, with aggregate grains and peloids as intracomponents and multiple micritic envelopes.

Dolostones with cemented non-fabric-selective porosity also occur (DMc). They are very fine to finely crystalline dolomites with intercrystalline mesopores and very large megapores (16 mm × 41 mm, vug to channel types). Large vuggy to channelised cavities can reach up 25–30 % of the rock volume and display multi-episodic fillings (Fig. 8a; see section 6).

5.2. Limestone clasts microfacies (LM)

The most frequent limestones are calcimicrobe- and calcimicrobe–archaeocyath-bearing clasts (63 thin-sections). Calcimicrobes and/or archaeocyaths are primary to accessory allochems that form calcimicrobial boundstone (LMd, 12.7 % of 63 thin-sections), calcimicrobial boundstone with archaeocyaths (LMe1, 5.5 %), calcimicrobe–archaeocyath boundstone (LMe2, 6.3 %), archaeocyath cementstone (LMe3, 15.9 %) and archaeocyath floatstone (LMf, 9.5 % of 63 thin-sections). Bioclastic wackestone to packstone (LMg) and peloid-intraclastic-bioclastic packstone to grainstone (LMh) are uncommon.

In the boundstone microfacies, calcimicrobes correspond to *Angusticellularia* (also named *Angulocellularia*), *Epiphyton*, *Renalcis*, *Tarthinia*, *Girvanella* and *Botomaella* (Fig. 8). *Epiphyton* or *Angusticellularia* are the main dendrolitic microframe-

https://doi.org/10.1017/S1755691022000111 Published online by Cambridge University Press

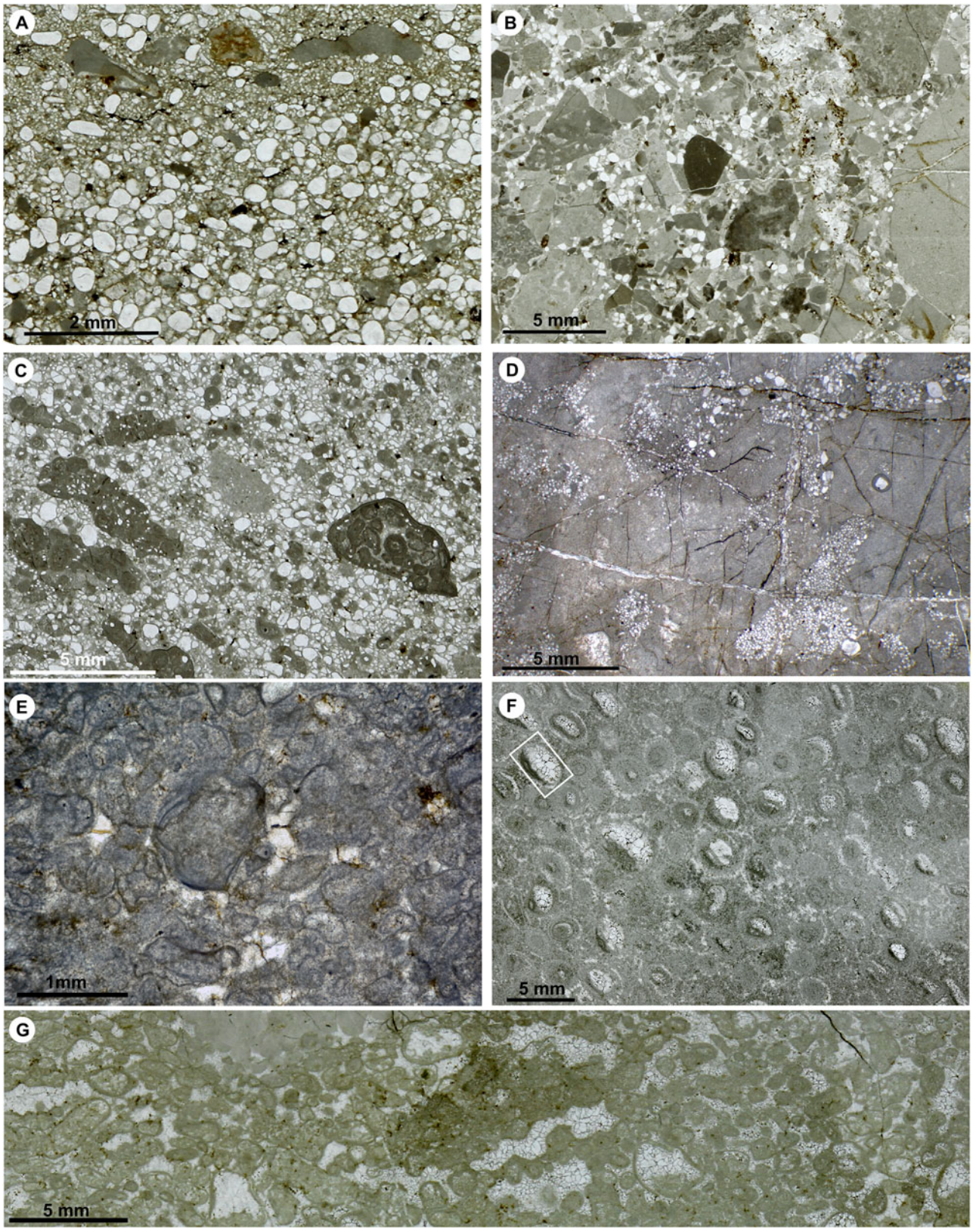

Figure 7 Cambrian dolostone clast microfacies from the Cambrian Mount Wegener Formation and the Cenozoic glacial erratics. Dolomitic sandstone: (A) coarse, poorly sorted, intraclastic, dolomitic sandstone. (B–D) Sandy dolostones (B) coarse, very poorly sorted, massive, clast-supported, intraclastic dolorudite; (C) medium, poorly to moderately sorted, oolitic, intraclastic, dolorudite; (D) dolomicrite with large megapores with siliciclastic filling. (E–G) Aggregate grain- to ooid-rich dolostones (E) aggregate grain dolopackstone; (F) loosely packed oolitic dolopackstone (the inset corresponds to Fig. 9b); (G) fenestral, aggregate grain-oolitic dolograinstone.

builders, while the archaeocyaths range from 10 to 25 %, 25 to 30 %, up to 40 to 50 % of the rock volume in the calcimicrobial boundstone with archaeocyaths, calcimicrobe–archaeocyath boundstone and archaeocyath cementstone, respectively. In the boundstone microfacies dominated by *Epiphyton* or *Angusticellularia* dendritic microframes (Fig. 8b, c), the associated skeletal components, mainly archaeocyaths or calcimicrobes, are extremely low. Few clusters of *Renalcis* (Fig. 8d) appear irregularly distributed among the dendrolites of *Angusticellularia* or *Epiphyton* or attached to the walls of

https://doi.org/10.1017/S1755691022000111 Published online by Cambridge University Press

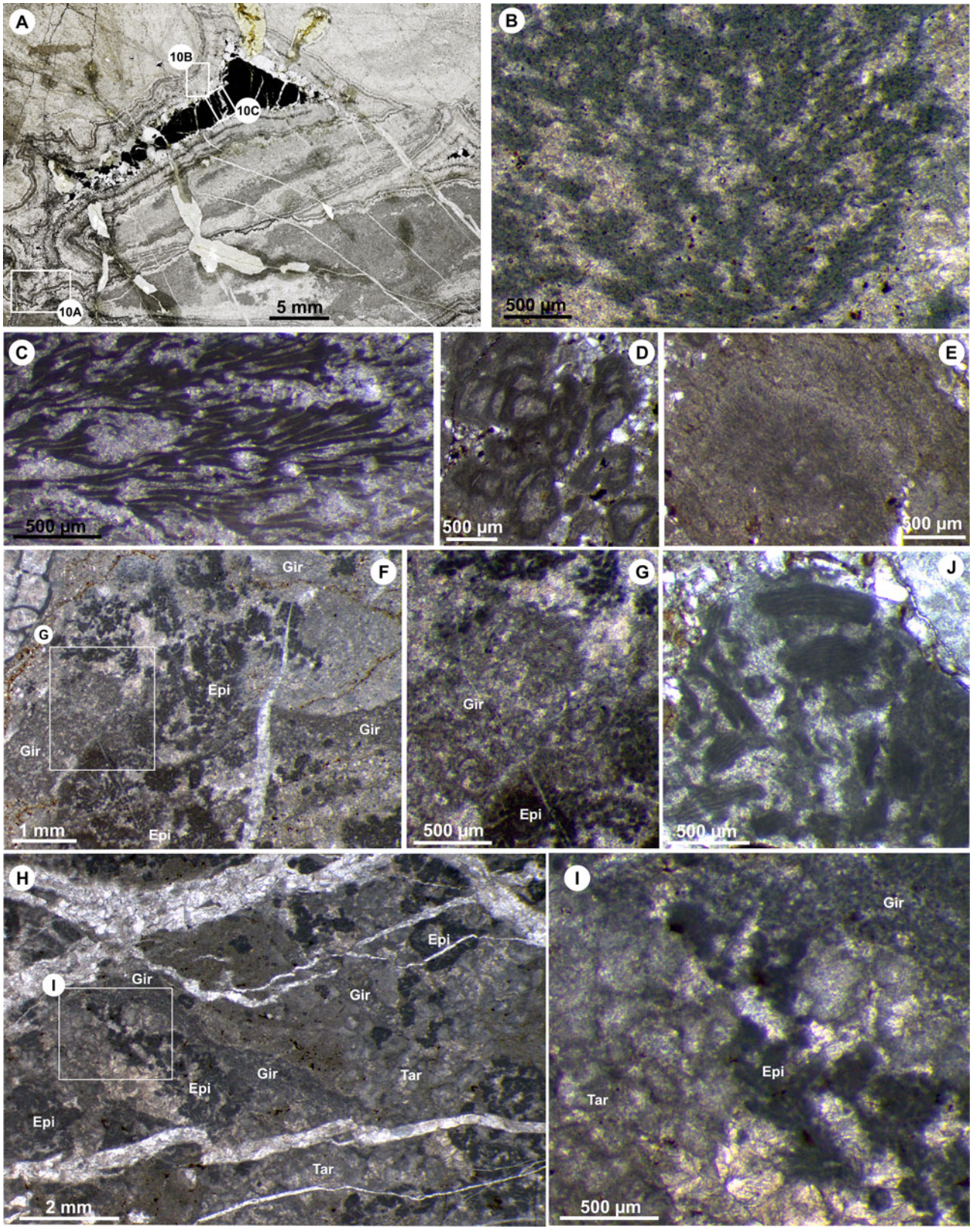

Figure 8 Cambrian dolostone and limestone clasts microfacies from the Cambrian Mount Wegener Formation and the Cenozoic glacial erratics. (A) Dolostone with meso- and megapores filled with multiple phases of dolomite cements, including black bitumen. The boxes correspond to Fig. 10a–c. Calcimicrobes from calcimicrobial-rich microfacies: (B) *Angusticellularia* dendrolitic microframe; (C) *Epiphyton* dendrolitic microframe; (D) broken *Renalcis* bunches surrounded by detrital grains; (E) *Botomaella* fan-like forms; (F, G) *Epiphyton–Girvanella* intergrowth. (H, I) *Tarthinia–Epiphyton–Girvanella* intergrowth. (J) Calcimicrobe grainstone clast with *Subtifloria* remains.

archaeocyaths, which may be exceptionally covered by *Girvanella* crusts.

Epiphyton–Girvanella or *Epiphyton–Tarthinia–Girvanella* intergrowths form complex microframes, but they are not very common (Fig. 8f–i). *Botomaella* fan-shaped radiant filaments/tubes (Fig. 8e) are extremely rare in the boundstone microfacies. *Tarthinia*-dominated microframes are rare but are found surrounded by wackestone to packstone pockets with a rich

https://doi.org/10.1017/S1755691022000111 Published online by Cambridge University Press

associated fauna of echinoderms, brachiopods, trilobites, hyoliths, chancelloriids, coralomorphs and sponge megascleres. This rich associated fauna has also been observed in the calcimicrobe–archaeocyath boundstone microfacies. However, in the archaeocyath cementstone, the associated fauna is restricted to accessory hyoliths and chancelloriids.

The archaeocyath-bearing microfacies are clearly dominated by regular archaeocyaths (149 specimens versus 40 irregular specimens). In addition, in the archaeocyath cementstone the presence of irregular archaeocyaths is totally accessory. Regarding archaeocyaths distribution, a total number of 16 families of archaeocyaths occur in the boundstones (see Appendix 1). *Rotundocyathus glacius*, *Cadniacyathus* sp. and *Archaeopharetra irregularis* are the dominant species. Fifteen families are represented in the calcimicrobial boundstone with archaeocyaths, six in the calcimicrobe–archaeocyath boundstones and seven in the archaeocyath cementstones. Ajacicyathidae is the dominant family in the archaeocyath cementstones and calcimicrobial boundstones with archaeocyaths. The calcimicrobe–archaeocyath boundstones are dominated by Densocyathidae and Ajacicyathidae. Common families in all boundstones are Ajacicyathidae, Densocyathidae, Shackletoncyathidae, Loculicyathidae and Archaeopharetridae, while Kaltatocyathidae are only found in the calcimicrobe–archaeocyath boundstones.

The presence of skeletal components, other than archaeocyaths, in the rest of the analysed microfacies (limestone- or dolostone-derived clasts) is very rare in terms of volume and/or frequency. The archaeocyath floatstone consists of poorly sorted reworked archaeocyaths (25–35 % of the rock volume), hyoliths (1–5 % rock volume), allochthonous calcimicrobe remains (*Proaulopora*, *Subtifloria*) and calcimicrobial boundstone intraclasts (*Renalcis*- or *Epiphyton*-dominated microframes). The archaeocyath debris varies from septum to large cup remains. The archaeocyathan walls are mostly free of calcimicrobe encrustations but are unusually encrusted by *Girvanella*. Eleven families of archaeocyaths are represented in the archaeocyath floatstones – Bronchocyathidae and Ajacicyathidae are the dominant ones. Bronchocyathidae, Kymbecyathidae, Dictyocyathidae and Copleicyathidae are only found in the floatstones (see Appendix 1). *Thalamocyathus trachealis* is dominant in the floatstones.

In the peloid-intraclastic-bioclastic packstone to grainstone, fine- to medium-grained sand size, algal peloids, mud peloids and bioclasts are the most common allochems. The largest bioclasts correspond to archaeocyathan remains (>1 mm), while indeterminate thin-walled, conical crenulated shells and hyoliths are minor bioclastic components. This microfacies (Fig. 9j–l) contains small to enlarged fenestral megapores that are filled with characteristic sedimentary fillings and cements (see section 6).

6. Principal diagenetic processes and tectonic fabrics recorded in the carbonate clasts from the Cambrian Mount Wegener Formation and the Cenozoic tills

6.1. Early diagenetic phases

The dolomitic sandstones, sandy dolostones and aggregate grain- to ooid-rich dolostones display evidence of early marine phreatic cementation, such as yellow fibrous to bladed isopachous rims (M1RD1) and pore-filling equant cement (M2RD1) (Fig. 9a, f). Meteoric vadose diagenesis processes, such as partial dissolution producing secondary moldic porosity, are common in aggregate grain- to ooid-rich dolostones. Some samples show partial to complete intraparticle dissolution and internal collapse that produced geopetal infills in aggregate grains and ooids ('half-moon' ooids *sensu* Wherry 1916). The evidence of selective leaching (oomoldic porosity and selective destructive replacive fabrics of some cortical laminae; Figs 7f, 9c) suggests a differentiation of the primary mineralogical composition of the ooids (high magnesium calcite, aragonite). Likewise, fenestral aggregate grain-oolitic dolograinstones display dark microcrystalline crusts and meniscus fabrics with distinctive rounded pores (Fig. 7g) produced during meteoric vadose diagenesis (Dunham 1971; Longman 1980).

Many dolostone microfacies exhibit early pervasive mimetic dolomitisation of allochems (e.g., concentric ooids, aggregate grains), micrite and early marine phreatic and vadose cements (Figs 7, 9a–f). Early mimetic dolomitisation (RD1) predates compaction and is followed by different stages of dolomitisation and silicification linked with secondary porosity and fractures (Figs 9a–f; see section 3). In the aggregate grain- to ooid-rich dolostones an early authigenic and diagenetic phase of silica occurs as chalcedony void-filling cement (Schc) within the remaining interparticle and/or within the secondary moldic intraparticle porosities (e.g., oomoldic porosity, Fig. 9b). Chalcedony cement post-dates early mimetic dolomitisation (RD1) and predates all other fracture-related cements. Some cortices and nuclei from ooids and aggregate-grains exhibit replacive cryptocrystalline and microcrystalline silica fabrics (RS1c-m in Fig. 9c, d, f).

The calcimicrobial boundstone with archaeocyaths, calcimicrobe–archaeocyath boundstone and archaeocyath cementstone exhibit the largest fabric-selective porosity that is filled with early marine phreatic cementation. The inter-, intra-skeletal and growth framework meso- and megapores are filled with yellow, inclusion-rich, fibrous calcite cements (M1Cc) and bladed to equant non-ferroan calcite mosaics (M2Cc) that precede the formation of stylolites. In the archaeocyath cementstones, the isopachous marine fibrous calcite crusts (up to 2.5 mm thick) constitute around 30–40 % of the rock volume (Fig. 9g). Early marine phreatic cementation occluded a significant part of the primary mesopores in the calcimicrobe- and archaeocyath-bearing clasts. Nevertheless, the larger fabric-selective porosity registered successive diagenetic phases (see below).

6.2. Breakup and brecciation of platform and downslope transport of carbonate clasts

Irregular vugs with very angular silt to sand-sized crystal and quartz grain sedimentary fillings post-date early marine phreatic cements (M1Cc and M2Cc) in boundstone microfacies (Fig. 9h). Furthermore, the orientations of the geopetals within irregular vugs and the calcimicrobe microframework show inconsistent polarity relationships between them (Fig. 9i). Therefore, these irregular vugs cut and eroded the early pre-existing marine cements and the calcimicrobe microframework, suggesting meteoric diagenesis related to the breakup and sedimentary brecciation of the carbonate platform. These sedimentary fillings are equivalent to those observed in enlarged fenestral megapores developed in the peloid-intraclastic-bioclastic grainstone clasts (Fig. 9j).

The enlarged fenestral megapores are filled with two sedimentary fillings (SI1, SI2 in Fig. 9j) and drusy mosaic cement with crystals showing compositional zoning. Drusy zoned mosaic cement begins with non-ferroan calcite (pink-stained) and ends with ferroan calcite (mauve-stained) (Fig. 9k). However, not all megapores are occluded by the complete succession of drusy zoned mosaic cement. The sedimentary fills correspond to an early very fine-grained geopetal crystal silt (SI1) that is followed by a second fill (SI2). The latter fill has angular silt to sand-sized quartz grains and eroded crystals derived from the non-ferroan calcite drusy mosaic (Fig. 9l). The SI2 is observed in those fenestral pores close to the margins of the limestone clast. Furthermore, SI2 is equivalent to the surrounding conglomerate

https://doi.org/10.1017/S1755691022000111 Published online by Cambridge University Press

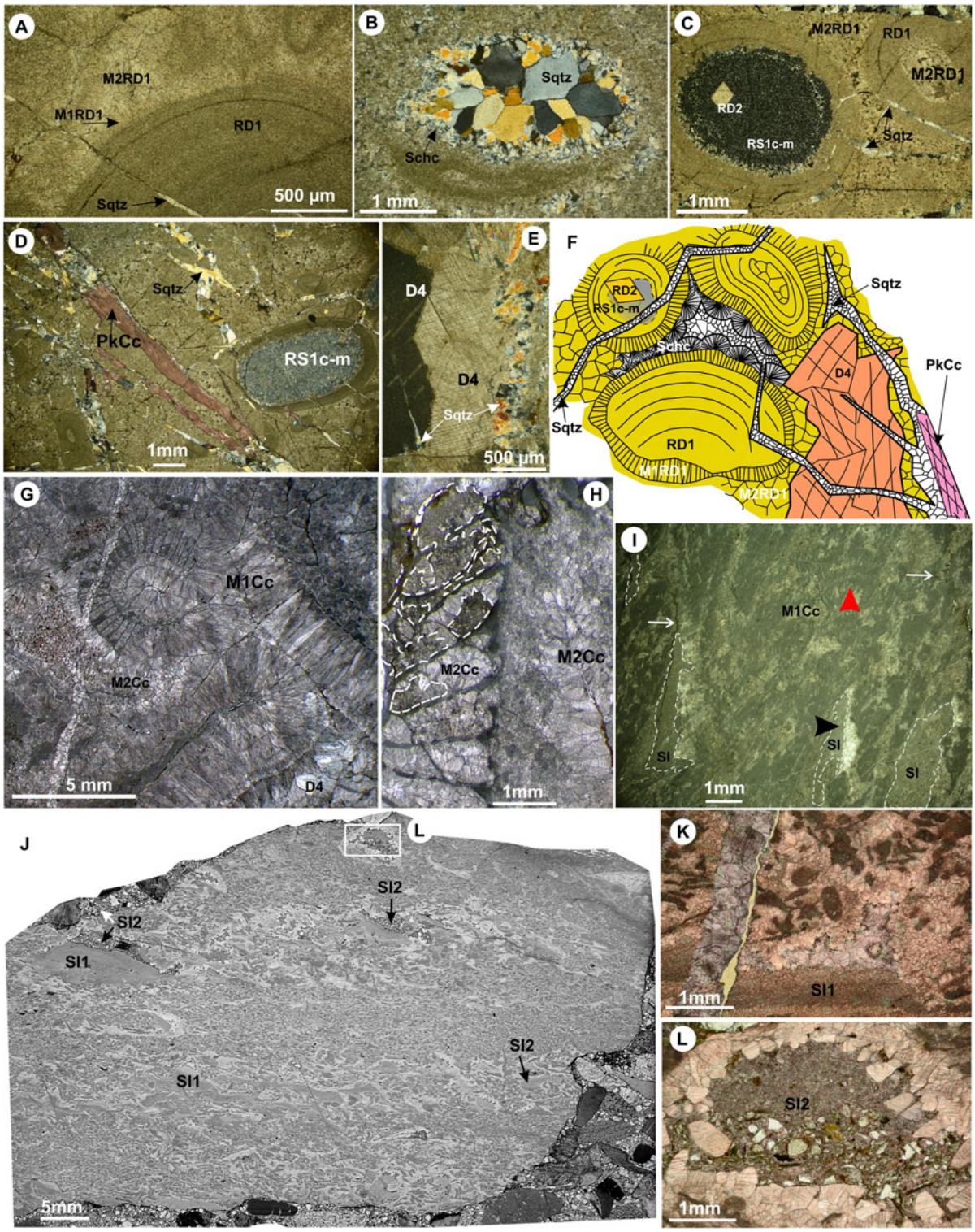

Figure 9 Diagenetic processes recorded in the Cambrian carbonate clasts of the Cambrian Mount Wegener Formation and the Cenozoic tills. (A–E) Dolostone clasts showing different processes of dolomitisation and silicification. (A) Detail of oolitic dolograinstone showing evidence of early mimetic dolomitisation of ooids (RD1), early marine fibrous and equant phreatic cements (M1RD1 and M2RD1, respectively). (B) Detail of oolitic dolopackstone (see Fig. 7f) where the oomoldic porosity is filled with an early authigenic silica phase (Schc = chalcedony cement) and a fracture-related silica phase (Sqtz = megaquartz mosaic). (C) The replacive cryptocrystalline to microcrystalline silicification (RS1c-m) post-dates early marine phreatic cements and mimetic dolomitisation and predates D2 dolomitisation stage (RD2). Megaquartz mosaics (Sqtz) are associated with late cement veins (LVA and LVB). (D) LVA (quartz–calcite vein) system with non-ferroan to slightly ferroan poikilotopic calcite cement (PkCc). (E) LVA system post-dates the dolomitisation stage D4. (F) Scheme with some of the main diagenetic processes recorded in the dolostone clasts. (G–L) Limestone clasts. (G) Detail of the archaeocyath cementstone with large fabric selective porosity infilled by early marine phreatic cement (M1Cc = fibrous calcite cement; M2Cc = bladed to equant non-ferroan calcite cement) and late diagenetic phases (D4). (H) Archaeocyathan intervallum (left) showing irregular vugs that post-date early marine phreatic cements. (I) *Epiphyton* microframe with secondary non-fabric selective porosity with geopetal sedimentary fillings (SI). Note how the growth polarity of the calcimicrobe (red arrowhead) does not match the polarity of the geopetal fillings (black arrowhead). Note how the stylolites (white arrows) post-date the sedimentary infillings. (J) Polymictic conglomerate showing a large peloid-intraclastic-bioclastic grainstone clast with enlarged fenestrae. Megapores are filled with sedimentary fillings (SI1 and SI2) and (K) drusy mosaic with compositional zoning starting with non-ferroan calcite and ending with fracture-related ferroan calcite cement. White box outlines area of (L). (L) Sedimentary filling (SI2) is composed of sandy-silty matrix (identical to the host rock conglomerate matrix) and eroded crystals derived from the non-ferroan calcite cement.

https://doi.org/10.1017/S1755691022000111 Published online by Cambridge University Press

matrix (Fig. 9j). Thus, SI2 was infiltrated into the still-open fenestral pores during sedimentation of the carbonate clasts as part of the matrix-supported polymictic gravels on the marine slope, after the early non-ferroan calcite drusy mosaic. The succeeding ferroan calcite cement is fracture-related cement and occludes the remaining fenestral porosity (Fig. 9k).

6.3. Late diagenetic phases and mechanical overthrust-emplacement processes

In general, clasts in the sandy polymictic conglomerates from the Mount Wegener Formation and Cenozoic tills show dominant tangential contacts due to their deposition as matrix-supported gravels. However, the contacts between sandy matrix and clasts are sutured due to tectonic deformation (Fig. 5d, e). In carbonate clasts, mechanical compaction features were inhibited mostly by early cementation (M1, M2), dolomitisation (RD1) and silicification (Schc and RS1c-m) (Fig. 9). Thus, loosely packed fabrics are the most common, except for sandy intraclastic dolorudites (Fig. 7c), where tangential and long contacts dominate and there are also concavo–convex contacts between quartz and dolomite grains. Evidence of chemical compaction occurs as simple to sutured stylolites in some limestone clasts. These stylolites post-date both shallow marine cements (M1Cc, M2Cc) as well as geopetal sedimentary infillings produced during the downslope transport of the clasts.

Burial dolomites correspond to three different stages of dolomitisation (D2, D3 and D4). Stage D2 consists of coarsely crystalline (0.25–0.5 mm up to 1 mm), planar-s to planar-e type dolomite (types according to Sibley & Gregg, 1987). D2 occurs mainly as replacive/cement dolomite in the interparticle, secondary intraparticle, intercrystal and fracture-associated porosities of the aggregate grain- to ooid-rich dolostones. D2 post-dates silica Schc cement and RS1c-m replacement (Fig. 9c, f). Stage D2 is also the first dolomite cement in the vug to channel cemented dolostones where the large megapores are lined by multiple isopachous layers of cement crusts (1.5–2.5 mm thick) (Figs 8a, 10a, b). In some cases, cavity-cement crusts may start with early yellow inclusion-rich fibrous cement (like those previously described as M1Cc) but now being a dolomite, so it could represent early mimetic dolomitisation of a fibrous marine aragonite/calcite cement precursor (M1RD1). However, most mesopores, megapores and fractures are rimmed by a first generation of cloudy to clear, coarsely crystalline (>0.25 mm) rhombic D2 dolomite (Fig. 10a). The boundary between the rhombic crystals D2 and the next stage D3 can be locally irregular and rich in black hydrocarbon residues. Stage D3 corresponds to a black inclusion-rich zoned, fibrous to elongated-bladed dolomite crust (up to 2 mm thick) (Fig. 10a). In some cavities, the D3 dolomite crusts show a clearer, less inclusion-rich epitaxial late D4 stage (Fig. 10b). There are traces of bitumen after the growth of D4 dolomite. Therefore, the hydrocarbon migration post-dates the D2 and D4 dolomite stages and was coeval with the D3 dolomite stage. In addition, the partial migration of the trapped hydrocarbon in the D3 cement left an open microporosity that was filled with the fracture-related cement. Stage D3 is not observed in the aggregate grain- to ooid-rich dolostones (Fig. 7e–g). However, a possible equivalent to stage D4 is recorded as a fracture-related phase of brown, thick twinning, very coarsely crystalline (1–4 mm), planar-s dolomite in the aggregate-grain to ooid-rich dolostones (Fig. 9e, f) and in the archaeocyath cementstones and floatstones (Fig. 9g). The abundance of black bitumen inclusions in D3–D4 suggests that they are burial diagenetic dolomites. The occurrence of black bitumen in mesopores and megapores from dolostones and the observed cross-cutting relationships suggest that hydrocarbon migration predates the void-late-fracture-related remnant cements (LVA, late cement vein system A) (Figs 8a, 10c). The appearance of black bitumen residues is recorded in thin hair-like fractures, intercrystalline mesopores and megapores in dolostones, calcimicrobial boundstones and polymictic conglomerates.

The late cement veins correspond to different mineral-filled fracture systems (LVA and LVB, respectively). The LVA system consists of quartz-calcite veins and the LVB system consist of (ferroan saddle dolomite)-quartz-ferroan calcite-quartz veins. LVA and LVB fluids precipitated in remnant open porosity in dolostone and limestone clasts and host rock conglomerates. Cross-cutting relationships, mineralogies and fabrics support LVB postdating LVA. In the LVA system (Fig. 9d, f), dissolved silica fluids first produced chert and microquartz replacement from the host rock and later precipitated as megaquartz mosaics within the remaining porosity and fractures. Second, dissolved non-ferroan to very slightly ferroan carbonate fluids precipitated as very to extremely coarse poikilotopic calcite cement with thin twin planes (and minor thick twin planes) in pores and fractures. In the LVB system, the fracture walls are sometimes lined with ferroan saddle dolomite relics (turquoise/greenish stain and curved faces; FeD in Fig. 10d) and, generally, by megaquartz crystals with euhedral terminations, which are embedded by coarsely to very coarsely crystalline zoned ferroan calcite with tabular thick twin planes (FeCc in Fig. 10d–g). Dissolved silica fluids from the LVB system also produced partial and selective host rock cryptocristalline and microcrystalline silica replacement (RS2c-m), syntaxial overgrowths of detrital quartz grains and megaquartz mosaics in remnant porosity (Sqtz).

Some limestone clasts show obliterative diagenetic fabrics and they have been classified here as sparstone clasts. However, the distribution pattern of clots, the size of cavities and the appearance of archaeocyath ghosts suggest that they were calcimicrobe–archaeocyath-bearing microfacies that underwent neomorphism and partial replacement processes that were associated with fracture-related fluids during burial (Fig. 10h, i). In fact, replacive microdolomite crystals occur in the limestone clasts associated with hair-like fractures with ferroan carbonate fluids from the LVB system. This replacive microdolomite is observed in host rock, calcimicrobes, archaeocyaths and shallow marine cements (Fig. 10j, k).

Some samples from the Cambrian Mount Wegener Formation and the Cenozoic erratics show evidence of low-grade tectonically induced fabrics. Furthermore, in the Mount Wegener Formation, the tectonically induced fabrics occur close to the overthrust. Buggisch *et al.* (1994b) described how the sandstones and polymictic conglomerates from the Mount Wegener Formation are tightly folded and deformed above the decollement zone. They observed how the limestone clasts were extremely stretched while feldspars were brittly deformed and described the growth of illite/sericite, chlorite and minor biotite. They recognised two stages of deformation: a first isoclinal folding with penetrative schistosity and distinct crenulation cleavage, and a later recumbent open folding development during the final emplacement of the Mount Wegener Nappe.

We have recognised in the carbonate clasts several features associated with the low-grade tectonically induced fabrics produced during the deformation and emplacement of the Mount Wegener Nappe. In some samples, archaeocyaths and cements can be distorted by the effects of plastic deformation (Fig. 10l), as well as flattened ooids produced by pervasive tectonic shear. Calcite cements associated with late cement veins (LVA and LVB) present different degrees of twin lamellae development. The non-ferroan to very slightly ferroan coarsely poikilotopic calcite cement that precipitated from the LVA system (PkCc in Figs 9d, 10c, h) exhibits mostly type I and rare type II calcite twins. However, the coarse to very coarse crystalline

https://doi.org/10.1017/S1755691022000111 Published online by Cambridge University Press

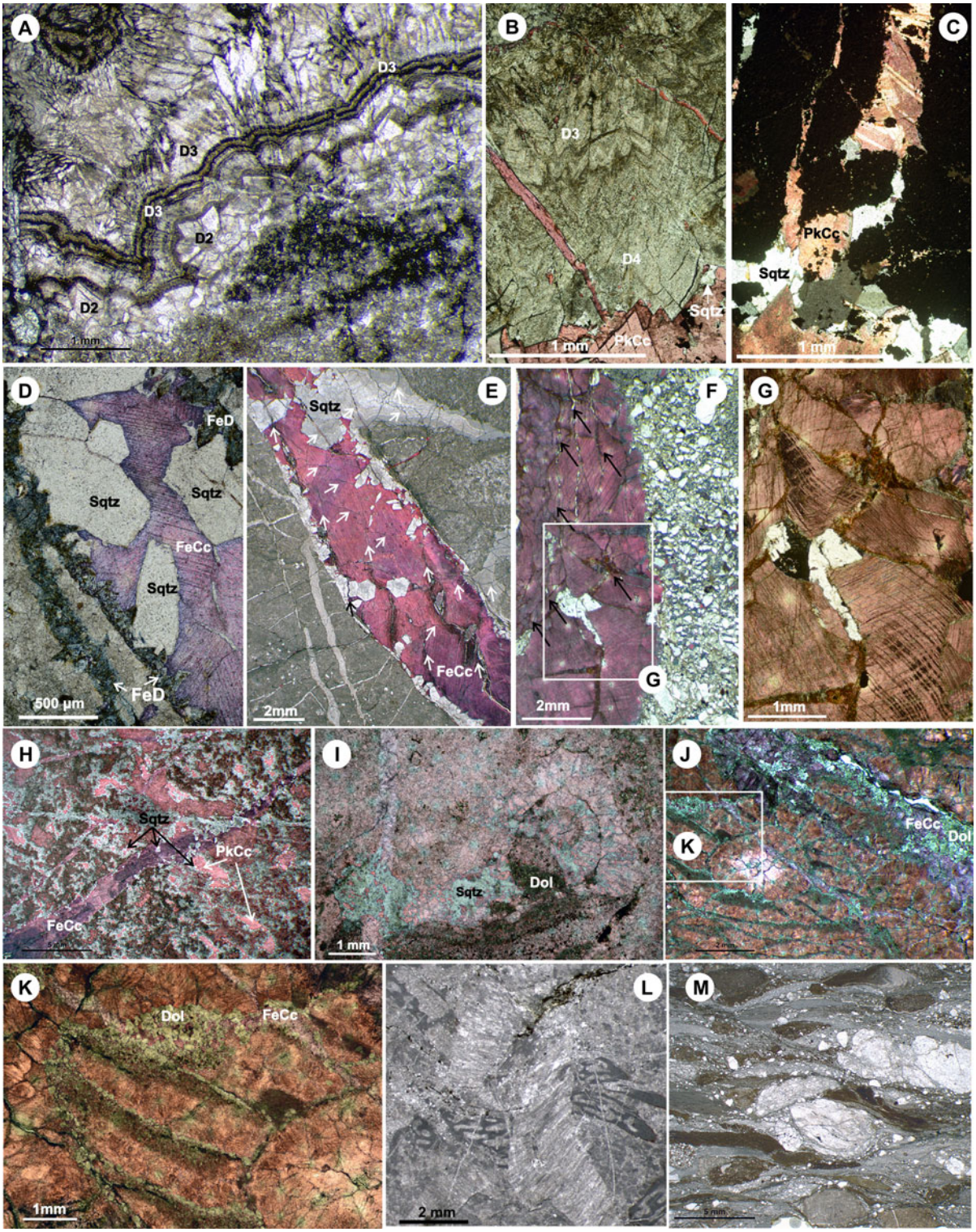

Figure 10 Late diagenetic and tectonically induced fabrics in Cambrian carbonate clasts of the Mount Wegener Formation and the Cenozoic tills. Details of dolostone with large vuggy to channelised cavities with multi-episodic fillings, locations of (A)–(C) in Fig. 8a. (A) Burial dolomites D2 and D3. D3 is rich in black bitumen residues. (B) D3 dolomite crust grading into epitaxial D4 stage. Late cement vein (LVA) with quartz (Sqtz) and poikilotopic non-ferroan to slightly ferroan calcite (PkCc) cuts the pore-lining dolomite crust cements (D2, D3, D4). (C) Late cement vein (LVA) cuts the remains of black bitumen from the cavity, thus post-dating the burial D2–D4 dolomites and the migration of hydrocarbons. (D) Detail of late cement vein (LVB) with ferroan saddle dolomite (FeD), megaquartz crystals (Sqtz) and zoned ferroan calcite cements (FeCc). (E) Late cement vein (LVB). Note the euhedral terminations of the megaquartz crystals and the posterior superimposed tectonically induced cataclastic fabric (white arrows). (F) Detail of late cement vein (LVB) that crosses the sandy matrix of the polymictic conglomerate. Notice how the remaining intergranular porosity of the matrix is filled with ferroan calcite cement. Note the posterior superimposed tectonically induced cataclastic fabric (black arrows). (G) Detail of the zoned ferroan calcite cement showing type III calcite twins. (H) Calcimicrobe boundstone where secondary porosity has been filled with quartz (Sqtz) and poikilotopic non-ferroan to slightly ferroan calcite (PkCc), which are both late fracture-related cements (LVA). Notice how the second fracture system (LVB) is posterior to the LVA cements. (I) Sparstone clast where it is possible to recognise the inner and outer walls of an archaeocyathan cup. Note the presence of partial replacement processes such as dolomitisation (Dol) and silicification (Sqtz). (J) Archaeocyath cementstone where early marine cementation is crossed by late cement veins (LVB) with dolomite (Dol) and ferroan calcite (FeCc). White box outlines are of (K). (K) Detail of archaeocyathan intervallum. Note how dolomitisation is associated with hair-like fractures with ferroan carbonate fluids and is higher in substrates with precursor mineralogies with high magnesium content, such as archaeocyaths. (L, M) Tectonically induced fabrics in limestone clast (L) and conglomerate (M).

https://doi.org/10.1017/S1755691022000111 Published online by Cambridge University Press

zoned ferroan calcite cement that precipitated from the LVB system exhibits types II (tabular thick) and III (tabular thick curved) calcite twins (Fig. 10d–g). Calcite twin morphologies can be used as a low-temperature geothermometer based on data collection and analysis from Ferrill *et al*. (2004). These authors correlate the average calcite twin with the temperature of deformation, so that the thin twins dominate below 170 °C, and the thick twins dominate above 200 °C. On the other hand, late cement vein systems (LVA and LVB) show the coexistence of calcite and quartz in the veins. Experimental work on calcite and quartz solubility shows that the quartz solubility increases with rising temperatures while the solubility of calcite decreases; between 150 °C and 300 °C, all proportions are possible (Sharp 1965). These temperature values are in agreement with the very low-grade metamorphism conditions reached by the Mount Wegener Formation at the southern Read Mountains according with the illite crystallinities of °$\Delta 2\theta > 0.25$ (Buggisch *et al*. 1994b).

The analysed conglomerates and carbonate clasts may show different degrees of cataclastic deformation (Fig. 5b–e), from minor to dense anastomosing cleavage and incipient brecciation to strongly sheared fabrics (Fig. 10m) with finer seams of solution residues. This deformation post-dates all observed cementation and replacement phases, including late cement veins (LVA and LVB systems; Fig. 10e–g). K–Ar analysis in phyllosilicates (2–6 μm fraction) indicates that low-grade metamorphic overprint and southwards transport of the Mount Wegener Nappe were around 490 Ma (i.e., Furongian) as a result of the Ross (Pan-African) orogeny (Buggisch *et al*. 1994b).

7. Systematic palaeontology

Phylum Porifera Grant, 1836
Class Archaeocyatha Bornemann, 1884

Order Monocyathida Okulitch, 1935
Family Tumuliolynthidae Rozanov in Rozanov & Missarzhevskiy, 1966
Genus *Tumuliolynthus* Zhuravleva, 1963

Tumuliolynthus irregularis (Bedford & Bedford, 1934)
(Fig. 11a, b)

1934 *Monocyathus irregularis* R. Bedford & W. R. Bedford, p. 2, pl. 1, fig. 2.
1995 *Tumuliolynthus irregularis* (R. Bedford & W. R. Bedford) – Zhuravlev & Wood, fig. 2a (top).
2020 *Tumuliolynthus irregularis* (R. Bedford & W. R. Bedford) – Kruse & Debrenne, p. 17, figs 14, 44A, *cum syn*.

Material. Two specimens: MGM-7209X-8; MGM-7213X-5 (see Appendix 2 for localities).

Description. One-walled cup 1.2 to 1.7 mm diameter. The wall is 0.08 to 0.12 mm thick and bears scarce single-pore tumuli with 0.22 to 0.28 mm diameter.

Remarks. This species is characterised by the irregularity of the size and spacing of its tumuli pores.

Occurrence. Australia: Arrowie Basin, Ajax Mine, Ajax Limestone (Bedford & Bedford 1934, 1939; Zhuravleva 1963; Debrenne 1969, 1974b; Kruse & Debrenne 2020); Gnalta Shelf, Mount Wright, Cymbric Vale Formation (Kruse 1982). Allochthonous clasts: South America, Falkland Islands, Hill Cove, Fitzroy Tillite Formation, erratics from the Late Carboniferous (Stone *et al*. 2012). Antarctica, King George Island, erratic deposits (Zhuravlev & Wood 1995); King George Island, Admiralty Bay-Melville Peninsula, Oligocene Polonez Cove and Early Miocene Cape Melville Formations, glacio-marine deposits (Wrona & Zhuravlev 1996); Shackleton Range, Trueman Terraces, carbonate clasts from the Mount Wegener Formation; Stephenson Bastion, Cenozoic glacial erratic tills. Cambrian *Series 2*, Botoman.

Order Ajacicyathida Bedford & Bedford, 1939
Suborder Dokidocyathina Vologdin, 1957

Superfamily Dokidocyathoidea Bedford & Bedford, 1936
Family Dokidocyathidae Bedford & Bedford, 1936
Genus *Dokidocyathus* Taylor, 1910

Dokidocyathus sp.
(Fig. 11c–e)

Material. Thirteen specimens: MGM-7203X-1, MGM-7206X-1, MGM-7208X-6, MGM-7208X-13; MGM-7208X-15, MGM-7208X-19, MGM-7209X-9, MGM-7209X-17, MGM-7209X-22; MGM-7214X-10; MGM-7235X-8; MGM-7235X-9; MGM-7235X-13 (see Appendix 2 for localities).

Description. Cup 0.7 to 3.8 mm in diameter and intervallum 0.20–1.20 mm wide. Intervallar coefficient IK 0.24–0.40. Outer wall with 3–5 rows of simple pores per intersept (diameter 0.06–0.16 mm, lintels 0.06–0.12 mm, wall thickness 0.04–0.20 mm). Inner wall with 1–2 rows of simple rounded pores per intersept (diameter 0.10–0.20 mm, lintels 0.06–0.20 mm, wall thickness 0.04–0.14 mm). Intervallum traversed by radial bars (thickness 0.02–0.16 mm), the transverse distance of bars 0.18–0.20 mm and longitudinal distance of bars 0.20–0.24 mm.

Remarks. The narrower spacing of intervallar bars and the values of IK distinguish from *Dokidocyathus simplicissimus* present in Nimrod Glacier (Debrenne & Kruse 1986) and other Australian described species. Although for similar diameters the intervallar bar spacing is in the range of the Australian species *zero*, the small size of the cups does not allow us to assign them to a specific species.

Occurrence. Allochthonous clasts: Antarctica, Shackleton Range, Trueman Terraces, carbonate clasts from the Mount Wegener Formation; Stephenson Bastion, Cenozoic glacial erratic tills. Cambrian *Series 2*, Botoman.

Superfamily Kaltatocyathoidea Rozanov in Zhuravleva, Konyushkov & Rozanov, 1964
Family Kaltatocyathidae Rozanov in Zhuravleva, Konyushkov & Rozanov, 1964
Genus *Kaltatocyathus* Rozanov in Zhuravleva, Konyushkov & Rozanov, 1964

Kaltatocyathus gregarius (Gravestock, 1984)
(Fig. 11f)

1984 *Aroonacyathus gregarius* Gravestock, p. 46, fig. 31e–l.
1989 *Kaltatocyathus gregarius* (Gravestock) – Debrenne, Zhuravlev & Rozanov, p. 114.
1990 *Kaltatocyathus gregarius* (Gravestock) – Debrenne, Rozanov & Zhuravlev, p. 148.

Material. One specimen: MGM-7218X-29/30 (see Appendix 2 for locality).

Description. Branching cups 1.3–1.6 mm in diameter and intervallum 0.40 mm wide with radial bars 0.02 mm thick. Outer wall with simple tumuli 0.10 mm in height (pore diameter 0.08 mm, wall thickness 0.02 mm). Inner wall with 1–2 rows of simple pores (diameter 0.08 mm, lintels 0.02 mm, wall thickness 0.02–0.04 mm).

Remarks. The porosity of the walls is characteristic of this genus and the branching cups are similar to the transverse section assigned to *K. gregarius* (Gravestock 1984, fig. 31g). This is the first recorded occurrence of the *Kaltatocyathus* from Antarctica.

https://doi.org/10.1017/S1755691022000111 Published online by Cambridge University Press

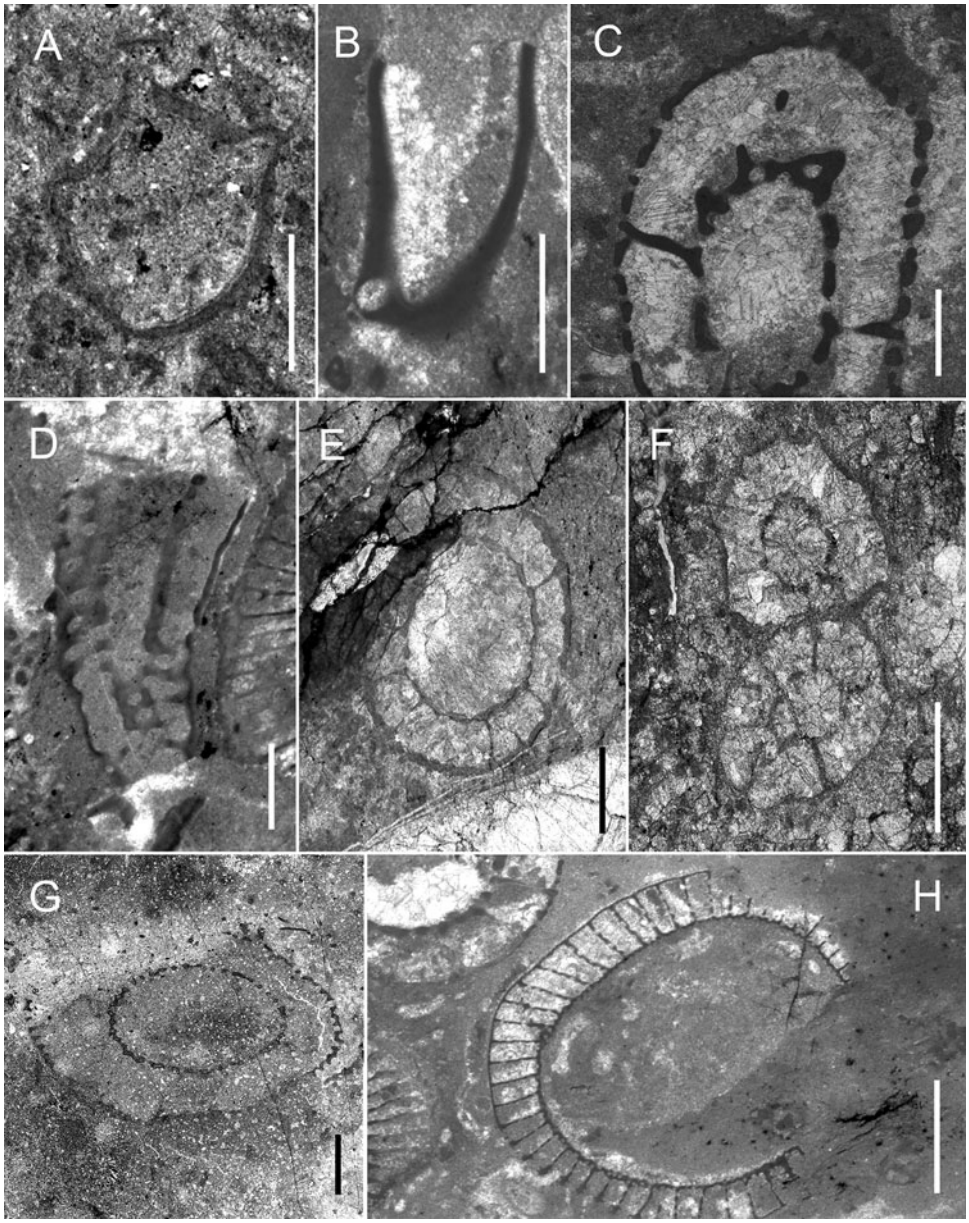

Figure 11 (A, B) *Tumuliolynthus irregularis* (Bedford & Bedford, 1934): (A) MGM-7209X-8, Stephenson Bastion; (B) MGM-7213X-5, Trueman Terraces. (C–E) *Dokidocyathus* sp.: (C) MGM-7208X-13, Stephenson Bastion; (D) MGM-7209X-17, Stephenson Bastion; (E) MGM-7235X-8, Oldhamia Terraces. (F) *Kaltatocyathus gregarius* (Gravestock, 1984): MGM-7218X-29/ 30, Trueman Terraces. (G) *Kymbecyathus avius* Debrenne & Kruse, 1986: MGM-7249X-2, Stephenson Bastion. Negative. (H) *Nochoroicyathus hystrix* Kruse, 1982: MGM-7209X-15, Stephenson Bastion. Scale bars = 1 mm (A–F); 2 mm (G, H).

Occurrence. Australia: Arrowie Basin, Mount Scott Range, Ajax Limestone, *Spirillicyathus tenuis* Zone (Gravestock 1984). Allochthonous clasts: Antarctica, Shackleton Range, Trueman Terraces, carbonate clasts from the Mount Wegener Formation. Cambrian *Series 2*, Botoman. *Kaltatocyathus gregarius* has been recorded in Australia and correlated with the Atdabanian stage, the type species from Mount Scott Range appears in the Lower Faunal Assemblage II (Gravestock 1984) or the equivalent *Spirillicyathus tenuis* Zone (Zhuravlev & Gravestock 1994). In Shackleton Range, *K. gregarius* occurs with *Nochoroicyathus lawrencei*, *Rotundocyathus glacius*, *Cadniacyathus* sp., *Buggischicyathus microporus*, *Shackletoncyathus buggischi*, *Paranacyathus sarmaticus* and *Archaeopharetra irregularis* in the same calcimicrobe–archaeocyath boundstone thin section. Therefore, *K. gregarius* extends its stratigraphic range to the Botoman.

Superfamily Kymbecyathoidea Debrenne, Rozanov & Zhuravlev in Debrenne, Zhuravlev & Rozanov, 1989

Family Kymbecyathidae Debrenne, Rozanov & Zhuravlev in Debrenne, Zhuravlev & Rozanov, 1989

Genus *Kymbecyathus* Debrenne & Kruse, 1986

Kymbecyathus avius Debrenne & Kruse, 1986 (Fig. 11g)

1986 *Kymbecyathus avius* Debrenne & Kruse, p. 241, fig. 6.
1989 *Kymbecyathus avius* Debrenne & Kruse – Debrenne, Zhuravlev & Rozanov, p. 116.
1990 *Kymbecyathus avius* Debrenne & Kruse – Debrenne, Rozanov & Zhuravlev, p. 149.
2002 *Kymbecyathus avius* Debrenne & Kruse – Debrenne, Zhuravlev & Kruse, p. 1558, figs 14M, N.
2012 *Kymbecyathus avius* Debrenne & Kruse – Debrenne, Zhuravlev & Kruse, p. 10, fig. 9.
2015 *Kymbecyathus avius* Debrenne & Kruse – Debrenne, Zhuravlev & Kruse, p. 932, figs 532a, b.

https://doi.org/10.1017/S1755691022000111 Published online by Cambridge University Press

Material. One specimen: MGM-7249X-2 (see Appendix 2 for locality).

Description. Cup 6.3–8 mm in diameter with intervallum 1.49 mm in width. Outer wall with pore canals (diameter 0.20 mm, lintels 0.12–0.32 mm, wall thickness 0.36 mm). Inner wall with simple, rounded to elliptical pores (diameter 0.20 mm, lintels 0.12 mm, wall thickness 0.12 mm). The presence of possible scattered bars in the intervallum is not confirmed.

Remarks. The diameter of the Byrd Glacier specimens is bigger than specimens described here, but the wall porosity is very similar between all specimens. The bars are rare, scattered and even not visible in some sections (Debrenne & Kruse 1986, fig. 6).

Occurrence. Antarctica: TAM, Byrd Glacier, Crackling Cwm, Shackleton Limestone (Debrenne & Kruse 1986). Allochthonous clasts: Shackleton Range, Stephenson Bastion, Cenozoic glacial erratic tills. Cambrian *Series 2*, Atdabanian?–Botoman?. In the TAM, the type species from Byrd Glacier was assigned to the Botoman stage (Debrenne & Kruse 1986), but now may possibly be of Atdabanian (Zhuravlev & Gravestock 1994; Kruse & Debrenne 2020). In the Shackleton Range, *K. avius* occurs with other unidentified specimens; therefore, the age of this sample cannot be clearly specified.

Suborder Ajacicyathina Bedford & Bedford, 1939
Superfamily Bronchocyathoidea Bedford & Bedford, 1936
Family Ajacicyathidae Bedford & Bedford, 1939
Genus *Nochoroicyathus* Zhuravleva, 1951

Nochoroicyathus hystrix Kruse, 1982
(Fig. 11h)

1982 *Nochoroicyathus hystrix* Kruse, p. 175–176, pl. 5, figs 1–4.

Material. One specimen: MGM-7209X-15 (see Appendix 2 for locality).

Description. Cup 5.6–6.8 mm in diameter. Intervallum 0.8 mm in width. Radial coefficient RK 7.3–8.9. Intervallar coefficient IK 0.14. Ratio of sides of interseptal loculi IC 1:2.8–1:3.3. Outer wall with 3–4 rows of diaphragm pores per intersept (diameter 0.06 mm, lintels 0.02 mm, wall thickness 0.02 mm). Inner wall with 2–3 rows of simple pores per intersept (diameter 0.08 mm, lintels 0.03–0.08 mm, wall thickness 0.02–0.03 mm) with a short spine projecting inward into central cavity of each pore. Septa with 4–5 rows of rounded pores (diameter 0.10 mm, lintels 0.04 mm, septa thickness 0.02 mm). Tabulae pectinate.

Remarks. The presence of pectinate tabulae and the inner wall with short spines allows us to assign our specimen to the species from Gnalta Shelf.

Occurrence. Australia: Gnalta Shelf, Mount Wright, Cymbric Vale Formation (Kruse 1982). Allochthonous clasts: Antarctica, Shackleton Range, Stephenson Bastion, Cenozoic glacial erratic tills. Cambrian *Series 2*, Botoman.

Nochoroicyathus lawrencei (Kruse, 1982)
(Fig. 12a, b)

1982 *Aldanocyathus lawrencei* Kruse, p. 160–161, text-figs 13g–m.
1989 *Nochoroicyathus lawrencei* (Kruse) – Debrenne, Zhuravlev & Rozanov, p. 120.
1990 *Nochoroicyathus lawrencei* (Kruse) – Debrenne, Rozanov & Zhuravlev, p. 152.

Material. Twelve specimens: MGM-7202X-3; MGM-7209X-2; MGM-7209X-4; MGM-7209X-13; MGM-7217X-19; MGM-7218X-28; MGM-7219X-6; MGM-7221X-1; MGM-7222X-5; MGM-7235X-7; MGM-7248X-2; MGM-7248X-5 (see Appendix 2 for localities).

Description. Cup 1–4.8 mm in diameter. Intervallum 0.3–0.8 mm in width. Radial coefficient RK 3.8–7. Intervallar coefficient IK 0.2–0.4. Ratio of sides of interseptal loculi IC 1:1–1:2.5. Outer wall with 2–5 (8) rows of simple pores per intersept (diameter 0.04–0.14 mm, lintels 0.02–0.10 mm, wall thickness 0.02–0.10 mm). Inner wall with 2–4 rows of simple pores per intersept (diameter 0.08–0.16 mm, lintels 0.02–0.12 mm, wall thickness 0.02–0.10 mm). Septa with 2–5 rows of rounded pores (diameter 0.06–0.16 mm, lintels 0.04–0.12 mm, septa thickness 0.02–0.04 mm).

Remarks. The Shackleton Range specimens are smaller than those described from the Gnalta Shelf and *N.* cf. *lawrencei* from Ajax Mine, but the porosity of the walls and septa are similar. The radial and intervallar coefficients vary proportionally during the growth of the cups. The porosity coefficient in both walls is greater in the smaller cups and decreases when the diameter of the cup increases, as observed in Shackleton Range specimens, until it stabilises since it presents little variability from diameters of 4 mm with coefficient values from 1 to 1.5, as observed in *N. lawrencei* and *N. andersoni* from Australia. This pattern does not hold for *N.* cf. *lawrencei*. The septal porosity coefficient tends to decrease with increasing cup diameter, with values >1, except for some *N. lawrencei* specimens (~0.6 outer wall Ø/l); this trend is not followed by *N.* cf. *lawrencei*.

Occurrence. Australia: Gnalta Shelf, Mount Wright, Cymbric Vale Formation (Kruse 1982). Allochthonous clasts: Antarctica, Shackleton Range, Trueman Terraces, Oldhamia Terraces, Swinnerton Ledge, carbonate clasts from the Mount Wegener Formation; Stephenson Bastion, Du Toit Nunataks, Cenozoic glacial erratic tills. Cambrian *Series 2*, Botoman.

Nochoroicyathus sp.
(Fig. 12g)

Material. Seven specimens: MGM-7202X-1; MGM-7214X-1; MGM-7214X-3 = MGM-7215X-3 (two different sections of the same specimen); MGM-7227X-9; MGM-7228X-10; MGM-7229X-13; MGM-7245X-2 (see Appendix 2 for localities).

Description. Cup 1.6–9.5 mm in diameter. Intervallum 0.48–1.49 mm in width. Radial coefficient RK 3.3–3.5. Intervallar coefficient IK 0.11–0.30. Ratio of sides of interseptal loculi IC 1:1.7–1:2.8. Outer wall with 2–5 rows of simple pores per intersept (diameter 0.10 mm, lintels 0.06 mm, wall thickness 0.04–0.08 mm). Inner wall with 1–3 rows of simple pores per intersept (diameter 0.12–0.20 mm, lintels 0.04–0.08 mm, wall thickness 0.04–0.08 mm). Septa with 2–6 rows of rounded pores (diameter 0.12 mm, lintels 0.04–0.08 mm, septa thickness 0.04 mm).

Remarks. The poor state of preservation of the cups, affected by recrystallisation and deformation processes, does not allow us to assign them to a described species.

Occurrence. Allochthonous clasts: Antarctica, Shackleton Range, Trueman Terraces, Oldhamia Terraces, carbonate clasts from the Mount Wegener Formation; Stephenson Bastion, Du Toit Nunataks, Cenozoic glacial erratic tills. Cambrian *Series 2*, Botoman.

Genus *Rotundocyathus* Vologdin, 1960
Rotundocyathus glacius Perejón, Menéndez & Moreno-Eiris sp. nov.
(Fig. 12c–f)

https://doi.org/10.1017/S1755691022000111 Published online by Cambridge University Press

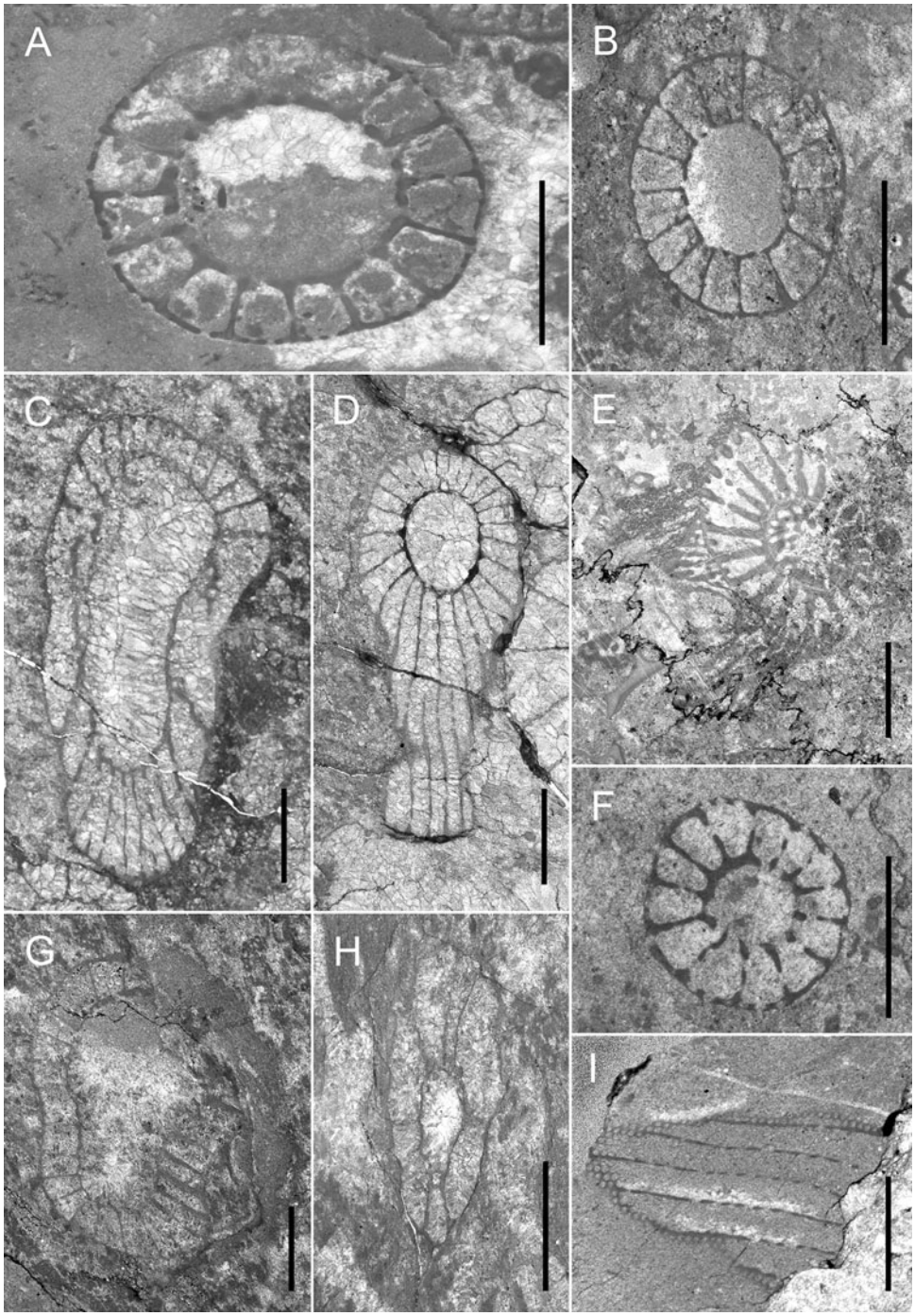

Figure 12 (A, B) *Nochoroicyathus lawrencei* Kruse, 1982: (A) MGM-7209X-13, Stephenson Bastion; (B) MGM-7202X-3, Du Toit Nunatak. (C–F) *Rotundocyathus glacius* sp. nov.: (C) holotype, MGM-7217X-6; (D) holotype, MGM-7216X-6, Trueman Terraces; (E) MGM-7204X-2, Stephenson Bastion; (F) MGM-7208X-8, Stephenson Bastion. (G) *Nochoroicyathus* sp.: MGM-7245X-2, Stephenson Bastion. (H, I) Ajacicyathidae gen. et sp. indet: (H) MGM-7239X-5, Oldhamia Terraces; (I) MGM-7238X-3, Oldhamia Terraces. Scale bars = 2 mm (A–E, G, H); 1 mm (F, I).

Etymology. From Latin 'glacies', meaning 'ice'.

Material. Twenty specimens: MGM-7216X-6 = MGM-7217X-6 (holotype, two different sections of the same specimen); MGM-7210X-6, MGM-7210X-9, MGM-7212X-5, MGM-7214X-2 = MGM-7215X-2, MGM-7218X-40, MGM-7218X-41, MGM-7219X-14 (paratypes); MGM-7204X-1; MGM-7204X-2; MGM-7206X-2; MGM-7208X-8, MGM-7208X-11; MGM-7208X-16; MGM-7208X-21; MGM-7223X-2, MGM-7223X-3, MGM-7223X-4, MGM-7246X-2; MGM-7247X-7 (see Appendix 2 for localities).

Diagnosis. Outer wall with two to six rows of diaphragm pores. Inner wall with one row of simple pores per intersept, without small spines. Septa completely porous, with two to five rows of pores.

Description. Cup 0.8–5.8 mm in diameter. Intervallum 0.3–1.2 mm in width. Radial coefficient RK 2.8–13.9. Intervallar coefficient IK 0.19–0.36. Ratio of sides of interseptal loculi IC 1:1.5–1:4.3. Outer wall with 2–6 rows of diaphragm pores per intersept (diameter 0.06–0.16 mm, lintels 0.02–0.10 mm, wall thickness 0.02–0.20 mm). Inner wall with one row of simple pores per intersept (diameter 0.08–0.24 mm, lintels 0.02–0.12 mm, wall thickness 0.02–0.14 mm). Septa with 2–5 (6) rows of rounded pores (diameter 0.06–0.20 mm, lintels 0.04–0.20 mm, septa thickness 0.02–0.20 mm).

https://doi.org/10.1017/S1755691022000111 Published online by Cambridge University Press

Remarks. Note the existence of endostructures in some specimens and somewhat thickened walls. Some cups have redimiculi (Fig. 12e) at internal and external sides of the outer wall. But they are not similar to *Rotundocyathus pelmani* Zhuravleva 1997 (Zhuravleva *et al*. 1997) for having diaphragm pores and greater number of pores in the outer wall, similar cup diameters and absence of pectinate tabulae. It is the first occurrence of this genus in Antarctica, the species *Rotundocyathus magnipora* was described in Ajax Mine by Kruse & Debrenne (2020), which differs from the size of the pores of both walls and septa.

Occurrence. Allochthonous clasts: Antarctica, Shackleton Range, Trueman Terraces, Swinnerton Ledge, carbonate clasts from the Mount Wegener Formation; Stephenson Bastion, Cenozoic glacial erratic tills. Cambrian *Series 2*, Botoman.

Ajacicyathidae gen. et sp. indet.
(Fig. 12h, i)

Material. Twenty-one specimens: MGM-7225X-1; MGM-7227X-4; MGM-7227X-7; MGM-7228X-6; MGM-7228X-9; MGM-7229X-1; MGM-7229X-2; MGM-7229X-3; MGM-7229X-6; MGM-7229X-7; MGM-7229X-8; MGM-7229X-10; MGM-7229X-11; MGM-7229X-12; MGM-7229X-17; MGM-7229X-18; MGM-7235X-19; MGM-7238X-2; MGM-7238X-3; MGM-7239X-5; MGM-7242X-10 (see Appendix 2 for localities).

Remarks. The poor preservation and the fragmentary state of these specimens do not allow us to assign them to a specific genus and species.

Occurrence. Allochthonous clasts: Antarctica, Shackleton Range, Oldhamia Terraces, carbonate clasts from the Mount Wegener Formation. Cambrian *Series 2*, Botoman.

Family Densocyathidae Vologdin, 1937
Genus *Cadniacyathus* Bedford & Bedford, 1937

Cadniacyathus sp.
(Fig. 13a, b)

Material. Fifteen specimens: MGM-7210X-5 = MGM-7211X-5; MGM-7216X-2 = MGM-7217X-2; MGM-7216X-7 = MGM-7217X-7; MGM-7216X-8 = MGM-7217X-8; MGM-7216X-14 = MGM-7217X-14; MGM-7218X-31; MGM-7218X-34; MGM-7218X-39; MGM-7219X-10; MGM-7225X-4; MGM-7225X-6; MGM-7227X-10; MGM-7233X-9; MGM-7237X-1 = MGM-7239X-1; MGM-7241X-5 (see Appendix 2 for localities).

Description. Cup 1.8–8.6 mm in diameter. Intervallum 0.5–2.5 mm in width. Radial coefficient RK 2.6–7.7. Intervallar coefficient IK 0.18–0.32. Ratio of sides of interseptal loculi IC 1:1–1:3.7. Outer wall with 2–4 rows of simple pores per intersept (diameter 0.06–0.20 mm, lintels 0.04–0.12 mm, wall thickness 0.02–0.08 mm). Inner wall with 1–3 rows of simple pores per intersept (diameter 0.12–0.48 mm, lintels 0.04–0.20 mm, wall thickness 0.02–0.30 mm); each pore with planar fused bract (length 0.08–0.18 mm). Septa with 2–6 rows of pores (diameter 0.10–0.32 mm, lintels 0.08–0.24 mm, septa thickness 0.02–0.24 mm).

Remarks. The poor state of preservation of many of these specimens and high degree of fragmentation, making many of them incomplete, do not allow us to assign them to some Australian or Antarctic species of *Cadniacyathus*. There are some differences with the Australian species *Cadniacyathus asperatus* such as the non-bulging outer wall and its smaller number of pores and the septal porosity.

Occurrence. Allochthonous clasts: Antarctica, Shackleton Range, Trueman Terraces, Oldhamia Terraces, carbonate clasts from the Mount Wegener Formation. Cambrian *Series 2*, Botoman.

Genus *Buggischicyathus* Perejón, Menéndez & Moreno-Eiris gen. nov.

Etymology. In memory of Werner Buggisch, a German geologist who sampled and studied this Antarctic material.

Type species. *Buggischicyathus microporus* Perejón, Menéndez & Moreno-Eiris sp. nov. Cambrian *Series 2*, Botoman. Shackleton Range, Trueman Terraces, carbonate clast from Mount Wegener Formation.

Diagnosis. Outer wall with several simple pores. Inner wall with one row of pores per intersept, bearing upwardly projecting cupped bracts. Septa with two to six rows of pores, stirrup pores are absent.

Remarks. *Buggischicyathus* Perejón, Menéndez & Moreno-Eiris differs from *Dailycyathus* Debrenne (1970) by the absence of stirrup pores and the porosity of the septa. From *Deceptioncyathus* Gravestock (1984) for the absence of synapticulae. From *Leptosocyathus* Vologdin (1937) for not having upwardly S scales in the inner wall and the different septal porosity.

Buggischicyathus microporus Perejón, Menéndez & Moreno-Eiris gen. et sp. nov.
(Fig. 13c–e)

Etymology. From Latin 'microporous', meaning 'small pores'.

Material. Seven specimens: MGM-7210X-3 = MGM-7211X-3 (holotype); MGM-7214X-4, MGM-7218X-32 (paratypes); MGM-7229X-14; MGM-7230X-1; MGM-7234X-7; MGM-7236X-1 (see Appendix 2 for localities).

Diagnosis. Cup 2.8–10 mm in diameter. Outer wall with two to four pore rows, inner wall with one pore row per intersept, bearing upwardly projecting cupped bracts. Septa completely porous with rounded to elliptical pores and two to six pore rows.

Description. Cup 2.8–10 mm in diameter. Intervallum 0.80–1.32 mm in width. Radial coefficient RK 6–7.4. Intervallar coefficient IK 0.19–0.36. Ratio of sides of interseptal loculi IC 1:3.7–1:5. Outer wall with 2–4 rows of simple pores per intersept (diameter 0.06–0.16 mm, lintels 0.02–0.08 mm, wall thickness 0.02–0.10 mm). Inner wall one row of simple pores per intersept (diameter 0.14–0.26 mm, lintels 0.04–0.12 mm, wall thickness 0.02–0.10 mm); each pore bearing upwardly cupped bract (length 0.08–0.24 mm). Septa with 2–6 rows of pores (diameter 0.10–0.16 mm, lintels 0.04–0.08 mm, septa thickness 0.02–0.06 mm).

Remarks. The septa of our specimens have numerous pores of small size, unlike the other genera of the Densocyathidae that have only one pore in the inner wall, besides other notable differences, such as *Dailycyathus* in the septal porosity and absence of stirrup pores; it differs from *Deceptioncyathus* by not presenting synapticulae and from *Leptosocyathus* by not having scales on the inner wall.

Occurrence. Allochthonous clasts: Antarctica, Shackleton Range, Trueman Terraces, Oldhamia Terraces, carbonate clasts from the Mount Wegener Formation. Cambrian *Series 2*, Botoman.

Densocyathidae gen. et. sp. indet.
(Fig. 14a, b)

Material. Ten specimens: MGM-7218X-36; MGM-7224X-5; MGM-7224X-6; MGM-7225X-7; MGM-7227X-8; MGM-7229X-21; MGM-7239X-6; MGM-7239X-7; MGM-7244X-10; MGM-7244X-11 (see Appendix 2 for localities).

Remarks. The poor state of preservation does not allow us to observe clearly the number of pore rows of the internal wall or the type of bracts.

Occurrence. Allochthonous clasts: Antarctica, Shackleton Range, Trueman Terraces, Oldhamia Terraces, Swinnerton Ledge, carbonate clasts from the Mount Wegener Formation; Stephenson Bastion, Cenozoic glacial erratic tills. Cambrian *Series 2*, Botoman.

https://doi.org/10.1017/S1755691022000111 Published online by Cambridge University Press

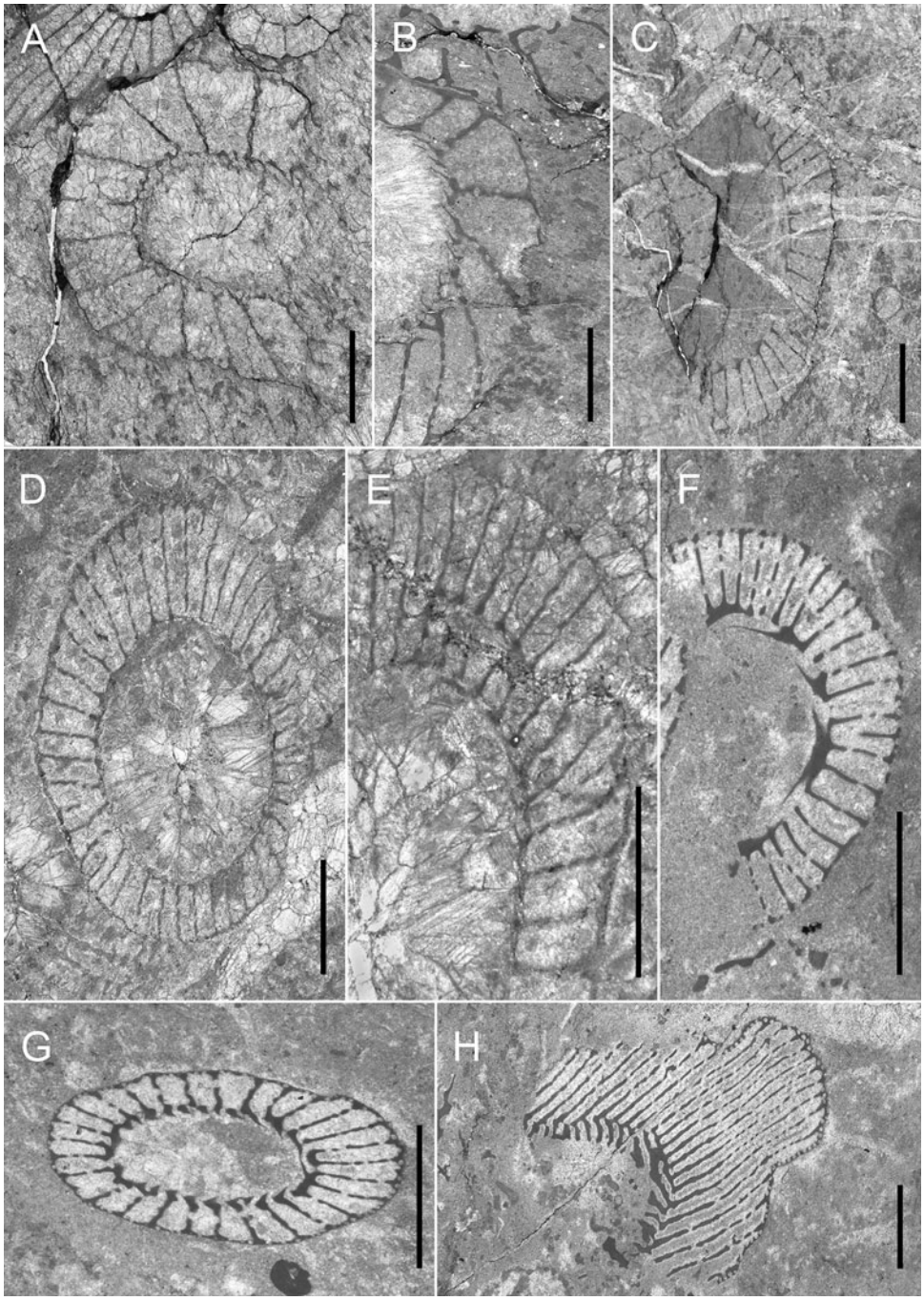

Figure 13 (A, B) *Cadniacyathus* sp.: (A) MGM-7216X-7; Trueman Terraces; (B) MGM-7241X-5, Oldhamia Terraces. (C–E) *Buggischicyathus microporus* gen. et sp. nov.: (C) MGM-7234X-7, Oldhamia Terraces; (D) holotype, MGM-7210X-3; (E) holotype, MGM-7211X-3, Trueman Terraces. (F–H) *Thalamocyathus trachealis* (Taylor, 1910): (F) MGM-7208X-18; (G) MGM-7208X-14; (H) MGM-7208X-9, Stephenson Bastion. Scale bars = 2 mm.

Family Bronchocyathidae Bedford & Bedford, 1936
Genus *Thalamocyathus* Gordon, 1920

Thalamocyathus trachealis (Taylor, 1910)
(Fig. 13f–h)

1910 *Archaeocyathus trachealis* Taylor, p. 125, text-fig. 22, pl. 1, figs 11n–p, pl. 2, fig. 6 left, pl. 3, figs 11a, pl. 5, figs 27–29i, 28–30 g, pl. 6, fig. 31 pars, pl. 8, figs 45–47 (7–8).
2002 *Thalamocyathus trachealis* (Taylor) – Debrenne, Zhuravlev & Kruse, p. 1567, figs 19a–d.
2012 *Thalamocyathus trachealis* (Taylor) – Stone, Thomson & Rushton, p. 211, fig. 6c.
2020 *Thalamocyathus trachealis* (Taylor) – Kruse & Debrenne, p. 42, figs 31a–c, 37, *cum syn*.

Material. Nine specimens: MGM-7208X-9; MGM-7208X-14; MGM-7208X-17; MGM-7208X-18; MGM-7208X-23; MGM-7209X-5; MGM-7209X-10; MGM-7209X-16; MGM-7209X-19 (see Appendix 2 for localities).

Description. Cup 1.6–7 mm in diameter. Intervallum 0.48–0.96 mm in width. Radial coefficient RK 5.6–12.7. Intervallar coefficient IK 0.18–0.33. Ratio of sides of interseptal loculi IC 1:3–1:6. Outer wall with 1–3 rows of simple and rounded pores per intersept (diameter 0.08–0.10 mm, lintels 0.02–0.08 mm, wall thickness 0.04–0.06 mm), pores with planar diaphragms. Inner wall annulated with one row of pores per intersept (diameter 0.10–0.20 mm, lintels 0.04–0.14 mm, wall thickness 0.04–0.08 and including annuli 0.36 mm); annuli V-shaped. Septa with 2–4 rows of pores (diameter 0.08–0.12 mm, lintels 0.04–

https://doi.org/10.1017/S1755691022000111 Published online by Cambridge University Press

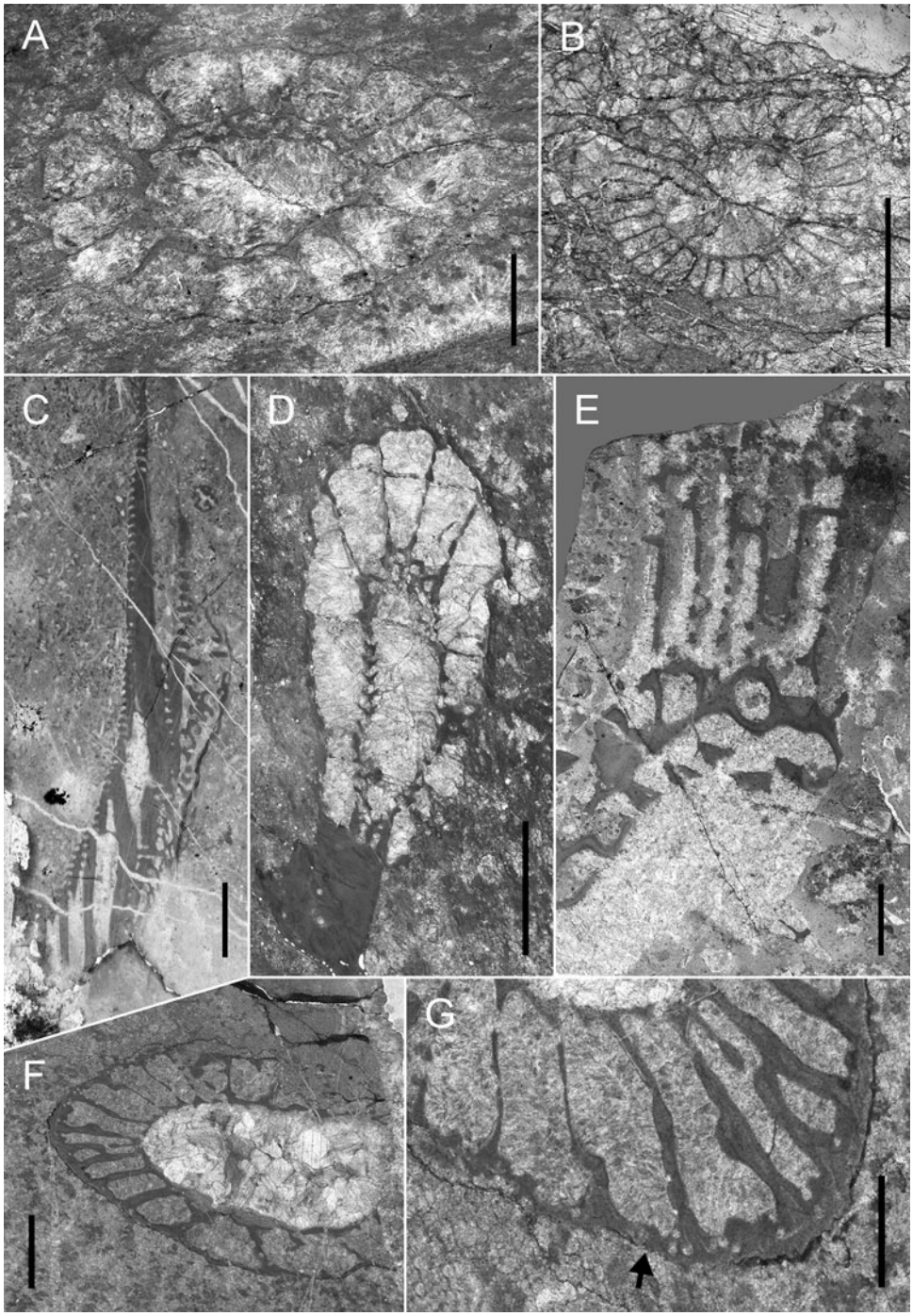

Figure 14 (A, B) Densocyathidae gen. et. sp. indet.: (A) MGM-7239X-6; (B) MGM-7227X-8, Oldhamia Terraces. (C) ?*Ussuricyathellus* sp.: MGM-7207X-1, Stephenson Bastion. (D) ?*Baikalocyathus* sp.: MGM-7233X-10, Oldhamia Terraces. (E) *Paragnaltacyathus hoeflei* gen. et sp. nov.: holotype, MGM-7205X-3, Stephenson Bastion. (F, G) *Ladaecyathus* sp.: (F) MGM-7234X-1; (G) detail, arrow points to the attached microporous sheath, Oldhamia Terraces. Scale bars: 1 mm (A, G); 2 mm (B–F).

0.10 mm, septa thickness 0.04–0.08 mm), the pores are distributed predominantly in the outer half of the septum.

Remarks. The wall and septal porosity are characteristic of *T. trachealis*, a common species in the Australia–Antarctica province. It differs from *Gordonicyathus* because the latter presents a greater number of pores in the septa, in cups of similar diameter.

Occurrence. Australia: Arrowie Basin, Ajax Mine (Taylor 1910; Bedford & Bedford 1939; Debrenne 1973; Kruse & Debrenne 2020), Mount Scott Range (Gravestock 1984); Stansbury Basin, Ardrossan (Taylor 1910; Zhuravlev & Gravestock 1994), Curramulka-Stansbury (Zhuravlev & Gravestock 1994), Cape d'Estaing (Kruse & Moreno-Eiris 2013). Antarctica: TAM, Holyoake Range, Nimrod Glacier, Shackleton Limestone (Debrenne & Kruse 1986, 1989); Argentina Range, Schneider Hills limestone (Konyushkov & Shulyatin 1980). Allochthonous clasts: Africa, main Karoo Basin, Zwartskraal, Dwyka tillites (Debrenne 1975). South America, Falkland Islands, Fitzroy Tillite Formation (Stone *et al*. 2012). Antarctica, King George Island, erratic glaciomarine deposits (Morycowa *et al*. 1982, Wrona & Zhuravlev 1996); Weddell Sea area (Gordon 1920); Whichaway Nunataks (Hill 1965); Shackleton Range, Stephenson Bastion, Cenozoic glacial erratic tills. Cambrian *Series 2*, Botoman.

https://doi.org/10.1017/S1755691022000111 Published online by Cambridge University Press

Family Ethmocyathidae Debrenne, 1969
Genus *Baikalocyathus* Yazmir in Zhuravleva, 1974

?*Baikalocyathus* sp.
(Fig. 14d)

Material. Two specimens: MGM-7233X-10; MGM-7242X-5 (see Appendix 2 for localities).

Description. Cup 2.6–2.7 mm in diameter. Intervallum 0.9 mm in width. Intervallar coefficient IK 0.32–0.33. Ratio of sides of interseptal loculi IC 1:3.1. Outer wall with several rows of pores per intersept (diameter 0.08–0.14 mm, lintels 0.04 mm, wall thickness 0.06–0.08 mm). Inner wall with one row of downwardly projecting, straight canals per intersept, bearing supplementary bracts on central cavity side forming V-shaped canals (diameter 0.14–0.16 mm, lintels 0.04–0.06 mm, wall thickness 0.04 and canal length 0.10 mm). Septa with two rows of pores (diameter 0.14 mm, lintels 0.08 mm, septa thickness 0.04 mm).

Remarks. The fragmentary nature of the specimens does not allow us to assign a specific species. Several species of *Baikalocyathus* have been described in Australia. It is the first find of *Baikalocyathus* in Antarctica.

Occurrence. Allochthonous clasts: Antarctica, Shackleton Range, Oldhamia Terraces, carbonate clasts from the Mount Wegener Formation. Cambrian *Series 2*, Botoman. Since in Australia it has been recorded during the Atdabanian age, all the species described from Mount Scott Range appear in the Lower Faunal Assemblage II (Gravestock 1984) or the equivalent *Spirillicyathus tenuis* Zone (Zhuravlev & Gravestock 1994). Our specimens are found in calcimicrobial boundstone with archaeocyaths together with *Cadniacyathus* sp., *Santelmocyathus santelmoi* and *Wegenercyathus sexangulae*. Therefore, *Baikalocyathus* extends its stratigraphic range to the Botoman.

Genus *Paragnaltacyathus* Perejón, Menéndez & Moreno-Eiris gen. nov.

Etymology. From Greek 'παρά', meaning similary to *Gnaltacyathus* Kruse, 1982.

Type species. *Paragnaltacyathus hoeflei* Perejón, Menéndez & Moreno-Eiris sp. nov. Cambrian *Series 2*, Botoman. Shackleton Range, Stephenson Bastion, Cenozoic glacial erratic tills.

Diagnosis. Outer wall with simple pores. Inner wall with straight canals, each canal span several intersepts. Septa completely porous, linked by synapticulae.

Remarks. This genus differs from *Gnaltacyathus* Kruse (1982) by presenting synapticulae.

Paragnaltacyathus hoeflei Perejón, Menéndez & Moreno-Eiris gen. et sp. nov.
(Fig. 14e)

Etymology. In memory of Hans-Christian Höfle, German glaciologist who sampled and studied the Cenozoic erratics of all this Antarctic material.

Material. One specimen: MGM-7205X-3 (see Appendix 2 for locality).

Diagnosis. Outer wall with two rows of simple pores. Inner wall with straight canals, each canal span several intersepts. Septa completely porous with five or more rows of pores. Synapticulae.

Description. A fragmented cup. Outer wall with two rows of pores per intersept (diameter 0.20 mm, lintels 0.28 mm, wall thickness 0.32 mm). Inner wall with straight canals, each canal spanning several (2–3) intersepts (diameter 1.10 mm, lintels 0.25 mm, wall thickness 1.50 mm). Septa with five or more rows of pores (diameter 0.50 mm, lintels 0.25 mm, septa thickness 0.17 mm). Sinapticulae thickness 0.17 mm.

Remarks. Although the cup is fragmented, it is possible to recognise the internal wall so characteristic of *Gnaltacyathus*, but the presence of synapticulae suggests that it is a different genus.

Occurrence. Allochthonous clasts: Antarctica, Shackleton Range, Stephenson Bastion, Cenozoic glacial erratic tills. Cambrian *Series 2*, Botoman.

Genus *Ussuricyathellus* Voronin, 1988

?*Ussuricyathellus* sp.
(Fig. 14c)

Material. One specimen: MGM-7207X-1 (see Appendix 2 for locality).

Description. Cup 7.5 mm in diameter. Intervallum 1.7 mm in width. Intervallar coefficient IK 0.22. Ratio of sides of interseptal loculi IC 1:2.9. Outer wall with several rows of pores per intersept (diameter 0.16 mm, lintels 0.16 mm, wall thickness 0.16 mm). Inner wall with two rows of horizontal to upwardly projecting, straight canals per intersept (diameter 0.20 mm, lintels 0.12–0.32 mm, wall thickness 0.32). Septa with one row of pores or aporose.

Remarks. The porosity of the inner wall and the aporose to sparsely porous septa allow us to assign it to the genus *Ussuricyathellus* Voronin (1988). This assumes that it is the first record of this genus in Antarctica. Australian species *Ussuricyathellus bellidoi* (Kruse & Moreno-Eiris 2013) and *Ussuricyathellus coronus* (Kruse & Debrenne 2020) are correlated with the Botoman.

Occurrence. Allochthonous clasts: Antarctica, Shackleton Range, Stephenson Bastion, Cenozoic glacial erratic tills. Cambrian *Series 2*, Botoman.

Superfamily Erbocyathoidea Vologdin & Zhuravleva in Vologdin, 1956
Family Erbocyathidae Vologdin & Zhuravleva in Vologdin, 1956
Genus *Ladaecyathus* Zhuravleva, 1960a

Ladaecyathus sp.
(Fig. 14f, g)

Material. Four specimens: MGM-7208X-4; MGM-7234X-1; MGM-7241X-6; MGM-7245X-3 (see Appendix 2 for localities).

Description. Cup 5.2–10 mm in diameter. Intervallum 1.2–2.7 mm in width. Intervallar coefficient IK 0.22–0.23. Ratio of sides of interseptal loculi IC 1:2.6–1:5. Outer wall with 2–3 rows of pores per intersept (diameter 0.20–0.58 mm, lintels 0.08–0.58 mm, wall thickness 0.08–0.58 mm); the attached microporous sheath has several micropores (diameter 0.12 mm, lintels 0.04 mm). Inner wall with two rows of simple pores per intersept (diameter 0.18–0.28 mm, lintels 0.08–0.12 mm, wall thickness 0.06–0.16 mm). Septa with 4–6 rows of pores (diameter 0.16–0.36 mm, lintels 0.04–0.20 mm, septa thickness 0.04–0.08 mm).

Remarks. *Ladaecyathus jagoi* Debrenne & Kruse (1986) has been described in Nimrod Glacier, but the bad preservation of our material does not allow us to assign it to a specific species.

Occurrence. Allochthonous clasts: Antarctica, Shackleton Range, Oldhamia Terraces, carbonate clasts from the Mount Wegener Formation; Stephenson Bastion, Cenozoic glacial erratic tills. Cambrian *Series 2*, Botoman.

Superfamily Lenocyathoidea Zhuravleva in Vologdin, 1956

Family Shackletoncyathidae Perejón, Menéndez & Moreno-Eiris fam. nov.

Etymology. From Shackleton Range.

Diagnosis. Inner wall with bracts or scales.

Generic composition. Two new genera are included: *Shackletoncyathus* and *Santelmocyathus*.

https://doi.org/10.1017/S1755691022000111 Published online by Cambridge University Press

Genus *Shackletoncyathus* Perejón, Menéndez & Moreno-Eiris gen. nov.

Etymology. From Shackleton Range.

Type species. *Shackletoncyathus buggischi* Perejón, Menéndez & Moreno-Eiris sp. nov. Cambrian *Series 2*, Botoman. Shackleton Range, Trueman Terraces, carbonate clast from the Mount Wegener Formation.

Diagnosis. Outer wall with multiperforated tumuli. Inner wall with several rows of pores per intersept, bearing supplementary bracts on central cavity side. Septa completely porous.

Remarks. This genus is characterised by inner wall with several rows of pores per intersept, bearing supplementary tubular bracts on central cavity side. Septa completely porous.

Shackletoncyathus buggischi Perejón, Menéndez & Moreno-Eiris gen. et sp. nov.
(Figs 15d, 16)

Etymology. In memory of Werner Buggisch, German geologist who sampled and studied this Antarctic material.

Material. Five specimens: MGM-7248X-3 (Holotype); MGM-7243X-7, MGM-7246X-1 (Paratypes); MGM-7202X-4; MGM-7218X-38 (see Appendix 2 for localities).

Diagnosis. Cup 0.8–3.2 mm in diameter. Outer wall with two to three rows of multiperforated tumuli per intersept. Inner wall with two to three rows of pores per intersept, bearing supplementary tubular bracts on central cavity side. Septa completely porous.

Description. Cup 0.8–3.2 mm in diameter. Intervallum 0.48–0.72 mm in width. Radial coefficient RK 3.1–7.6. Intervallar coefficient IK 0.26. Ratio of sides of interseptal loculi IC 1:1.1–1:2.4. Outer wall with 2–3 rows of multiperforated tumuli per intersept (diameter 0.08–0.12 mm, lintels 0.06 mm, wall thickness 0.02–0.04 mm, tumuli high 0.20 mm). Inner wall with 2–3 rows of pores per intersept (diameter 0.06–0.20 mm, lintels 0.08–0.40 mm, wall thickness 0.02–0.10 mm); each pore bearing supplementary tubular bracts on central cavity side (length up 0.14 mm). Septa with 2–3 (5) rows of pores (diameter 0.10 mm, lintels 0.04–0.06 mm, septa thickness 0.02–0.04 mm).

Remarks. The porosity of the inner wall and the septa are the distinctive character to distinguish our material from the other genera belonging to the other families of the Lenocyathoidea.

Occurrence. Allochthonous clasts: Antarctica, Shackleton Range, Trueman Terraces, carbonate clasts from the Mount Wegener Formation; Stephenson Bastion, Du Toit Nunataks, Cenozoic glacial erratic tills. Cambrian *Series 2*, Botoman.

Genus *Santelmocyathus* Perejón, Menéndez & Moreno-Eiris gen. nov.

Etymology. From the San Telmo Spanish ship, possibly the first to reach the coast of the Antarctic continent in 1819.

Type species. *Santelmocyathus santelmoi* Perejón, Menéndez & Moreno-Eiris sp. nov. Cambrian *Series 2*, Botoman. Shackleton Range, Trueman Terraces, Oldhamia Terraces, carbonate clasts from the Mount Wegener Formation; Stephenson Bastion, Cenozoic glacial erratic tills. Cambrian *Series 2*, Botoman.

Diagnosis. Outer wall with multiperforated tumuli. Inner wall with several rows of pores per intersept, bearing possibly upwardly projecting, S-shaped scales. Septa aporose to sparsely porous.

Remarks. This genus is characterised by inner wall with one to two rows of pores per intersept, bearing S-shaped scales. Septa aporose to sparsely porous.

Santelmocyathus santelmoi Perejón, Menéndez & Moreno-Eiris gen. et sp. nov.
(Fig. 15a, b)

Etymology. From the San Telmo Spanish ship, possibly the first to reach the coast of the Antarctic continent in 1819.

Material. Five specimens: MGM-7246X-4 (holotype); MGM-7246X-3 (paratype); MGM-7219X-8; MGM-7231X-2 = MGM-7232X-2; MGM-7242X-2 (see Appendix 2 for localities).

Diagnosis. Cup 2.8–8.3 mm in diameter. Outer wall with one to three rows of multiperforate tumuli. Inner wall with one to two rows of pores per intersept, bearing possibly upwardly projecting, S-shaped scales. Septa aporose to sparsely porous with one to three rows of pores. Radial coefficient RK 2.9–3.8.

Description. Cup 2.8–8.3 mm in diameter. Intervallum 0.5–1.7 mm in width. Radial coefficient RK 2.9–3.8. Intervallar coefficient IK 0.2–0.3. Ratio of sides of interseptal loculi IC 1:1.6–1:3.2. Outer wall with 1–3 rows of multiperforate tumuli per intersept (diameter 0.04–0.28 mm, lintels 0.04–0.20 mm, wall thickness 0.02–0.20 mm, tumuli high 0.14 mm). Inner wall with 1–2 rows of pores per intersept (diameter 0.16–0.24 mm, lintels 0.04–0.16 mm, wall thickness 0.04–0.30 mm); each pore bearing possibly upwardly projecting, S-shaped scales (length 0.12 mm). Septa with 1–3 rows of pores (diameter 0.08–0.12 mm, lintels 0.04–0.16 mm, septa thickness 0.04–0.24 mm).

Remarks. *Santelmocyathus santelmoi* differs from *Shackletoncyathus buggischi* in the inner wall, by having scales and not bracts, and the septal porosity, as it occurs in another new genus of family Shackletoncyathidae.

Occurrence. Allochthonous clasts: Antarctica, Shackleton Range, Trueman Terraces, Oldhamia Terraces, carbonate clasts from the Mount Wegener Formation; Stephenson Bastion, Cenozoic glacial erratic tills. Cambrian *Series 2*, Botoman.

Superfamily Ethmophylloidea Okulitch, 1937
Family Fallocyathidae Rozanov in Zhuravleva, Korshunov & Rozanov, 1969
Genus *Fallocyathus* Rozanov in Zhuravleva, Korshunov & Rozanov, 1969

?*Fallocyathus* sp.
(Fig. 15e)

Material. Two specimens: MGM-7234X-8 and MGM-7234X-9 (see Appendix 2 for localities).

Description. Cup 1–5.8 mm in diameter. Intervallum 0.5–1 mm in width. Radial coefficient RK 3.5. Intervallar coefficient IK 0.2–0.3. Ratio of sides of interseptal loculi IC 1:1.3–1:1.5. Outer wall with 3–4 rows of canals per intersept (diameter 0.10 mm, lintels 0.06–0.12 mm, wall thickness 0.10–0.20 mm). Inner wall with 2–3 rows of simple pores per intersept (diameter 0.14–0.16 mm, lintels 0.04–0.80 mm, wall thickness 0.04–0.06 mm). Septa with 1–3 rows of pores (diameter 0.10–0.16 mm, lintels 0.04–0.08 mm, septa thickness 0.04 mm).

Remarks. The canals of the outer wall and the simple pores of the inner wall are characteristic of *Fallocyathus*. The type of preservation of cup sections does not allow us to assign them to a specific species.

Occurrence. Allochthonous clasts: Antarctica, Shackleton Range, Oldhamia Terraces, carbonate clasts from the Mount Wegener Formation. Cambrian *Series 2*, Botoman.

Suborder Erismacoscinina Debrenne, Rozanov & Zhuravlev in Debrenne, Zhuravlev & Rozanov, 1989
Superfamily Salairocyathoidea Zhuravleva in Vologdin, 1956
Family Asterocyathidae Vologdin, 1956
Genus *Antoniocoscinus* Zhuravlev in Debrenne *et al.*, 1988

?*Antoniocoscinus* sp.
(Fig. 17b)

https://doi.org/10.1017/S1755691022000111 Published online by Cambridge University Press

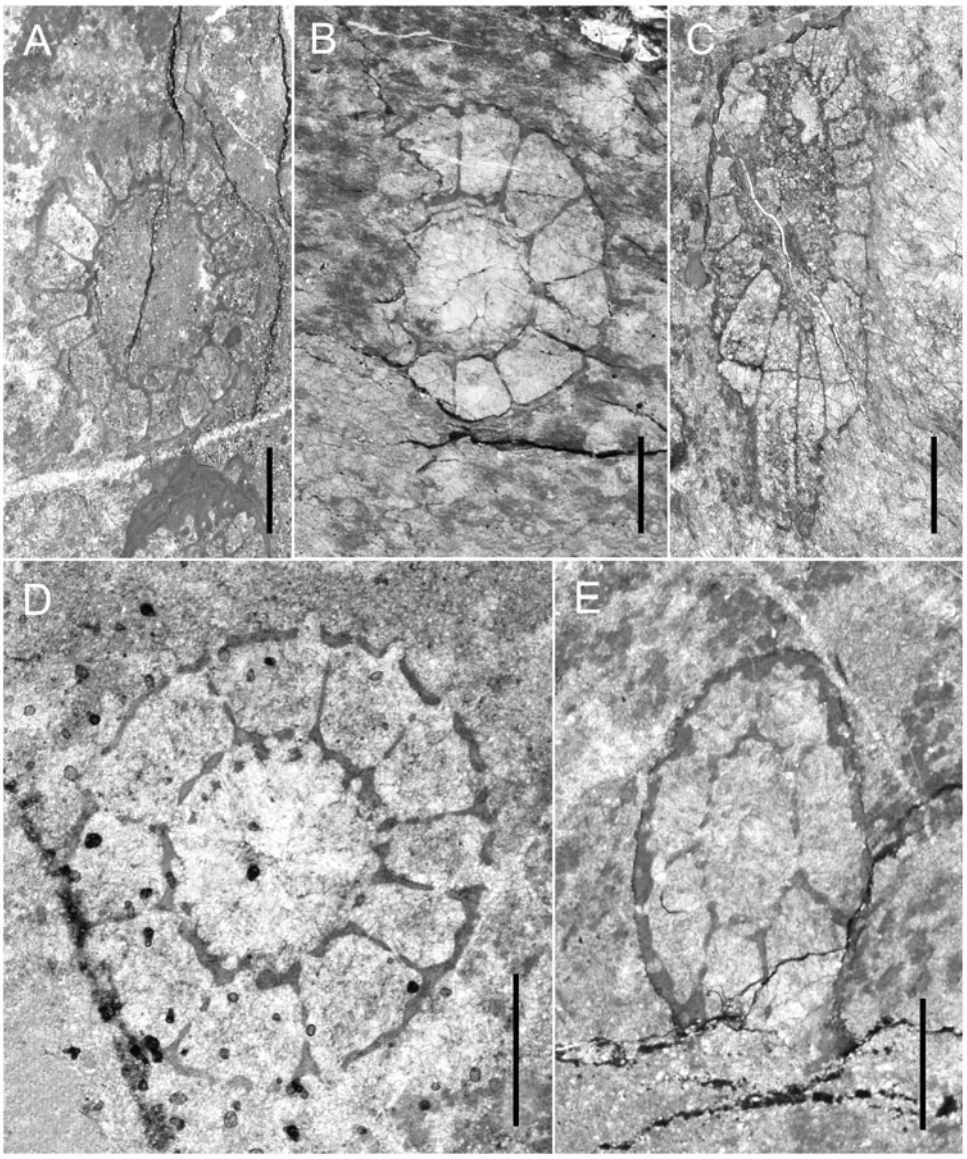

Figure 15 (A, B) *Santelmocyathus santelmoi* gen. et sp. nov.: (A) holotype, MGM-7246X-4, Stephenson Bastion; (B) MGM-7231X-2, Oldhamia Terraces. (C) *Coscinoptycta convoluta* (Taylor, 1910): MGM-7216X-5, Trueman Terraces. (D) *Shackletoncyathus buggischi* gen. et sp. nov.: holotype, MGM-7248X-3, Stephenson Bastion. (E) ?*Fallocyathus* sp.: MGM-7234X-9, Oldhamia Terraces. Scale bars = 2 mm (A–C); 1 mm (D, E).

Material. Two specimens: MGM-7227X-3; MGM-7231X-3 = MGM-7232X-3 (see Appendix 2 for localities).

Description. Cup 1.4–8.3 mm in diameter. Intervallum 0.52–0.80 mm in width. Radial coefficient RK 2.9–12.5. Intervallar coefficient IK 0.30–0.36. Ratio of sides of interseptal loculi IC 1:2.8–1:4.3. Outer wall with 2–3 rows of simple pores per intersept (diameter 0.06 mm, lintels 0.02–0.04 mm, wall thickness 0.02–0.08 mm). Inner wall with one row of simple pores per intersept (diameter 0.28 mm, lintels 0.16 mm, wall thickness 0.04 mm). Septa with three? rows of pores (diameter 0.04 mm, lintels 0.02 mm, septa thickness 0.02–0.04 mm). Tabulae 0.04 in thickness, with 3–4 rows of pores per loculus (diameter 0.10 mm, lintels 0.06 mm).

Remarks. The specimens are intensely affected by recrystallisation and tectonic deformation processes, which does not allow assigning them to a specific species. *Antoniocoscinus retifer* is present in Ajax Mine.

Occurrence. Allochthonous clasts: Antarctica, Shackleton Range, Oldhamia Terraces, carbonate clasts from the Mount Wegener Formation. Cambrian *Series 2*, Botoman.

Genus *Erismacoscinus* Debrenne, 1958

Erismacoscinus bilateralis (Taylor, 1910) (Fig. 17a)

1910 *Coscinoptycha bilateralis* Taylor, p. 142, text-fig. 6, pl. 2, fig. 6, pl. 6, fig. 32, pl. 11, figs 61–63.
2020 *Erismacoscinus bilateralis* (Taylor) – Kruse & Debrenne, p. 76, figs 65, 66, *cum syn*.

Material. Two specimens: MGM-7232X-5 and MGM-7232X-6 (see Appendix 2 for localities).

Description. Conical cup 3–5.5 mm in diameter. Intervallum 0.9–1.1 mm in width. Intervallar coefficient IK 0.20–0.29. Ratio of sides of interseptal loculi IC 1:1.4–1:3.6. Outer wall with several rows of simple pores per intersept (diameter 0.16 mm, lintels 0.16 mm, wall thickness 0.04–0.12 mm). Inner wall with 1–2 rows of simple pores per intersept (diameter 0.16–0.28 mm, lintels 0.04–0. 12 mm, wall thickness 0.04–0.28 mm). Septa with 2–3 rows of pores (diameter 0.16–0.20 mm, lintels 0.08–0.12 mm, septa thickness 0.04–0.12

https://doi.org/10.1017/S1755691022000111 Published online by Cambridge University Press

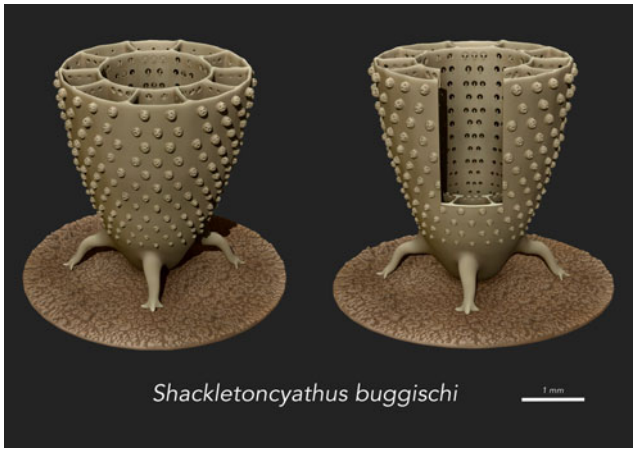

Figure 16 3D reconstruction of *Shackletoncyathus buggischi* (designed by F. Cebrián).

mm). Tabulae spacing 1–1.6 mm, with 3–6 radial rows of pores (diameter 0.06–0.12 mm, lintels 0.02–0.08 mm, thickness 0.02–0.04 mm).

Remarks. Measurements and coefficients of Shackleton specimens fall within the range of the species *Erismacoscinus bilateralis* described by Kruse & Debrenne (2020), which includes some specimens of Gordon's 1920 *E. endutus* and *E. fultus* from Weddell Sea.

Occurrence. Australia: Amadeus and Georgina Basins (Kruse & West 1980); Arrowie Basin, Ajax Mine, Ajax Limestone (Taylor 1910; Kruse & Debrenne 2020); Stansbury Basin, Cape d'Estaing, White Point Conglomerate (Kruse & Moreno-Eiris 2013). Allochthonous clasts: Antarctica, Weddell Sea area (Gordon 1920); Whichaway Nunataks (Hill 1965); Shackleton Range, Oldhamia Terraces, carbonate clasts from the Mount Wegener Formation. Cambrian *Series 2*, Botoman.

Genus *Retecoscinus* Zhuravleva 1960b

?*Retecoscinus* sp.
(Fig. 17c)

Material. One specimen: MGM-7227X-12 (see Appendix 2 for locality).

Description. Cup 3.2–5.6 mm in diameter. Intervallum 0.60 mm in width. Radial coefficient RK 13.8. Intervallar coefficient IK 0.19. Ratio of sides of interseptal loculi IC 1:3.7. Outer wall with 3–4 rows of simple pores per intersept (diameter 0.06 mm, lintels 0.02 mm, wall thickness 0.02 mm). Inner wall with 1–2 rows of simple pores per intersept (diameter 0.14 mm, lintels 0.06 mm, wall thickness 0.04 mm). Septa with 4–6 rows of pores (diameter 0.06 mm, lintels 0.04–0.08 mm, septa thickness 0.02 mm). Tabulae with two slit-like pores per intersept.

Remarks. The porosity of both walls is similar to *Retecoscinus* apart from the presence of tabulae with slit-like pores, but the designation is doubtful due to the poor preservation of this specimen.

Occurrence. Allochthonous clasts: Antarctica, Shackleton Range, Oldhamia Terraces, carbonate clasts from the Mount Wegener Formation. Cambrian *Series 2*, Botoman.

Family Rudanulidae Debrenne, Rozanov & Zhuravlev in Debrenne, Zhuravlev & Rozanov, 1989

Genus *Wegenercyathus* Perejón, Menéndez & Moreno-Eiris gen. nov.

Etymology. After Mount Wegener Formation from Shackleton Range.

Type species. *Wegenercyathus sexangulae* Perejón, Menéndez & Moreno-Eiris sp. nov. Cambrian *Series 2*, Botoman. Shackleton Range, Oldhamia Terraces, carbonate clasts from Mount Wegener Formation.

Diagnosis. Outer wall with normal pores. Inner wall with several rows of pores per intersept, bearing S-shaped bracts; septa completely porous; retiform tabulae with subpolygonal pores.

Remarks. *Wegenercyathus* shares the same septal porosity as *Rudanulus*, the difference is that *Rudanulus* has a longitudinally plicate outer wall and inner wall with scales. The new genus differs from *Pilodicoscinus* in that the latter has plicate outer wall, cupped inner wall bracts and aporose to sparsely porous septa. *Wegenercyathus* shares the same septal porosity as *Yhecyathus*, the difference is that the latter has plicate outer wall, and cupped inner wall bracts.

Wegenercyathus sexangulae Perejón, Menéndez & Moreno-Eiris gen. et sp. nov.
(Fig. 17d, e)

Etymology. From Latin 'sexangulae', meaning 'hexagonal pores'.

Material. Two specimens: MGM-7233X-11 (holotype); MGM-7242X-6 (paratype) (see Appendix 2 for localities).

Diagnosis. Outer wall with two or three rows of simple pores per intersept. Inner wall with several rows of pores per intersept, bearing S-shaped bracts; septa completely porous; retiform tabulae with hexagonal pores.

Description. Cup 5.2–7.5 mm in diameter. Intervallum 1.2–1.4 mm in width. Radial coefficient RK 2.3–3.1. Intervallar coefficient IK 0.23–0.26. Ratio of sides of interseptal loculi IC 1:1.5–1:2.8. Outer wall with 2–3 rows of normal pores per intersept (diameter 0.20 mm, lintels 0.20 mm, wall thickness 0.02–0.08 mm). Inner wall with 1–2 rows of pores per intersept (diameter 0.20 mm, lintels 0.08–0.20 mm, wall thickness 0.04–0.08 mm); each pore bearing S-shaped bract (length 0.10–0.20 mm). Septa with 4–6 rows of pores (diameter 0.06–0.08 mm, lintels 0.10 mm, septa thickness 0.04–0.08 mm). Tabulae with 5–6 large hexagonal pores per intersept (diameter 0.14–0.16 mm, lintels 0.04 mm, thickness 0.02–0.04 mm).

Remarks. In addition to the differences already indicated with the other genera of Rudanulidae, the presence of retiform tabulae with large subpolygonal pores distinguishes it, since these hexagonal pores are unusual.

Occurrence. Allochthonous clasts: Antarctica, Shackleton Range, Oldhamia Terraces, carbonate clasts from the Mount Wegener Formation. Cambrian *Series 2*, Botoman.

Superfamily Coscinoptyctoidea Debrenne, Rozanov & Zhuravlev in Debrenne, Zhuravlev & Rozanov, 1989
Family Coscinoptyctidae Debrenne, Rozanov & Zhuravlev in Debrenne, Zhuravlev & Rozanov, 1989
Genus *Coscinoptycta* Broili, 1915

Coscinoptycta convoluta (Taylor, 1910)
(Fig. 15c)

1910 *Coscinoptycha convoluta* Taylor, p. 141, text-figs 7, 8, 33, pl. 11, fig. 60.
2020 *Coscinoptycta convoluta* (Taylor) – Kruse & Debrenne, p. 102, fig. 87, *cum syn.*

Material. Two specimens: MGM-7214X-5; MGM-7216X-5 = MGM-7217X-5 (see Appendix 2 for localities).

Description. Cup in which both walls show slight synchronous transverse folds. Diameter 3.6–4.4 mm. Intervallum 0.8–1.2 mm in width. Radial coefficient RK 5.8–5.9. Intervallar coefficient IK 0.2–0.3. Ratio of sides of interseptal loculi IC

https://doi.org/10.1017/S1755691022000111 Published online by Cambridge University Press

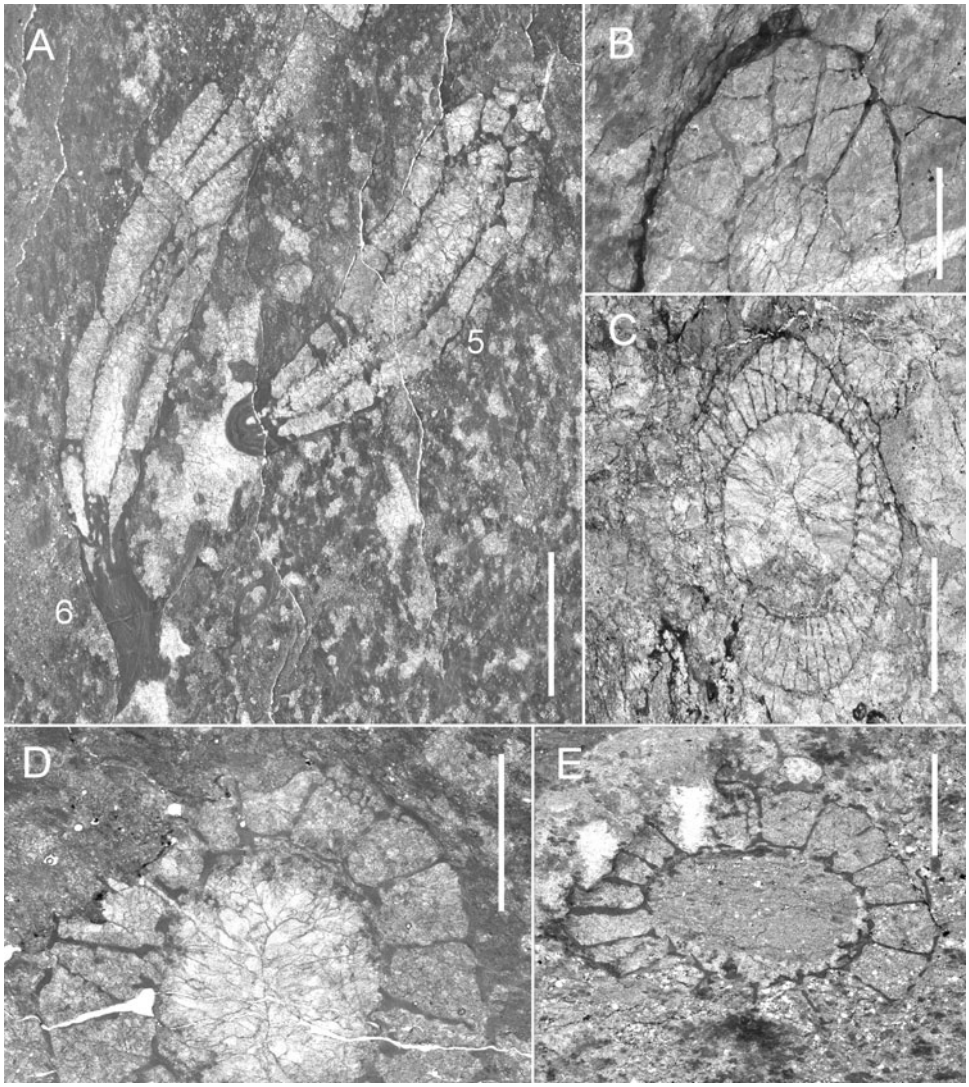

Figure 17 (A) *Erismacoscinus bilateralis* (Taylor, 1910): MGM-7232X-5 and 6, Oldhamia Terraces. (B) ?*Antoniococsinus* sp.: MGM-7231X-3, Oldhamia Terraces. (C) ?*Retecoscinus* sp.: MGM-7227X-12, Oldhamia Terraces. (D, E) *Wegenercyathus sexangulae* gen. et sp. nov.: (D) holotype, MGM-7233X-11; (E) paratype, MGM-7242X-6, Oldhamia Terraces. Scale bars = 4 mm (A); 2 mm (B–E).

1:2.5–1:3. Outer wall with 1–2 rows of pores per intersept (diameter 0.24–0.28 mm, lintels 0.14 mm, wall thickness 0.08 mm), each surmounted by a multiperforate tumulus. Tumuli 0.2–0.3 mm high. Inner wall with 1–3 rows of pores (diameter 0.20 mm, lintels 0.08 mm, wall thickness 0.08 mm), bearing cupped bracts. Septa with 1–3 rows of pores (diameter 0.12 mm, lintels 0.16 mm, septa thickness 0.04–0.08 mm). Tabulae with 3–5 radial rows of pores, tabulae thickness 0.07 mm.

Remarks. The porosity of both walls is characteristic of *C. convoluta*, including the other species described for the genus that are currently synonymous, which allows us to assign our specimens.

Occurrence. Australia: Arrowie Basin, Ajax Mine (Taylor 1910; Bedford & Bedford 1934; Ting 1937; Debrenne & Debrenne 1960; Debrenne 1969; Kruse & Debrenne 2020), Wirrealpa Mine (Zhuravlev & Gravestock 1994); Mount Scott Range (Gravestock 1984); Gnalta Shelf, Mount Wright (Kruse 1982); Stansbury Basin, Curramulka-Stansbury (Zhuravlev & Gravestock 1994), Cape d'Estaing (Kruse & Moreno-Eiris 2013). Allochthonous clasts: Antarctica, Beardmore Glacier (Hill 1964a); Shackleton Range, Trueman Terraces, carbonate clasts from the Mount Wegener Formation. Cambrian *Series 2*, Botoman.

Order Putapacyathida Vologdin, 1961
Superfamily Putapacyathoidea Bedford & Bedford, 1936
Family Putapacyathidae Bedford & Bedford, 1936
Genus *Putapacyathus* Bedford & Bedford, 1936

Putapacyathus sp.
(Fig. 18a)

Material. One specimen: MGM-7220X-4 (see Appendix 2 for locality).

Description. Cup narrowly conical, diameter 6–7 mm with intervallum 1–1.5 mm width. Intervallar coefficient IK 0.16–0.21. Outer wall secondarily thickened, with ten pores per intertabulum (diameter 0.08 mm, lintels 0.04–0.20 mm, wall thickness 0.12 mm). The presence of the microporous sheath is not clearly observed, although redimiculi and vesicular tissue are present. Inner wall with 3–8 rows of pores per intertabulum (diameter 0.10 mm, lintels 0.02 mm, wall thickness 0.10 mm); each pore bearing cupped bract (length 0.12 mm) projects downward. Tabulae flat with 4–8 pores across intervallum (diameter 0.10 mm, lintels 0.04 mm, thickness 0.04 mm).

Remarks. The poor state of preservation of the specimen does not allow the observation of all the diagnostic characters to be able to assign it to a described species, although our

https://doi.org/10.1017/S1755691022000111 Published online by Cambridge University Press

material may have slightly wider intervallum than *Putapacyathus regularis* does, but it is a small difference, and it is found on trend lines of the intervallar coefficient.

Occurrence. Allochthonous clasts: Antarctica, Shackleton Range, Swinnerton Ledge, carbonate clasts from the Mount Wegener Formation. Cambrian *Series 2*, Botoman.

Order Archaeocyathida Okulitch, 1935
Suborder Loculicyathina Zhuravleva, 1955
Superfamily Loculicyathoidea Zhuravleva, 1954
Family Loculicyathidae Zhuravleva, 1954
Genus *Neoloculicyathus* Voronin, 1974

Neoloculicyathus sp.
(Fig. 18b, c)

Material. Six specimens: MGM-7202X-2; MGM-7203X-2; MGM-7204X-5; MGM-7207X-2; MGM-7208X-1; MGM-7248X-1 (see Appendix 2 for localities).

Description. Cup conical, diameter 1.7–3.3 mm with intervallum 0.5–0.9 mm wide. Radial coefficient RK 3.7–4.7. Intervallar coefficient IK 0.3–0.4. Ratio of sides of interseptal loculi IC 1:2–1:2.6. Outer wall with 2–3 rows of cambroid pores per intersept (diameter 0. 08–0.12 mm, lintels 0.02–0.08 mm, wall thickness 0.02–0.40 mm). Inner wall with 1–2 (3?) rows of pores per intersept (diameter 0.06–0.20 mm, lintels 0.02–0.16 mm, wall thickness 0.02–0.12 mm). Pseudosepta with 1–5 rows of pores (diameter 0.10–0.18 mm, lintels 0.04–0.08 mm, thickness 0.04–0.06 mm).

Remarks. The poor preservation of our material does not allow us to assign it to a specific species. It is the first occurrence of this genus in Antarctica.

Occurrence. Allochthonous clasts: Antarctica, Shackleton Range, Stephenson Bastion, Du Toit Nunataks, Cenozoic glacial erratic tills. Cambrian *Series 2*, Botoman.

Genus *Paranacyathus* Bedford & Bedford, 1937

Paranacyathus sarmaticus Debrenne, 1974c
(Fig. 18d)

1937 *Paranacyathus parvus* Bedford & Bedford (part), p. 34, pl. 35, figs 137a–g.
1974c *Paranacyathus sarmaticus* Debrenne, p. 171, pl. 19, figs 5–7.
1992 *Paranacyathus sarmaticus* Debrenne & Zhuravlev, p. 128, 145.
1996 *Paranacyathus sarmaticus* Debrenne – Wrona & Zhuravlev, p. 27, pl. 6, figs 1, 2.

Material. Three specimens: MGM-7210X-4; MGM-7216X-1 = MGM-7217X-1 = MGM-7218X-1 (three different sections of the same specimen); MGM-7218X-35 (see Appendix 2 for localities).

Description. Cup 1.6–9.9 mm in diameter. Intervallum 0.6–2.9 mm in width. Radial coefficient RK 2–3.2. Intervallar coefficient IK 0.3–0.4. Ratio of sides of interseptal loculi IC 1:4.1–1:5.8. Outer wall with two rows of cambroid pores per intersept (diameter 0.20 mm, lintels 0.16 mm, wall thickness 0.12 mm). This wall is slightly bulged over pores producing diaphragms. Inner wall with one (two?) rows of pores per intersept (diameter 0.10–0.40 mm, lintels 0.06–0.08 mm, wall thickness 0.04–0.08 mm). Pseudosepta with 3–6 rows of pores (diameter 0.08–0.20 mm, lintels 0. 80 mm, thickness 0.08 mm).

Remarks. The difference between *P. parvus* and *P. sarmaticus* is the absence or presence, respectively, of diaphragms over the outer wall pores. The Shackleton Range specimens present exostructures especially developed in the apical part. Vesicular tissue occupies the intervallum and central cavity in some cups, as well as the specimens described by Wrona & Zhuravlev (1996) from King George Island.

Occurrence. Australia: Arrowie Basin, Ajax Mine, Ajax Limestone (Bedford & Bedford 1937; Debrenne 1974c). Allochthonous clasts: Antarctica, King George Island, Admiralty Bay-Melville Peninsula, Oligocene Polonez Cove and Early Miocene Cape Melville Formations, glacio-marine deposits (Wrona & Zhuravlev 1996); Shackleton Range, Trueman Terraces, carbonate clasts from the Mount Wegener Formation. Cambrian *Series 2*, Botoman.

Loculicyathidae gen. et sp. indet.
(Fig. 18f)

Material. Three specimens: MGM-7231X-4; MGM-7242X-3; MGM-7242X-8 (see Appendix 2 for localities).

Remarks. The poor preservation and small size of our material do not allow us to assign it to a specific species.

Occurrence. Allochthonous clasts: Antarctica, Shackleton Range, Oldhamia Terraces, carbonate clasts from the Mount Wegener Formation. Cambrian *Series 2*, Botoman.

Suborder Archaeocyathina Okulitch, 1935
Superfamily Dictyocyathoidea Taylor, 1910
Family Dictyocyathidae Taylor, 1910
Genus *Graphoscyphia* Debrenne in Zhuravleva, 1974

?*Graphoscyphia* sp.
(Fig. 18g)

Material. Three specimens: MGM-7209X-1; MGM-7209X-12; MGM-7209X-14 (see Appendix 2 for localities).

Description. Cup 2.9–10 mm in diameter and intervallum 0.7–2.1 mm wide. Radial coefficient RK 7.8–9.1. Intervallar coefficient IK 0.15–0.34. Ratio of sides of interseptal loculi IC 1:3–1:4.3. Outer wall with 1–6 rows of pores per intersept (diameter 0.04 mm, lintels 0.02 mm, wall thickness 0.02–0.24 mm). Inner wall with one row of simple pores per intersept (diameter 0.16–0.20 mm, lintels 0. 08–0.28 mm, wall thickness 0.04–0.12 mm). Pseudosepta with 1–2? rows of pores (diameter 0.16 mm, lintels 0.08 mm, thickness 0.04–0.12 mm). Synapticulae are less regularly disposed.

Remarks. Our material presents the porosity of inner wall, septal porosity, synapticulae and septal arrangement similar to the specimen described by Debrenne 1992 from EW, which in Kruse & Debrenne (2020) is included in the synonymy as ?*G. graphica*.

Occurrence. Allochthonous clasts: Antarctica, Shackleton Range, Stephenson Bastion, Cenozoic glacial erratic tills. Cambrian *Series 2*, Botoman.

Superfamily Archaeocyathoidea Hinde, 1889
Family Archaeopharetridae Bedford & Bedford, 1936
Genus *Archaeopharetra* Bedford & Bedford, 1936

Archaeopharetra irregularis (Taylor, 1910)
(Figs 18e, h, 19a)

1910 *Dictyocyathus irregularis* Taylor, p. 145, pl. 12, fig. 66.
2002 *Archaeopharetra irregularis* (Taylor) – Debrenne, Zhuravlev & Kruse, p. 1665, fig. 62e, g–h.
2012 *Archaeopharetra irregularis* (Taylor) – Debrenne, Zhuravlev & Kruse, p. 129, 132, fig. 103-1a-b.
2015 *Archaeopharetra irregularis* (Taylor) – Debrenne, Zhuravlev & Kruse, p. 1051, 1054, fig. 626-1a-b.
2019 *Archaeopharetra irregularis* (Taylor) – Perejón *et al.*, p. 17, fig. 9c, e, *cum syn*.

Material. Eleven specimens: MGM-7203X-4; MGM-7205X-1; MGM-7208X-2; MGM-7216X-11; MGM-7216X-12; MGM-7218X-27; MGM-7219X-9; MGM-7225X-3; MGM-7236X-4; MGM-7240X-6; MGM-7245X-1 (see Appendix 2 for localities).

https://doi.org/10.1017/S1755691022000111 Published online by Cambridge University Press

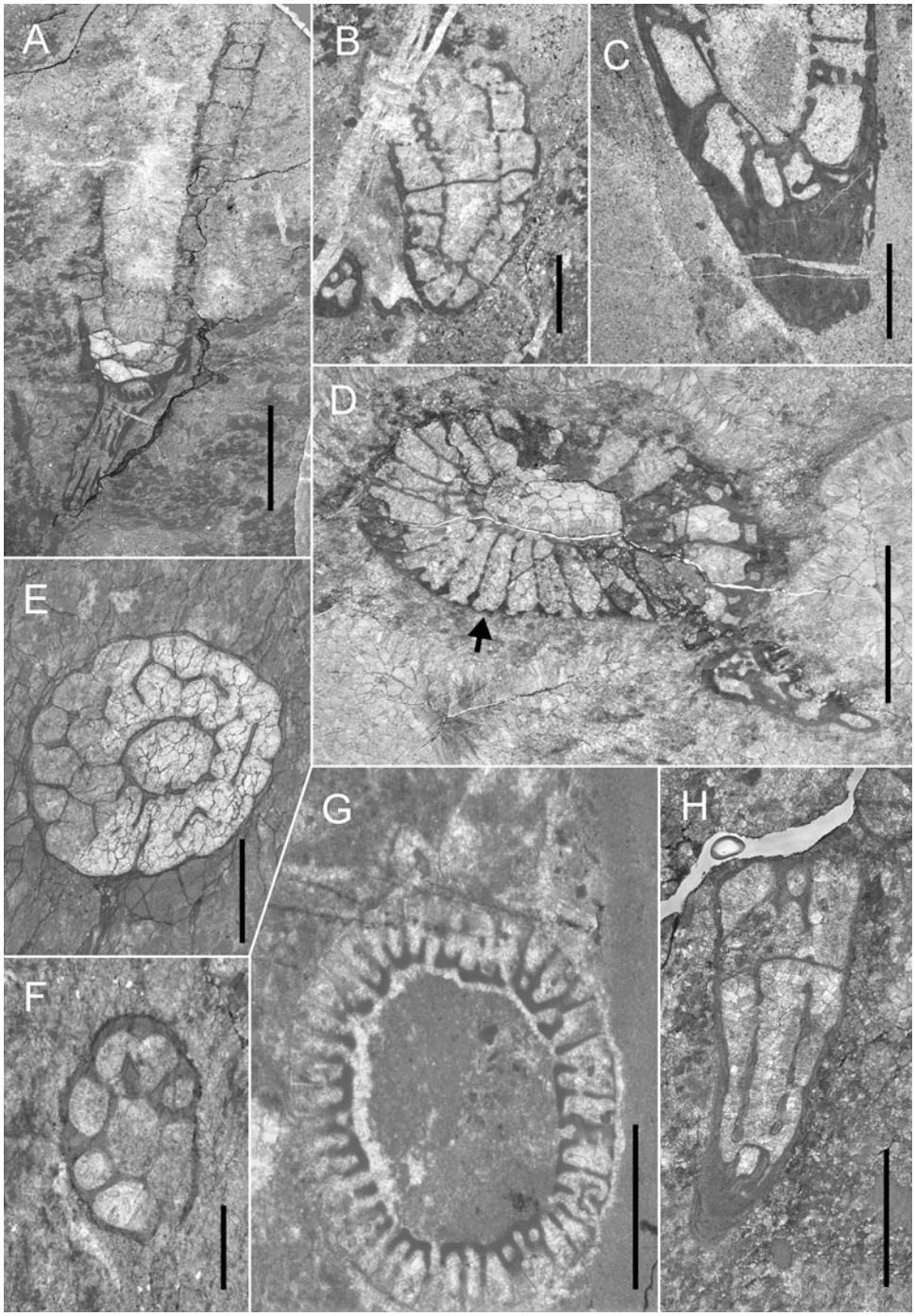

Figure 18 (A) *Putapacyathus* sp.: MGM-7220X-4, Swinnerton Ledge. (B, C) *Neoloculicyathus* sp.: (B) MGM-7203X-2; (C) MGM-7208X-1, Stephenson Bastion. (D) *Paranacyathus sarmaticus* Debrenne, 1974: MGM-7217X-1, arrow indicates diaphragm pores, Trueman Terraces. (E, H) *Archaeopharetra irregularis* (Taylor, 1910): (E) MGM-7225X-3, Oldhamia Terraces; (H) MGM-7218X-27, Trueman Terraces. (F) Loculicyathidae gen. et sp. indet.: MGM-7242X-8, Oldhamia Terraces. (G) ?*Graphoscyphia* sp.: MGM-7209X-1, Stephenson Bastion. Scale bars = 4 mm (A, D); 1 mm (B, C, F); 2 mm (E, G, H).

Description. Conical cup, 0.8–5.5 mm in diameter. Intervallum 0.8–1.8 mm in width. Outer wall imperforate in the juvenile cups, and with 1–2 rows of centripetal pores in larger cups (wall thickness 0.04–0.16 mm). Inner wall with one row of simple pores per intersept (diameter 0,16–0.36 mm, lintels 0.20–0,28 mm, wall thickness 0,04–0.12 mm). Intervallum with coarsely porous pseudotaeniae linked by synapticulae, both skeletal elements are 0.04–0.08 mm in thickness.

Remarks. Shackleton specimens are similar to *A. irregularis* as described by Zhuravlev & Gravestock (1994) and Wrona & Zhuravlev (1996).

Occurrence. Australia: Arrowie Basin, Ajax Mine, upper Ajax Limestone (Taylor 1910; Bedford & Bedford 1936) and Moorowie Mine, Moorowie Formation (Lafuste *et al*. 1991). Stansbury Basin, Yorke Peninsula, Tepper's Knoll, Aquitaine SYC101 and Minlaton-1 drillholes, Koolywurtie Member of Parara Limestone, 'Syringocnema favus beds' (Zhuravlev & Gravestock 1994). Allochthonous clasts: Africa, Namibia, Aranos Basin, Ganigobis, Botoman erratic cobbles in the Carboniferous Dwyka Group (Perejón *et al*. 2019). Antarctica, Ellsworth Mts, Sentinel Range, Mt Lymburner, erratic clasts in the Permo-Carboniferous Whiteout Conglomerate

https://doi.org/10.1017/S1755691022000111 Published online by Cambridge University Press

Formation (Debrenne 1992). King George Island, Admiralty Bay–Melville Peninsula, Oligocene Polonez Cove and Early Miocene Cape Melville Formation, glacio-marine deposits (Wrona & Zhuravlev 1996). Shackleton Range, Trueman Terraces and Oldhamia Terraces, carbonate clasts from the Mount Wegener Formation; Stephenson Bastion, Cenozoic glacial erratic tills. Cambrian *Series 2*, Botoman.

Family Archaeocyathidae Hinde, 1889
Genus *Archaeocyathus* Billings, 1861

Archaeocyathus sp.
(Fig. 19b)

Material. One specimen: MGM-7235X-16 (see Appendix 2 for locality).

Description. Cup on oblique section of 4.1 × 11.2 mm in diameter. Outer wall with centripetal pores (diameter 0.16 mm; lintels 0.06 mm; 0.08–0.12 mm in thickness). Microporous sheath with 3–4 micropores over outer wall pore (diameter 0.04 mm; lintels 0.01 mm). Inner wall with one row of pores, bearing upwardly projecting, straight pores tubes. Intervallum with pseudotaenial network coarsely porous (0.16–0.24 mm in thickness).

Remarks. Different species of *Archaeocyathus* genus have been identified in a wide geographic range: Europe, Africa, Asia, America, Australia and Antarctica. Note among these the assignment to *Archaeocyathus* sp. has been made in material from South Africa, main Karoo Basin, Zwartskraal, Dwyka tillites (Debrenne 1975; Debrenne & Kruse 1989) and in Antarctica, Ellsworth Mts, Heritage and Sentinel Ranges, erratic clasts in the Permo-Carboniferous Whiteout Conglomerate (Debrenne 1992).

Occurrence. Allochthonous clasts: Antarctica, Shackleton Range, Oldhamia Terraces, carbonate clasts from the Mount Wegener Formation. Cambrian *Series 2*, Botoman.

Superfamily Metacyathoidea Bedford & Bedford, 1934
Family Copleicyathidae Bedford & Bedford, 1937
Genus *Metacyathellus* Debrenne & Zhuravlev, 1990

?*Metacyathellus* sp.
(Fig. 19c)

Material. One specimen: MGM-7208X-3 (see Appendix 2 for locality).

Description. Cup on oblique section of 6.8 × 8.3 mm. Intervallum 2.5 mm in width. Outer wall with subdivided pores (diameter 0.08 mm, lintels 0.04 mm, wall thickness 0.04 mm). Inner wall with 1–2 rows of simple pores per intersept (diameter 0.16 mm, lintels 0.08 mm, wall thickness 0.16 mm). Intervallum with coarsely porous taeniae (0.08–0.12 mm in thickness). Vesicular tissue in intervallum and central cavity irregularly arranged.

Remarks. Our specimen presents a skeletal structure very similar to *Metacyathellus caribouensis* (Handfield) in Handfield (1971, p. 64, pl. 11, fig. 2a) from Canada. *Metacyathellus lairdi* (Hill 1964b) has been described in Antarctica, Nimrod Glacier (Hill 1964b). The poor preservation of our material does not allow us to assign it with certainty to a specific species.

Occurrence. Allochthonous clasts: Antarctica, Shackleton Range, Stephenson Bastion, Cenozoic glacial erratic tills. Cambrian *Series 2*, Botoman.

Archaeocyathina gen. et sp. indet.
(Fig. 19e–g)

Material. Twelve specimens: MGM-7204X-4; MGM-7204X-6; MGM-7204X-7; MGM-7204X-8; MGM-7209X-20; MGM-7218X-42; MGM-7234X-5; MGM-7247X-1; MGM-7247X-2; MGM-7247X-3; MGM-7247X-5; MGM-7247X-11 (see Appendix 2 for localities).

Remarks. The small size of the cups and their state of preservation do not allow us to assign these samples to a specific genus and species.

Occurrence. Allochthonous clasts: Antarctica, Shackleton Range, Trueman Terraces, Oldhamia Terraces, carbonate clasts from the Mount Wegener Formation; Stephenson Bastion, Cenozoic glacial erratic tills. Cambrian *Series 2*, Botoman.

Phylum Cnidaria Verrill, 1865
Class Anthozoa Ehrenberg, 1834
Subclass Zoantharia Scrutton, 1979
Order Tabulaconida Scrutton, 1979
Family Tabulaconidae Debrenne, Gangloff & Lafuste, 1987
Genus *Tabulaconus* Handfield, 1969

Tabulaconus kordae Handfield, 1969
(Fig. 19d)

1969 *Tabulaconus kordae* Handfield, p. 787, pl. 1, figs 2–5.
1979 *Tabulaconus kordae* Handfield – Scrutton, p. 179, fig. 2b (reproduced in Handfield 1969).
1981 *Tabulaconus kordae* Handfield – Debrenne, Lafuste & Gangloff, p.64.
1986 *Tabulaconus kordae* Handfield – Rozanov, fig. 28d.
1987 *Tabulaconus kordae* Handfield – Debrenne, Gangloff & Lafuste, p. 7–8, figs 5–10.
1987 *Tabulaconus kordae* Handfield – Voronova *et al.*, p. 43, pl. 10, fig. 5.
1988 *Tabulaconus kordae* Handfield – Zhuravlev, p. 109, pl. 12, fig. 2.
1993 *Tabulaconus kordae* Handfield – Mansy, Debrenne & Zhuravlev, pl. 1, fig. 1b, pl. 3, fig. 1.

Material. One specimen: MGM-7223X-1 (see Appendix 2 for locality).

Description. Solitary cup, 4 mm in height and 2.4 mm in diameter. Wall 0.01–0.04 mm thick with irregular undulations in the apical part. Inner cavity is crossed by thin tabulae (0.02 mm), most of which are complete, flat or arched upwards when they are recurved. Tabulae spacing ranges from 0.20 to 0.40 mm. Septa are not visible. The upper edge of cup is preserved.

Remarks. Our specimen shows the arrangement, distance and thickness of tabulae similar to the others described previously. Mansy *et al.* (1993) figured and do not describe a small specimen like our cup. The preservation of the skeletal parts of our specimen is clearly different from that observed in the neighbouring archaeocyath cups (in the same thin section), being a differentiating feature of its primary skeletal composition. It is the first occurrence of this genus in Antarctica.

Occurrence. Canada: Northwest Territories, Sekwi Formation and British Columbia, Cassiar Mountains, Atan Group, co-occurrence with *Polliaxis* Zone (Handfield 1969); Mackenzie Mountains, *Bonnia–Olenellus* Zone (Voronova *et al.* 1987); British Columbia, Rocky Mountains, Gataga River. Geological Survery of Canada locality 98754 (Mansy *et al.* 1993). USA, Alaska, Tatonduk River, Adams Argillite (Debrenne *et al.* 1987). Russia, Koryakia, Koryak Highlands (Zhuravlev 1988). Allochthonous clasts: Antarctica, Shackleton Range, Swinnerton Ledge, carbonate clasts from the Mount Wegener Formation. Cambrian *Series 2*, Botoman.

8. Biostratigraphical and palaeobiogeographical correlations

The stratigraphic distribution of the archaeocyathan genera from the Shackleton Range ranges from Tommotian 1 to Toyonian 3

https://doi.org/10.1017/S1755691022000111 Published online by Cambridge University Press

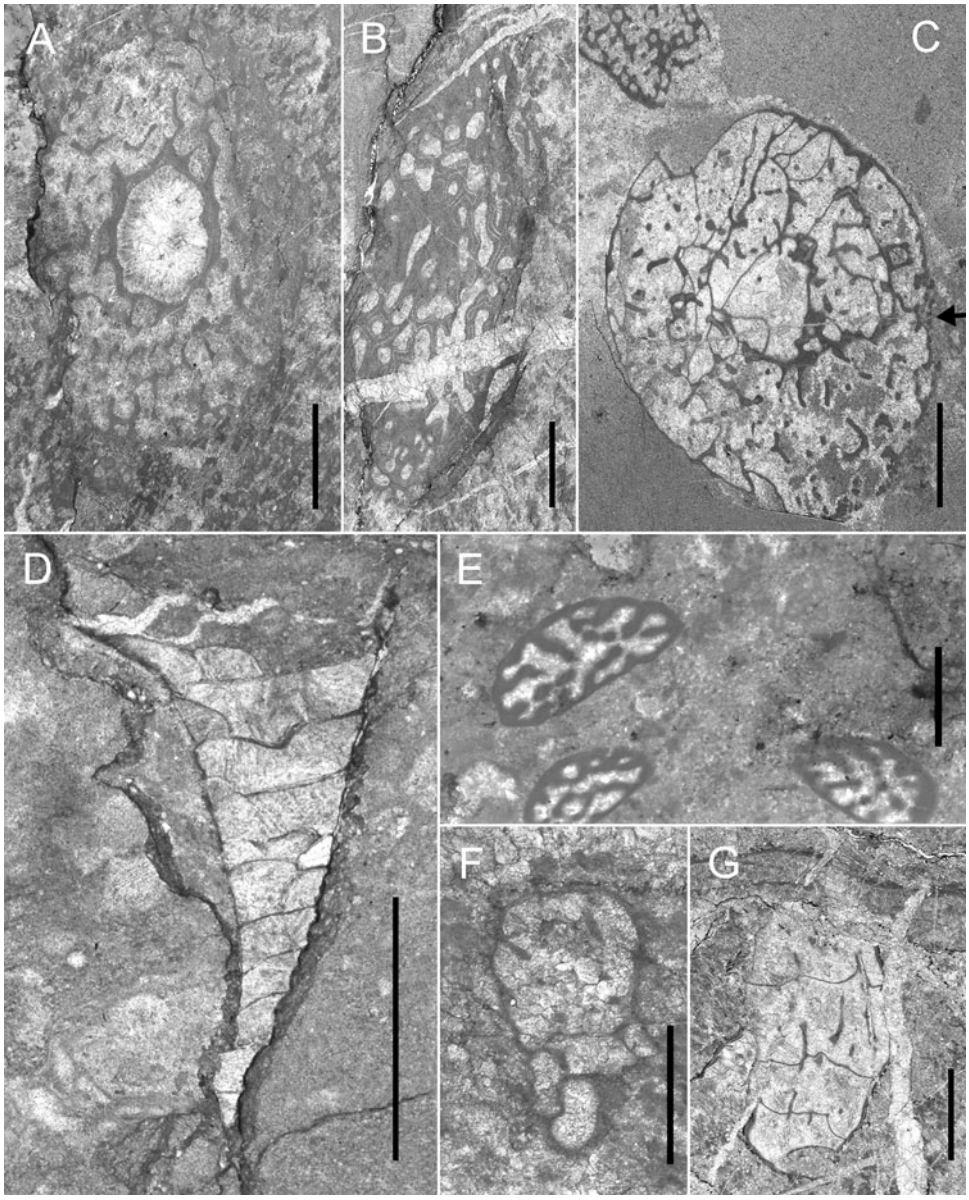

Figure 19 (A) *Archaeopharetra irregularis* (Taylor, 1910): MGM-7245X-1, Stephenson Bastion. (B) *Archaeocyathus* sp.: MGM-7235X-16, Oldhamia Terraces. (C) ?*Metacyathellus* sp.: MGM-7208X-3, arrow points to subdivided pores, Stephenson Bastion. (D) *Tabulaconus kordae* Handfield, 1969: MGM-7223X-1, Swinnerton Ledge. (E–G) Archaeocyathina gen. et sp. indet.: (E) MGM-7204X-6, 7, 8, Stephenson Bastion; (F) MGM-7218X-42, Trueman Terraces; (G) MGM-7234X-5, Oldhamia Terraces. Scale bars = 2 mm (A–D, G); 1 mm (E, F).

(Siberian stages, Cambrian *Stage 2* to *Stage 4*) according to Debrenne *et al*. (2015) (see Appendix 3). There are no biozones based on archaeocyaths in Antarctica. The Antarctic archaeocyathan fauna has usually been compared with Australian species (see Debrenne & Kruse 1989; Wrona & Zhuravlev 1996) since many species are common and support the concept of a unified Australia–Antarctica province (Australian archaeocyath fauna from Arrowie and Stansbury basins, Gnalta Shelf and fauna from Antarctica, South Africa and Falkland Islands, according to Kruse & Shi in Brock et al. 2000). Thus, we compare the Shackleton Range species with the Australian biostratigraphic schemes. In Arrowie and Stansbury Basins, Australia, Zhuravlev & Gravestock (1994) designated three biozones (*Warriootacyathus wilkawillinensis*, *Spirillicyathus tenuis* and *Jugalicyathus tardus*) and informally named two younger biozones ('*Syringocnema favus* beds' and '*Archaeocyathus abacus* beds').

Syringocnema favus beds were originally based on an assemblage that comprises 28 archaeocyathan species and two non-archaeocyathan taxa from Koolywurtie Member, Parara Limestone, Stansbury Basin (Zhuravlev & Gravestock 1994). The Shackleton Range fauna can be closely correlated to the *Syringocnema favus* beds assemblage based on shared species: *Tumuliolynthus irregularis*, *Nochoroicyathus hystrix*, *Nochoroicyathus lawrencei*, *Thalamocyathus trachealis*, *Erismacoscinus bilateralis*, *Coscinoptycta convoluta*, *Paranacyathus sarmaticus* and *Archaeopharetra irregularis*. The *Syringocnema favus* beds were initially correlated with the *Pararaia janeae* Zone (Zhuravlev & Gravestock 1994; Gravestock *et al*. 2001; Jago *et al*. 2006), which belongs to the Australian trilobite zonation based on Jell in Bengtson *et al*. (1990). Other authors correlate the *Syringocnema favus* beds with the *Pararaia bunyerooensis* Zone (Paterson *et al*. 2007; Jago *et al*. 2012, 2020; Kruse & Jago 2016; Betts *et al*. 2018; Kruse & Debrenne 2020). Moreover, Kruse *et al*. (2017) indicated that the archaeocyathan assemblage recognised in the *Syringocnema favus* beds is the most widespread in the Australia–Antarctica province, and some of their genera are restricted to the Botoman stage. Therefore, the Shackleton Range archaeocyath assemblage suggests a Botoman age (= provisional upper *Stage 3* and/or lower *Stage 4*) according to Peng *et al*. (2012), Ogg *et al*. (2016) and Geyer (2019). The Botoman age is also

https://doi.org/10.1017/S1755691022000111 Published online by Cambridge University Press

confirmed by the presence of the excellently preserved coralomorph *Tabulaconus kordae* (Swinnerton Ledge, Mount Wegener Formation). This coralomorph is reported from Botoman fauna in the Koryak Highlands, Penzhina River basin, Russia, according to Zhuravlev (1988).

Kaltatocyathus gregarius and ?*Baikalocyathus* sp. are reported in the Atdabanian *Spirillicyathus tenuis* Zone in Australia (Gravestock 1984), but they coexisted with Botoman taxa in the Shackleton Range (see Appendices 2 and 3). Thus, they expand their stratigraphic ranges in the Australia–Antarctica province.

Debrenne & Kruse (1986) also reported the presence of *Kymbecyathus avius* from samples of central TAM and it was assigned questionably to the Atdabanian *Jugalicyathus tardus* Zone by Zhuravlev & Gravestock (1994), and may possibly be of Atdabanian age, rather than stated Botoman age, due to structural complexity (Kruse & Debrenne 2020, p. 53). In the Shackleton Range, *K. avius* occurs in a Cenozoic glacial erratic sample from Stephenson Bastion with other undetermined taxa. Therefore, it would have an uncertain ?Atdabanian–?Botoman stratigraphic range in the Shackleton Range (see Appendix 3).

In the Shackleton Range, a total of 189 specimens have been identified in the Mount Wegener Formation from Trueman Terraces (41), Swinnerton Ledge (8), Oldhamia Terraces (66) and in the Cenozoic erratics from the Stephenson Bastion (70) and Du Toit Nunataks (4) (see Appendix 2). The Shackleton Range archaeocyathan assemblage comprises 34 different taxa corresponding to five new genera, six new species, ten specific species, seven doubtful genera, 14 sp. and four gen. and sp. indeterminate. A new archaeocyath family has been proposed. Therefore, the Shackleton Range archaeocyathan fauna is one of the most diverse records of allochthonous Antarctic assemblages described so far.

The Mount Wegener Formation and the Cenozoic erratics share the following 9 species out of the total taxa described: *Tumuliolynthus irregularis*, *Dokidocyathus* sp., *Nochoroicyathus lawrencei*, *Nochoroicyathus* sp., *Rotundocyathus glacius* sp. nov., *Ladaecyathus* sp., *Shackletoncyathus buggischi* gen. et sp. nov., *Santelmocyathus santelmoi* gen. et sp. nov. and *Archaeopharetra irregularis*. The archaeocyaths that only occur in the Mount Wegener Formation are *Kaltatocyathus gregarius*, *Cadniacyathus* sp., *Buggischicyathus microporus* gen. et sp. nov., ?*Baikalocyathus* sp., ?*Fallocyathus* sp., ?*Antoniocoscinus* sp., *Erismacoscinus bilateralis*, ?*Retecoscinus* sp., *Wegenercyathus sexangulae* gen. et sp. nov., *Coscinoptycta convoluta*, *Putapacyathus* sp., *Paranacyathus sarmaticus* and *Archaeocyathus* sp. The taxa that are only recorded in Cenozoic erratics from the Stephenson Bastion and Du Toit Nunataks are *Kymbecyathus avius*, *Nochoroicyathus hystrix*, *Thalamocyathus trachealis*, *Paragnaltacyathus hoeflei* gen. et sp. nov., ?*Ussuricyathellus* sp., *Neoloculicyathus* sp., ?*Graphoscyphia* sp. and ?*Metacyathellus* sp. (see Appendix 3).

This study describes the first reported occurrence of *Kaltatocyathus*, *Rotundocyathus*, ?*Baikalocyathus*, ?*Ussuricyathellus*, ?*Fallocyathus*, ?*Antoniocoscinus*, ?*Retecoscinus* and *Neoloculicyathus* in Antarctica. It also undoubtedly confirms the presence of *Cadniacyathus*. *Tumulocyathus* (?*Tumulocyathus*) *curvatus* sp. nov. was previously described by Hill (1965) from the Whichaway Nunataks, and has subsequently been reassigned to ?*Cadniacyathus curvatus* by Debrenne & Kruse (1989).

8.1. Comparison with autochthonous archaeocyathan assemblages

These new records in Antarctica allow the establishment of new paleobiogeographic relationships (Fig. 20). In Australia, the occurrence of *Cadniacyathus* and *Rotundocyathus* had only been reported in the Ajax Limestone, Ajax Mine, Arrowie Basin (Bedford & Bedford 1937; Debrenne 1974b; Kruse & Debrenne 2020). *Ussuricyathellus* has been described in the White Point Conglomerate, Stansbury Basin, Kangaroo Island (Kruse & Moreno-Eiris 2013) and Ajax Mine, Arrowie Basin (Kruse & Debrenne 2020), Australia, as well as in the Burgasutay Formation, Seer Mountains, western Mongolia (Voronin 1988). *Fallocyathus* has been described in Pestrotsvet Formation, Siberian Platform, Russia (Zhuravleva *et al.* 1969) and from the Santo Domingo Formation, Córdoba, Iberia (Perejón *et al.* 2008).

The remaining newly reported genera from the Shackleton Range (?*Baikalocyathus*, ?*Antoniocoscinus*, ?*Retecoscinus* and *Neoloculicyathus*) have a wide geographical distribution. However, the Shackleton Range fauna have three species that have only been described in Australia – *Kaltatocyathus gregarius* (Arrowie Basin; Gravestock 1984), *Nochoroicyathus hystrix* and *Nochoroicyathus lawrencei* (Gnalta Shelf; Kruse 1982) (see Appendix 4).

The Shackleton Range fauna show an extremely limited specific affinity with the autochthonous fauna from Antarctica. A total of 45 species have been previously described in the early Cambrian record of Antarctica, including 37 from the Shackleton Limestone, central TAM (Hill 1964b; Debrenne & Kruse 1986, 1989; 1 and 2 in Fig. 20) and 17 from the Schneider Hills limestone, Argentina Range (Konyushkov & Shulyatin 1980; Debrenne & Kruse 1989; 4 in Fig. 20). However, only *Kymbecyathus avius* (Shackleton Limestone) and *Thalamocyathus trachealis* (Shackleton Limestone and Schneider Hills limestone) are in common with the Shackleton Range assemblage (see Appendix 4).

The Shackleton Range archaeocyathan assemblage shares nine species and 21 genera with the Australian fauna. It shares eight species with the fauna of Arrowie Basin: *Tumuliolynthus irregularis*, *Kaltatocyathus gregarius*, *Nochoroicyathus* cf. *lawrencei*, *Thalamocyathus trachealis*, *Erismacoscinus bilateralis*, *Coscinoptycta convoluta*, *Paranacyathus sarmaticus* and *Archaeopharetra irregularis* (Etheridge 1890; Taylor 1910; Bedford & Bedford 1934, 1936; Debrenne & Debrenne 1960; Debrenne 1969, 1974a, 1974b; Daily 1973; Lafuste *et al.* 1991; Zhuravlev & Gravestock 1994; Kruse & Debrenne 2020); one with Amadeus and Georgina Basins: *Erismacoscinus bilateralis* (Kruse & West 1980); five with Gnalta Shelf: *Tumuliolynthus irregularis*, *Nochoroicyathus hystrix*, *Nochoroicyathus lawrencei*, *Coscinoptycta convoluta* and *Archaeopharetra irregularis* (Kruse 1978, 1982); and six with Stansbury Basin: *Tumuliolynthus irregularis*, *Kaltatocyathus* aff. *gregarius*, *Thalamocyathus trachealis Erismacoscinus bilateralis*, *Coscinoptycta convoluta* and *Archaeopharetra irregularis* (Gravestock 1984; Debrenne & Gravestock 1991; Zhuravlev & Gravestock 1994; Kruse & Moreno-Eiris 2013) (see Appendix 4).

8.2. Comparison with allochthonous archaeocyathan assemblages

The Shackleton Range fauna only share ?*Ladaecyathus* and ?*Erismacoscinus* with the allochthonous archaeocyathan record from the marine Cambrian El Jagüelito Formation in South America (González *et al.* 2011 and references therein).

The Shackleton Range archaeocyathan assemblage shows greater affinity with the allochthonous assemblages described in Permo-Carboniferous tillites of the Australia–Antarctica province. The Shackleton Range fauna share five of the eight species described in the Permo-Carboniferous Whiteout Conglomerate, Ellsworth Mountain, Antarctica (Debrenne 1992; 9 in Fig. 20): *Erismacoscinus* cf. *bilateralis*, *Paranacyathus*, ?*Graphoscyphia graphica*, *Archaeopharetra irregularis* and *Archaeocyathus* sp. The number of described genera from the Falkland Islands (Stone *et al.* 2012), the main Karoo Basin (Debrenne 1975),

https://doi.org/10.1017/S1755691022000111 Published online by Cambridge University Press

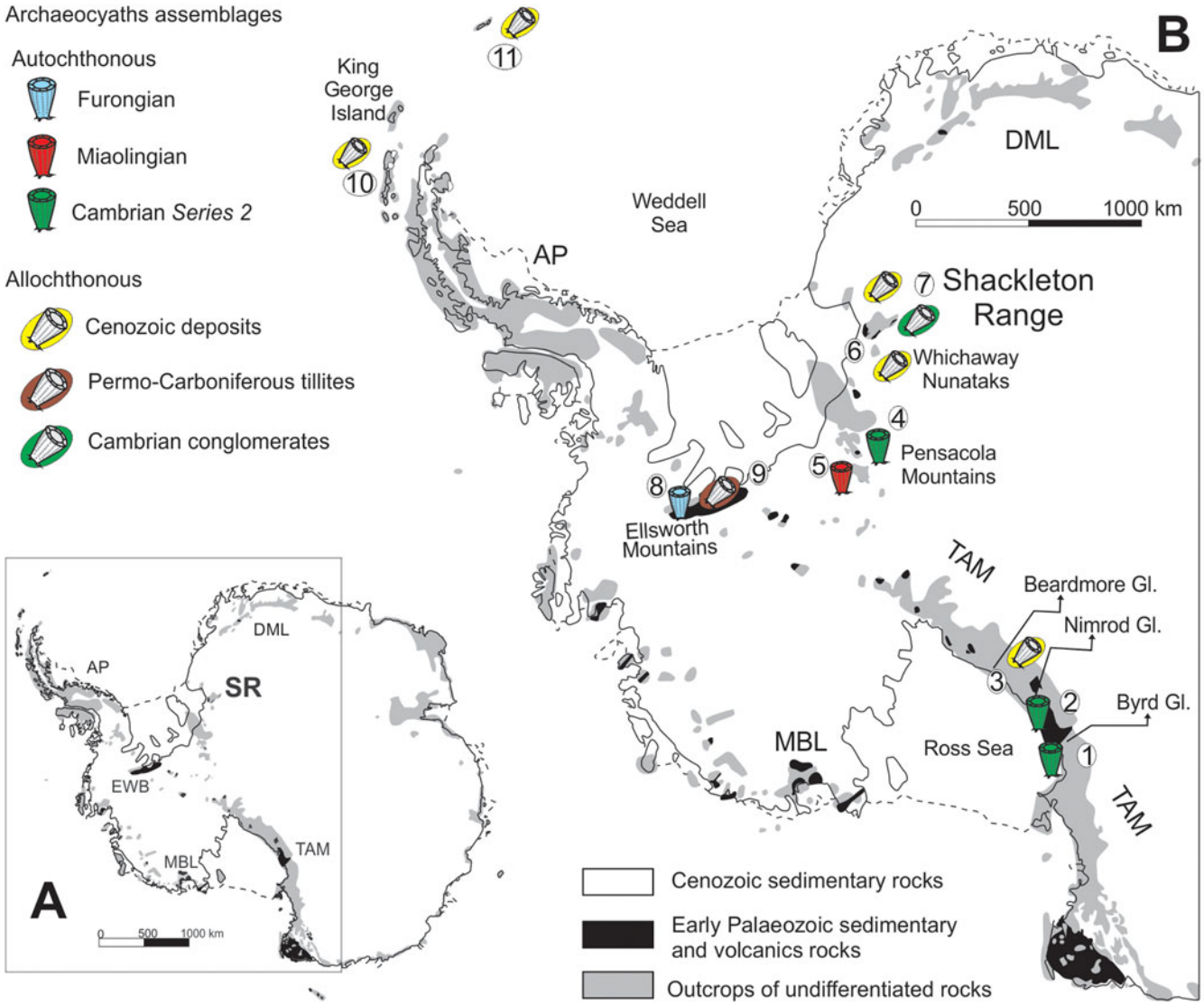

Figure 20 (A) Schematic geologic map of the Antarctic outcrops (modified from Tingey 1991). (B) Distribution of the archaeocyathan assemblages that have been previously reported and/or studied. Key: 1 = Debrenne & Kruse (1986); 2 = Hill (1964b); Debrenne & Kruse (1986, 1989)(; 3 = Hill (1964a); 4 = Konyushkov & Shulyatin (1980); 5 = Wood *et al*. (1992); 6 = Hill (1965); 7 = Höfle & Buggisch (1995); Buggisch & Henjes-Kunst (1999); 8 = Debrenne *et al*. (1984); Henderson *et al*. (1992); 9 = Debrenne (1992); 10 = Morycowa *et al*. (1982); Wrona (1989); Wrona & Zhuravlev (1996); 11 = Gordon (1920). Abbreviations: AP = Antarctic Peninsula; EWB = Ellsworth–Whitmore Block; MBL = Marie Byrd Land; TAM = Transantarctic Mountains; DML = Dronning Maud Land; SR = Shackleton Range; Gl. = glacier.

the Aranos Basin (Perejón *et al*. 2019) and the Sierras Australes (González *et al*. 2013) is 16, 13, 12 and 1, respectively. The Falkland Islands (Stone *et al*. 2012), main Karoo Basin (Debrenne 1975), Aranos Basin (Perejón *et al*. 2019) and the Sierras Australes (González *et al*. 2013) share three (*Tumuliolynthus*, *Thalamocyathus* and ?*Erismacoscinus*), four (*Thalamocyathus*, ?*Ladaecyathus*, *Archaeopharetra* and *Archaeocyathus*), three (*Erismacoscinus*, *Graphoscyphia* and *Archaeopharetra*) and one (?*Thalamocyathus*) genera with the Shackleton Range, respectively (see Fig. 1 and Appendix 4).

The archaeocyath-bearing clasts in Cenozoic glacial erratics are very common in Antarctica. It should be noted that the Shackleton Range fauna have only one common species with the Beardmore Glacier assemblage reported from present moraines in central TAM (Hill 1964a; 3 in Fig. 20) – *Coscinoptycta convoluta*. However, the highest affinity is with the Cenozoic deposits of King George Island, the Oligocene Polonez Cove (Morycowa *et al*. 1982; Wrona & Zhuravlev 1996) and the Miocene Cape Melville Formations (Wrona & Zhuravlev 1996) (10 in Fig. 20), sharing *Tumuliolynthus irregularis*, *Thalamocyathus trachealis*, *Erismacoscinus*, *Putapacyathus*, *Paranacyathus sarmaticus*, *Archaeopharetra irregularis* and ?*Archaeocyathus* from a total of 28 species described. ?*Nochoroicyathus*, ?*Cadniacyathus*, *Thalamocyathus trachealis*, *Erismacoscinus bilateralis*, *Putapacyathus*, ?*Graphoscyphia* and *Archaeocyathus* have been also reported from present-day moraines in the Whichaway Nunataks, the closest allochthonous record to the Shackleton Range, where an assemblage of 24 species has been described (Hill 1965; 6 in Fig. 20) (see Appendix 4).

In Cenozoic Weddel Sea gravels (11 in Fig. 20), Gordon (1920) described an archaeocyath assemblage of 14 taxa where *Thalamocyathus trachealis*?, *Erismacoscinus bilateralis*, ?*Graphoscyphia* and *Archaeopharetra* are in common with the Shackleton Range fauna.

9. Cambrian synorogenic record of the Shackleton Range and new age constraints on the Mount Wegener Formation

The Cambrian record currently crops out at the Shackleton Range as part of the Mount Wegener Formation, as Cenozoic glacial erratics derived from the Mount Wegener Formation

https://doi.org/10.1017/S1755691022000111 Published online by Cambridge University Press

(Stephenson Bastion and Du Toit Nunataks), and as locally sourced middle Cambrian erratics (trilobite shales) in the Mount Provender area (MP in Fig. 4a). Thus, all the information on the ages and sedimentary data of the Cambrian synorogenic marine sedimentation in the Shackleton Range sector (a-b in Fig. 21) comes from these units. Subsequently, the tectonic evolution of the Shackleton Range sector is synthesised, and possible synorogenic Cambrian sedimentation ages are reviewed and discussed.

The Mount Wegener Formation consists of marine clastic deposits sedimented from the upper slope to deep basinal settings in synorogenic conditions (Buggisch & Henjes-Kunst 1999). The high proportion of plagioclase, volcanoclastic and unstable heavy minerals suggest that the lower Cambrian Mount Wegener Formation was deposited in a back-arc basin (Buggisch *et al*. 1990; Kleinschmidt & Buggisch 1994; Buggisch *et al*. 1994a). However, the carbonate platform that generated the clasts that eventually formed the conglomerates and breccias of this formation does not outcrop in the Shackleton Range. Furthermore, this concealed platform developed on the Northern Belt, northwards of the Read Group (part of the EAC) and its sedimentary cover (Watts Needle Formation) (Fig. 3a; b in Fig. 21).

The Shackleton Range is interpreted as a composite terrane by Will *et al*. (2009, 2010) based on uranium–lead (U–Pb) zircon and monazite ages, geochemical and isotope data. The southern terrane would show similar characteristics to the Mawson Continent (Will *et al*. 2009; Boger 2011). In the Northern Terrane (Fig. 21), the magmatism associated with the subduction of the oceanic crust occurred at ~530 Ma (Zeh *et al*. 1999; Will *et al*. 2009). The K–Ar amphibole cooling ages from the ophiolitic complex, a relic of the Mozambique Ocean? (Tessensohn *et al*. 1999a), oscillate between 510 and 490 Ma (Talarico *et al*. 1999). In addition, the final continent–continent collision with eclogite facies metamorphism of 800–850 °C/23–25 kbar at approximately 70 km depth (Schmädicke & Will 2006; Romer *et al*. 2009) developed at 525–520 Ma (ultramafic rocks, Romer *et al*. 2009) and ~510 Ma (felsic country rocks, Will *et al*. 2009). Thus, ultramafic–mafic rocks and ophiolitic relics are related to the final amalgamation between E and W Gondwana (Tessensohn *et al*. 1999a; Kleinschmidt *et al*. 2001; Schmädicke & Will 2006; Will *et al*. 2009, 2010). In fact, different hypothetical traces of the E–W Gondwana sutures have been suggested (Moyes *et al*. 1993; Grunow *et al*. 1996; Shackleton 1996; Jacobs *et al*. 1998, 2017; Fitzsimons 2000; Yoshida *et al*. 2003; Boger & Miller 2004; Schmädicke & Will 2006; Kleinschmidt & Boger 2009, among others).

In the Northern Belt of the Shackleton Range, the Precambrian basement rocks with Pan-African overprinting and the northern neighbouring Coats Land Block (Kleinschmidt & Boger 2009; Loewy *et al*. 2011) are separated from the EAC (northernmost part of the Mawson Continent, Will *et al*. 2009; Boger 2011) by an E–W suture. Aeromagnetic data suggest that the E–W Shackleton Range suture could extend at least 500 km into E Antarctica and shift to an N–S orientation in the Recovery Lakes area (Golynsky *et al*. 2018). It should be noted that the Coats Land Block is separated from the Kalahari and Grunehogne cratons (K and G in Fig. 21) by the Grenvillian-age Maud Belt, which is interpreted as the continuation of the Namaqua-Natal Belt of southernmost Africa (Jacobs *et al*. 2003; Wang *et al*. 2020, fig. 11).

The sedimentation age of the Mount Wegener Formation has been estimated in different ways (Fig. 3). Shales give an Rb–Sr isochron age of ~526 Ma that was interpreted as a pre-cleavage event, such as diagenesis of sediments (Pankhurst *et al*. 1983). K–Ar dating ages around 547–506 Ma (2–6 μm whole rock fraction) were interpreted as mixtures of inherent sedimentation/diagenesis ages and around 490 Ma as the upper limit of deformation and metamorphism (Buggisch *et al*. 1994b). However, the K–Ar dating of detrital muscovites from greywacke turbidites of the Mount Wegener Formation ranges between 572 and 534 Ma, reflecting source rocks with different Pan-African primary cooling and exhumation histories; thus, the minimum cooling age limited a maximum age of sedimentation of the Mount Wegener Formation up to *ca*. 535 Ma (Buggisch & Henjes-Kunst 1999). In fact, this minimum cooling age of detrital muscovites matches with the age of magmatism in the northern terrane, which is associated with subduction of oceanic crust by ~530 Ma (Zeh *et al*. 1999; Will *et al*. 2009). Therefore, the Rb–Sr and K–Ar dating ages support an unknown Ediacaran–Terreneuvian rock source that does not crop out in the Shackleton Range (Figs 3, 21). The only known Ediacaran rocks are the EAC's autochthonous sedimentary cover, Watts Needle Formation. However, the paleocurrents of the Mount Wegener Formation point to a source area located to the N (Buggisch & Henjes-Kunst 1999), whereas the paleocurrents from the Watts Needle Formation point to the S (Buggisch *et al*. 1990). Furthermore, the neodymium (Nd) isotope values of the Mount Wegener Formation are more like Pan-African Grenville-age basement rocks such as Pioneers Group, than those from the Read Group (Buggisch & Henjes-Kunst 1999).

The fossil content of the Mount Wegener Formation was analysed in an incipient way (Buggisch *et al*. 1990, 1994a), so the previous given age is a wide early Cambrian Atdabanian age (Buggisch & Henjes-Kunst 1999). It should also be considered that there are two groups of fossils, one within the allochthonous carbonate clasts in the conglomerates, and another in the autochthonous presence of the *Oldhamia* ichnotaxon on the turbidite levels (*Oldhamia* cf. *antiqua* and *Oldhamia* cf. *radiata* according to Buggisch *et al*. 1990). The First Appearence Datum (FAD) of *Oldhamia* is placed in the Fortunian (Mángano & Buatois 2016). However, Herbosch & Verniers (2011) reviewed the biostratigraphic value of the cosmopolitan Cambrian *Oldhamia* ichnospecies and suggested that of 19 occurrences observed worldwide, 14 (Mount Wegener Formation included) occurred in a well-constrained time interval, ranging from the base of *Stage 3* to the lower three quarters of Wuliuan. Furthermore, these authors conclude that *Oldhamia* taxa from the Mount Wegener Formation just above the archaeocyaths, have an age that could extend from the base of *Stage 3* (appearance of trilobites) to the lower half of *Stage 4* (high diversity of archaeocyaths). The stratigraphic section of the Mount Wegener Formation records around 770 m at the Trueman Terraces but probably exceeds 1000 m (see Figs 4d, 5), although the total thickness of the unit is unknown. *Oldhamia* is recorded in the intermediate levels of the Oldhamia Terraces. However, we cannot rule out the presence of archaeocyath-bearing clasts or ichnotaxa in the rest of the mapped thickness of the Mount Wegener Formation (see Fig. 4d) since polymictic conglomerates crop out throughout the Oldhamia Terraces and because the exact position of the studied samples from Oldhamia Terraces is unknown.

Furthermore, from analysis of detrital zircons, MacNaughton *et al*. (2016) determined a younger, early Guzhangian age limit for new occurrences of Cambrian *Oldhamia* ichnospecies (*O. antiqua*, *O. curvata* and *O. flabellata*) in the Selwyn Basin, Canada. They also suggested a possible Last Appearance Datum (LAD) for *O. radiata* in the top of the Arrowhead Lake Member. This LAD for *O. radiata* would be below the basal conglomerate of the Gull Lake Formation, in the transition between the *Nevadella* and *Bonnia–Olenellus* Zones. The basal limestone conglomerate contains archaeocyath- and *Tabulaconus*-bearing clasts that may represent debris flows from coeval platform deposits of the Sekwi Formation (Gordey & Anderson 1993). In fact, this basal limestone conglomerate is correlated by

https://doi.org/10.1017/S1755691022000111 Published online by Cambridge University Press

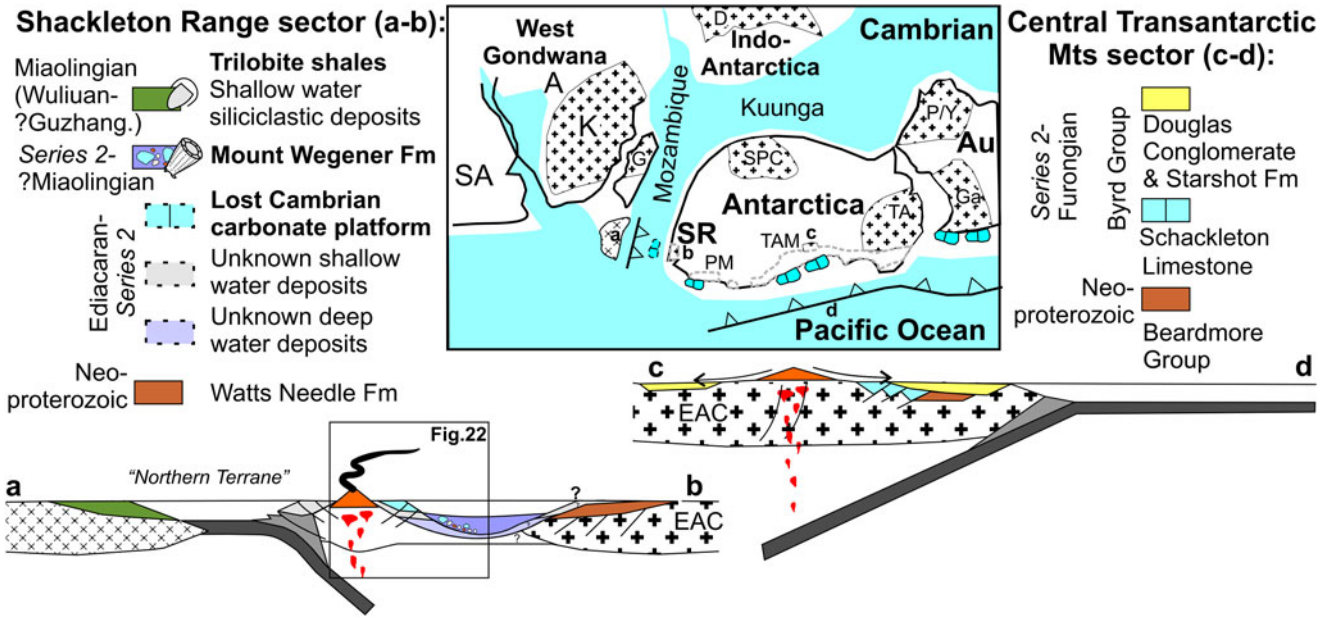

Figure 21 Cambrian paleogeography before the final amalgamation of Gondwana (modified from Boger & Miller 2004) showing the main cratonic areas, the location of the Shackleton Range sector (a-b), and the localities with Cambrian carbonate platform inboard sequences in the Pacific (initially passive) margin of Antarctica (PM, TAM) and Australia. The hypothetical seaways of the associated Ediacaran Mozambique and Cambrian Kuunga sutures are depicted. The so-called 'Northern Terrane' (see the text) is represented, but not the outboard terranes of Antarctica, Australia or South America. (a-b, c-d) Comparison of the geodynamic settings during synorogenic Cambrian sedimentation in the Shackleton Range sector (a-b, after Buggisch *et al.* 1990; Kleinschmidt & Buggisch 1994) and in the central Transantarctic Mountains sector (c-d, modified from Goodge 2020). In the Shackleton Range, the clasts from the Mount Wegener Formation and those from this unit present in the Cenozoic glacial tills suggest the existence of a volcanic arc and mixed sediment inputs of Ediacaran and Cambrian age (Terreneuvian *Series 2*). However, Terreneuvian *Series 2* shallow-water deposits on the Proterozoic Watts Needle Formation or their deep-water equivalents are unknown. Low sedimentation rates or even erosion at the EAC margin during that time cannot be ruled out. In this study we propose the reconstruction of a lost Cambrian carbonate platform (see Fig. 22) in the Shackleton Range sector. In the central Transantarctic Mountains sector (c-d), the *Series 2* Shackleton Limestone represents the platform development during the passive margin stage, while the Starshot Formation and the Douglas Conglomerate reflect syn- to late orogenic sedimentation (see Goodge 2020). Abbreviations: SA = South America; A = Africa; K = Kalahari craton; D = Dharwar craton; AU = Australia; P = Pilbara craton; Y = Yilgarn craton; Ga = Gawler craton; G = Grunehogne craton; EAC = East Antarctic craton; TA = Terre Adélie craton = Antarctic equivalent of Gawler craton that forms the 'Mawson continent' extending towards the Miller Range and Read Mountains; SPC = South Prince Charles Mountains; SR = Shackleton Range; PM = Pensacola Mountains; TAM = Transantarctic Mountains. The current contours of SR, PM and TAM are shown with a dashed grey line.

MacNaughton *et al.* (2016) with the regressive sandstone found within the Sekwi Formation in the Mackenzie Mountains, Northwest Territories. The Sekwi Formation contains trilobites from the *Fallotaspis*, *Nevadella* and *Bonnia–Olenellus* Zones (Fritz 1972) and three Botoman archaeocyath assemblages (archaeocyathan zonation for Laurentia according to Mansy *et al.* 1993, modified by McMenamin *et al.* 2000). Lower Botoman *Ethmophyllum withneyi–Sekwicyathus nahanniensis* belonging to the middle *Nevadella* strata and two middle Botoman assemblages *Claruscoscinus fritzi–M. caribouensis* and ?*Pycnoidocoscinus serratus–Tabulaconus kordeae* occurring within the middle *Bonnia–Olenellus* strata. Specifically, the carbon isotopic excursion cycle C recorded in the uppermost *Nevadella* Zone in the Sekwi Formation has been correlated with the VII positive excursion on the Siberian carbon isotope curve by Dilliard *et al.* (2007). Harvey *et al.* (2011) provided a maximum age of 514.45 ± 0.36 Ma for the Cambrian *Stage 3–Stage 4* boundary with the zircon $^{206}Pb/^{238}U$ dating of an ash from the upper part of the trilobite *Callavia* biozone (England). On the Siberian Platform, He *et al.* (2019) correlated the boundary of the uppermost Atdabanian archaeocyath *Fansycyathus lermontovae* Zone and the lowermost Botoman trilobite *Bergeroniellus micmaciformis–Erbiella* Zone with this radiometric age. Thus, the age of the Atdabanian/Botoman boundary remains uncertain on the Siberian Platform. The VII positive C-isotope excursion is recorded in the basal Botoman trilobite *B. micmaciformis–Erbiella* Zone, around 514 Ma (according to He *et al.* 2019). Thus, in the Selwyn Basin, *O. radiata* was coeval with lower Botoman archaeocyaths but did not coexist with middle Botoman archaeocyath assemblages or with the coralomorph *Tabulaconus kordeae*.

It is noteworthy to mention that the Cambrian fauna of the Mount Wegener Formation shares three species with the fauna of the Selwyn Basin: *O. radiata*, *O. antiqua* and *Tabulaconus kordeae*. The archaeocyathan fauna from the limestone clasts of the Mount Wegener Formation provide a correlation with Botoman fauna (see section 8) for the carbonate platform from which they were derived. Specifically, the archaeocyath assemblage of the Shackleton Range shares taxa with the *Syringocnema favus* beds fauna (see section 8). This archaeocyathan fauna is time-equivalent to the trilobite *Pararaia bunyerooensis* Zone (see Jago *et al.* 2020 and references therein), and the radiometric ("chemical abrasion" or CA-TIMS method) ages of three volcanic horizons within the *P. bunyerooensis* Zone from the Mernmerna Formation support ages of 514.46 ± 0.13 Ma, 514.56 ± 0.13 Ma and 515.38 ± 0.13 Ma (Betts *et al.* 2018). The archaeocyath-bearing clasts from the Mount Wegener Formation were deposited on upper slope to basinal settings after the breaking up and sedimentary brecciation of the carbonate platform, just after early marine phreatic to vadose diagenesis (see section 6). Therefore, at least the first 650–700 m of thickness (Fig. 5a) can be assigned to a maximum depositional age of terminal *Stage 3* (~515.5–514.3 Ma according to Australian data from Betts *et al.* 2018). The Shackleton Range record shows that *O. radiata* was partially contemporaneous with *Tabulaconus kordeae* and suggests certain diachronism with the *O. radiata* LAD from the Selwyn Basin. There are insufficient data to establish the final sedimentation age of the Mount Wegener Formation beyond the Wuliuan (according Herbosch & Verniers 2011) or beyond the early Guzhangian considering the LAD of Cambrian *Oldhamia* ichnospecies proposed by

https://doi.org/10.1017/S1755691022000111 Published online by Cambridge University Press

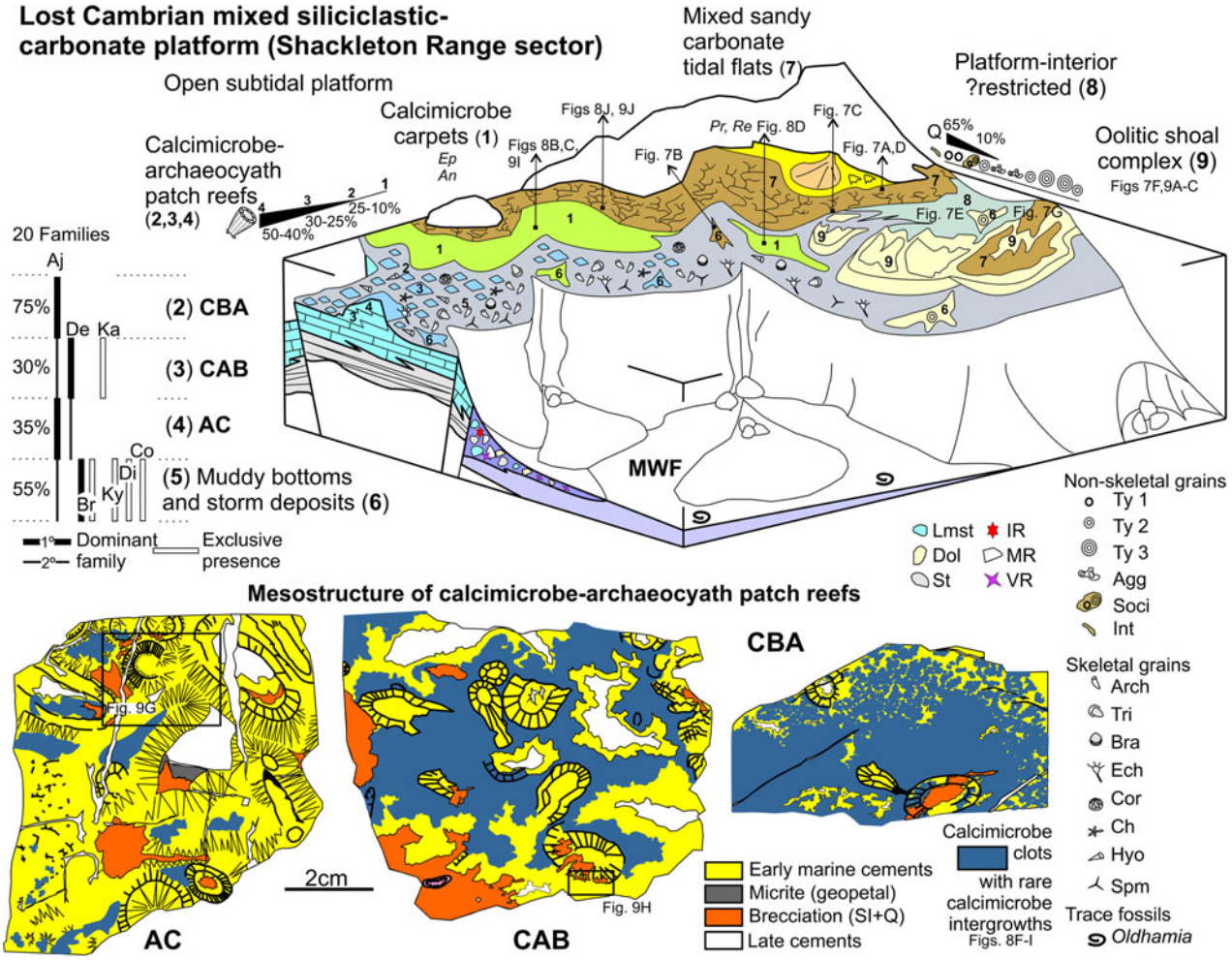

Figure 22 Hypothetical reconstruction of a hidden carbonate platform that was one of the source areas of upper slope to basinal facies of the Mount Wegener Formation. The combined analysis of microfacies, diagenesis and archaeocyaths from the carbonate clasts (Mount Wegener Formation and Cenozoic tills) allows differentiation between well-defined sedimentary sub-environments (1–9) in a lost Cambrian mixed siliciclastic–carbonate platform developed in a volcanic arc during the final amalgamation of E and W Gondwana. Abbreviations: Aj = Ajacicyathidae; De = Densocyathidae; Br = Bronchocyathidae; Ka = Kaltatocyathidae; Ky = Kymbecyathidae; Di = Dictyocyathidae; Co = Copleicyathidae; CBA = Calcimicrobial boundstones with archaeocyaths; CAB = Calcimicrobe–archaeocyath boundstones; AC = Archaeocyath cementstones; *Ep* = *Epiphyton*; *An* = *Angusticellularia*; *Pr* = *Proaulopora*; *Re* = *Renalcis*; MWF = Mount Wegener Formation; Lmst = limestones; Dol = dolostones; St = sandstones; IR = igneous rocks; MR = metamorphic rocks; VR = acidic to basic volcanic rocks; Ty 1–Ty 3 = ooid types; Agg = aggregate grains; Soci = sandy oolitic compound intraclasts; Int = intraclasts; Arch = archaeocyaths in muddy bottoms; Tri = trilobites; Bra = brachiopods; Ech = echinoderms; Cor = coralomorphs; Ch = chancelloriids; Hyo = hyoliths; Spm = sponge megascleres.

MacNaughton *et al*. (2016). Therefore, the minimum age of the unit is given by the deformation and metamorphism ages around 490 Ma (Buggisch *et al*. 1994b) during Furongian.

In the Shackleton Range, the middle Cambrian erratics are fossiliferous shales and calcareous siltstones containing trilobites, obolid brachiopods, hyoliths and other molluscs, and are informally known as the 'trilobite shales' (Fig. 3; see Thomson *et al*. 1995 and references therein). Solov'ev & Grikurov (1979) described nine trilobite assemblages from these erratics. The presence of the brachiopod *Notiobolus tenuis* (Popov & Solov'ev 1981) was assigned to a pre-Drumian age based on its co-occurrence with *Ptychagnostus gibbus* and *Ptychagnostus praecurrens* (Popov *et al*. 2015). Solov'ev and Grikurov's trilobite associations have been grouped as Fauna 2 and correlated with *gibbus* to *atavus* Zones, from late Templetonian to early Floran Australian stages by Cooper & Shergold (1991). However, Lieberman (2004) suggested that some of the Solov'ev & Grikurov (1979) figured material might be referred only questionably to *Ammagnostus laiwuensis*, showing a broad range in South China from the upper *Ptychagnostus atavus* Zone to the *Proagnostus bulbus* Zone (Peng & Robison 2000), late Floran to early Mindyallan (Drumian–Guzhangian). Therefore, the trilobite shales were deposited during the Wuliuan–Drumian or even Wuliuan–?Guzhangian, depending on whether Lieberman's subsequent reassignment is correct. Trilobite distortion and K–Ar ages (2–6 μm) of shales around 463–455 Ma are interpreted as weak deformation and very low-grade metamorphism (Buggisch *et al*. 1994a). Thus, the stratigraphic position of this *ex situ* record has been placed under the sedimentary molasse deposits of the Ordovician Blaiklock Glacier Group (Fig. 3; Thomson *et al*. 1995). The Blaiklock Glacier Group has yielded an Rb–Sr date of 482 ± 11 Ma isochron (Pankhurst *et al*. 1983), while the K–Ar date of micas from underlying leucogneiss, undeformed granitic clast and detrital micas from sandstones are around 516–498 Ma with palaeomagnetic declination data according to known Ordovician pole positions (Buggisch *et al*. 1999). Thus, the detrital micas from the Blaiklock Glacier Group support a Guzhangian–Furongian uplift and a history of exhumation for the northern basement of the Shackleton Range.

In summary, part of the upper slope to deep basinal deposits from the Mount Wegener Formation contains evidence of rock sources from late Ediacaran up to Cambrian *Series 2*, and locally sourced middle Cambrian erratics (trilobite shales) support that Cambrian shallow marine sedimentation continued during

https://doi.org/10.1017/S1755691022000111 Published online by Cambridge University Press

Wuliuan–?Guzhangian ages in the Shackleton Range sector (Fig. 21). However, the tectonic emplacement of the Mount Wegener nappe and its very low-grade metamorphic overprint is older (around 490 Ma) than the weak tectonic deformation and low-grade metamorphic overprint observed in the trilobite shales (463-455 Ma). This suggests that middle Cambrian shallow marine sedimentation did not develop in the same tectono-sedimentary environment (Fig. 21).

10. Palaeoenvironmental reconstruction of the lost Cambrian platform

The analysis of the microfacies of carbonate clasts allows us to reconstruct different sub-environments of the lost carbonate platform from which they were derived. The analysed carbonate clasts belong to different groups of lithofacies (dolomitic sandstones to sandy dolostones, aggregate grain- to ooid-rich dolostones, dolostones, calcimicrobe- and archaeocyath-rich limestones) – an outcome of the carbonate production in shallow waters from platform-interior ?restricted, oolitic shoal complex and open subtidal platform settings (Fig. 22). The high proportion of terrigenous sands in some dolostone lithofacies also suggests a mixed siliciclastic–carbonate platform attached to land.

The pervasive fabric-retentive dolomitisation observed in dolostone clasts (RD1 in Fig. 9a, c, f) could indicate conditions like those observed in present-day dolomites in restricted evaporative shallow-marine to supratidal environments (Tucker & Wright 1990 and references therein). Recent penecontemporaneous dolomites were found within microbial mats (Vasconcelos *et al*. 1995; Mazzullo 2000) and the recognised importance of low-temperature microbially mediated dolomite formation has strengthened in the last decades (Petrash *et al*. 2017 and references therein). It should be noted that microbially mediated dolomitisation produces small amounts of dolomite in modern shallow-marine sediments compared to other fossil examples (e.g., reflux dolomitisation by mesohaline brines is capable of pervasive dolomitisation of large areas of carbonate platform; see Machel 2004). However, DiLoreto *et al*. (2019) have found rhombohedral ordered dolomite in microbial mats in Qatari sabkhas dominated by filamentous anoxygenic photosynthetic bacteria. These authors propose that, in parallel to secular changes in ocean geochemistry, the evolution and structure of microbial mat communities may have favoured the predominant type of carbonate precipitation within the mat. Precambrian dolomites are primarily associated with shallow subtidal to intertidal facies related to microbial deposits, while limestones correspond to deeper waters facies (see discussion in Tucker 1992 and references therein). In Neoproterozoic oceans, the co-occurrence of marine aragonite, high magnesium calcite and dolomite (mimetic dolomitisation and primary cement) suggest extremely high magnesium/calcium ratios and marine anoxia (Hood & Wallace 2018). Furthermore, microbial sulphate reduction probably triggered precipitation of fibrous dolomites from euxinic porewaters (Hu *et al*. 2020). Evaporative conditions in combination with high rates of microbial activity (e.g., anoxygenic photosynthetic bacteria in biofilms) could have promoted the formation of extensive penecontemporaneous dolomites on those ancient microbe-dominated carbonate platforms, as suggested by Daye *et al*. (2019). Currently, we do not have any direct evidence of evaporite formation, since trace elements, fluid inclusions, oxygen and carbon isotopic data are not available; therefore, any dolomitisation model (microbial, evaporative, seepage-reflux, meteoric-marine mixing-zone) should be viewed with caution. Thus, the observed mimetic penecontemporaneous dolomitisation (RD1) seems to be a facies-selective process associated exclusively with platform-interior ?restricted and oolitic shoal complex settings, developed in a near-surface and/or shallow burial diagenetic setting.

10.1. Platform-interior ?restricted setting: mixed sandy carbonate peritidal and storm-related deposits

The dolomitic sandstones (Fig. 7a) with beach rock cements are interpreted as mixed sandy carbonate shore/flat deposits. Their very well rounded and sorted fine to medium detrital quartz grains suggest long-term abrasion due to the transport of the wind by saltation and surface creep. Therefore, mixed sandy carbonate shore/flat deposits (7 in Fig. 22) could have been fed by coastal eolian deposits. Silty/sandy dolomicrites with irregular vuggy to channelised cavities filled with clastic fillings (Fig. 7d) could reflect tidal flat sedimentation of mixed sandy carbonates with alternation of low energy (fallout of the suspended load during slack-water periods), exposure and/or burrowing (development of vuggy porosity), and sedimentation of the bed load as clastic fillings (pelletoids, superficial type 1 ooids, sand grains) by the action of current or waves under moderate energy conditions.

Sandy very poorly to moderately sorted dolorudites with a mixture of eroded and redeposited intraclasts (silty/sandy dolomicrites, sandy oolitic-type 2-compound intraclasts, oolitic-, aggregate-grain- and algal peloid-rich dolograinstones), fragments of type 3 oolitic cortices, abraded micritic coated clasts and orange fibrous cement crusts were produced during high-energy events such as strong storms (Fig. 7b, c; 6 in Fig. 22). The mixture of intraclasts can be correlated with alternating processes of sedimentation, erosion, reworking and deposition by waves, tides and/or storms in peritidal areas, where intraformational conglomerates are common (Flügel 2004). Indeed, the silty/sandy dolomicrite intraclasts could be rip-up clasts eroded from muddy and mixed tidal flat areas. Storms could produce the observed mix of ooids (types 1–3) that are derived from different sub-environments. Superficial ooids (type 1), mostly with quartz nuclei, point to sandy pelletal tidal flat environments, while larger micritic concentric ooids (type 2 and type 3) indicate high-energy environments such as oolitic shoals (see below), as suggested by the study of carbonate grain distribution developed by Steinhoff & Strohmenger (1996) in the Upper Permian Zechstein 2 of Germany. Therefore, the largest ooids were derived from active shoal settings, while the smallest were produced in moderate- to low-energy, platform-interior settings (8 in Fig. 22). In addition, large sandy oolitic (type 2) compound intraclasts (Fig. 7b), derived from oolitic shoals, also involve repeated reworking and sedimentation in storm-influenced platform-interior settings. The scarcity and low diversity of calcimicrobe remains (*Proaulopora*, *Renalcis*; Fig. 8d) in the storm-related deposits indicate that they occasionally colonised the platform-interior, while meanwhile a high siliciclastic input prevented the expansion of other calcimicrobes. *Proaulopora* remains have been described in fenestral, peloidal and microbial grainstones developed in high-energy peritidal settings of the lower Cambrian Láncara Formation, Spain (Álvaro et al. 2000).

10.2. Oolitic shoal complex

Another important group of carbonate clasts is formed by the aggregate grain- to ooid-rich dolostones. These are dominated by aggregate grains or ooids or a mixture of both, reflecting different but closely related sedimentary sub-environments in a shallow subtidal to intertidal shoal complex (9 in Fig. 22). The low detrital sand content suggests that sedimentation took place far from the influence of coastal siliciclastic input.

https://doi.org/10.1017/S1755691022000111 Published online by Cambridge University Press

Ooid-rich dolostones have noticeable diagenetic and microfacies characteristics linked with their paleoenvironmental settings (e.g., mimetic dolomitisation, concentric micritic laminae, ooid sizes). The type 2–3 ooids of the studied carbonate clasts are laminar concentric dolomicritic ooids (Figs 7f, 9a, c, f). The micritic laminae are considered secondary microfabrics produced by physical-chemical and/or microbial processes. Laboratory experiments suggest that mimetic concentric dolomite ooids may be useful indicators of precursor aragonite ooids and early dolomitisation (Zempolich & Baker 1993). The role of agitation and abrasion can be correlated with the size of the ooid, the density of the bands and the cortical fabric (Medwedeff & Wilkinson 1983), so equivalent rates of carbonate precipitation and cortex abrasion could produce micritic ooids (Wilkinson *et al*. 1984). However, micritic laminae have also been explained as micritisation by endolithic cyanobacteria and final filling of microborings with random microcrystalline cement (Margolix & Rex 1971; Reid & MacIntyre 2000). In addition, research in Bahamian ooids shows that microbes do not play an important role in early ooid genesis, but modify the chemistry and microfabrics of the cortices through extensive microboring activity and biotic aragonite cementation associated with cyanobacteria *Solentia* sp. and *Hyella* sp. (Duguid *et al*. 2010). Some Cambrian ooids show different types of microbial activity as well, such as encrusting filamentous cyanobacteria (e.g., *Girvanella*-cortex ooids; Liu & Zhang 2012) or the presence of microbial microborings, filaments and extracellular polymeric substances or EPS (Tan *et al*. 2018).

The selection, composition (type 2–3 ooids) and presence of broken and overgrown ooids indicate that oolitic dolograinstones correspond to highly turbulent environments caused by the action of waves, tides and/or currents that form oolitic shoal deposits. The development of giant ooids (type 3) is favoured by high saturation of seawater carbonate, low supply of nuclei, high accretion rates, high current velocities and ramp-style architecture according to Sumner & Grotzinger (1993). Other experiments carried out by Trower *et al*. (2017) indicate that both precipitation and abrasion play a significant role in the final size of ooids. They correlated the mode of transport and the size of ooids, so that the transport as suspended load produces larger ooids than those dominated by bed load transport. In the studied carbonate clasts, the different ooids (types 1–3) occur in characteristic microfacies, the small superficial ooids with quartz nuclei (type 1) suggest platform-interior settings with high siliciclastic contribution, while medium and giant ooids correspond to high-energy oolitic shoal settings. The most common examples of giant ooids come from Precambrian, Cambrian, Lower Triassic and Jurassic platforms (Lehrmann *et al*. 2012 and references therein). The lower Cambrian Qingxudong Formation, Sichuan Basin, could be a counterexample for giant ooids developed in deepening and moderate-energy subtidal environments affected by episodic hydrodynamic events (Tan *et al*. 2018).

Those depositional textures with abundant dolomicrite and varying proportions of ooids and/or aggregate grains indicate low- to moderate-energy conditions in the vicinity of oolitic shoal settings. The loosely packed oolitic dolowackestones represent a mixture of reworked ooids (type 3–2) that were redeposited by waves/storms in low-energy, depressed, muddy areas that were adjacent to an oolitic shoal setting, similar to washover deposits (6 in Fig. 22). The aggregate grain dolowackestones and dolopackstones (Fig. 7e) with the finest size sediment represent low-energy, depressed, muddy areas in a protected subtidal backshoal setting. Nowadays, aggregate-grains are characteristic allochems in shallow marine environments on tropical and subtropical carbonate platforms. For instance, the Bahama Banks grapestones are indicative of uneven water turbulence, low sedimentation rates and low-nutrient environments (Illing 1954; Purdy 1963a, b; Winland & Matthews 1974) developed in the vicinity of the shelf-margin reefs, and grading into oolitic shoals and algal-foraminiferal sands (Flügel 2004 and references therein).

The aggregate grain-oolitic dolograinstone (Fig. 7g) shows a characteristic laminoid fenestral fabric that can result from multiple processes such as degassing of decaying organic matter and desiccation of microbial mats and lime mud, among others, which are commonly associated with modern peritidal environments (Scholle & Ulmer-Scholle 2003; Flügel 2004). The lack of quartz sand grains suggests that sedimentation took place far from the coastal siliciclastic inputs. The mixture of components (e.g., aggregate grains, medium and giant ooids, large compound intraclasts) reflects that the fenestral aggregate grain-oolitic dolograinstones developed in transition zones between aggregate-rich areas and active oolitic shoals. Finally, the observed diagenetic vadose fabrics (e.g., intraparticle secondary porosity as oomolds, internal geopetal infills, microcrystalline crust, meniscus cement; Figs 7f, g, 9b) indicate that they developed in intertidal conditions, likely on a partially/episodically subaerially exposed oolitic shoal setting.

10.3. Open subtidal platform setting: calcimicrobe carpets, calcimicrobe–archaeocyath patch reefs and storm-related deposits

The calcimicrobe-rich and/or archaeocyath-rich limestone clasts from the Mount Wegener Formation and Cenozoic erratics evidence different environmental conditions in an open subtidal platform (1–5 in Fig. 22). The co-occurrence of calcimicrobes and archaeocyaths points out photic, normal conditions. As above, the low content of detrital quartz sand grains suggests shallow subtidal conditions far away from the coarse detrital siliciclastic coastal inputs. Calcimicrobe-rich microfacies are derived from calcimicrobial boundstones (calcimicrobe carpets; 1 in Fig. 22) and/or calcimicrobial boundstones with varying proportions of archaeocyaths (calcimicrobe–archaeocyath patch reefs; 2–4 in Fig. 22). The diversity of archaeocyath-rich microfacies shows that the archaeocyaths colonised diverse subenvironments, forming calcimicrobe–archaeocyath patch reefs under varying conditions of water turbulence (calcimicrobe–archaeocyath boundstones and archaeocyath cementstones), and living in open spaces (calcimicrobe-free spaces; 5 in Fig. 22), on muddy substrates that could be disturbed during storms (archaeocyath floatstones; 6 in Fig. 22).

The affinities of calcimicrobes have been a controversial issue; they have been interpreted as cyanobacteria, green and red algae, diagenetic microfossils, fossilised biofilm clusters or fossilised microbial colonies (Pratt 1984; Riding 1991, 2001; Stephens & Sumner 2002; Woo & Chough 2010 and references therein). However, many of them have been considered mostly fossil calcified cyanobacteria (Riding 1991; Latif *et al*. 2019) and others such as *Renalcis* and *Epiphyton* are regarded as algae (Luchinina 2013 and references therein), as problematic calcified microfossils (Liu *et al*. 2017) or as colonies of calcified coccoid cyanobacteria (Zhang *et al*. 2019). In the Shackleton Range, calcimicrobes clearly linked to filamentous cyanobacteria are *Girvanella*, *Subtifloria* (calcified oscillatorialean cyanobacteria) or *Proaulopora* (calcified nostocalean cyanobacterium) according to Liu *et al*. (2020).

The occurrence of calcimicrobes in different microfacies of the carbonate clasts allows us to reconstruct their distribution on the platform. Calcimicrobe carpets are dominated by low-diverse calcimicrobial microframeworks. The frequency and prevalence of *Epiphyton* and/or *Angusticellularia* suggest that they could easily colonise substrates forming carpets or meadows on the

https://doi.org/10.1017/S1755691022000111 Published online by Cambridge University Press

Cambrian seabed, where grazing pressure was low (Debrenne & Zhuravlev 1997). In contrast to *Epiphyton* and *Angusticellularia*, *Proaulopora* and *Renalcis* appear to have no problem forming carpets/meadows near to siliciclastic inputs. Extensive calcimicrobial colonisation of the substrate may inhibit larval settlement of sessile benthic organisms such as filter-feeding archaeocyaths, where competition for available 'open space' is important when grazing pressure is low. The growth rate of archaeocyaths is considered relatively slow so they were easily overgrown by calcimicrobes or buried by mud (Zhuravlev 2001 and references therein). In fact, in the *Epiphyton*-group-dominated bioherms, some archaeocyaths are smaller and have a thick exotheca (Zhuravlev 1996 and references therein).

Calcimicrobe–archaeocyath patch reefs correspond to boundstone microfacies where calcimicrobes were the main framebuilders (except in the archaeocyath cementstone), while sessile heterotrophs such as archaeocyaths and coralomorphs played a minor or passive framebuilder role together with chancelloriids and hyoliths (part of an accessory heterozoan assemblage). The most common framebuilder in Cambrian reefs is *Renalcis*, encrusting archaeocyath cups, which form *Renalcis*-archaeocyath boundstones (Debrenne 2007) or calcimicrobial thrombolytic framestones (type 2 of Gandin & Debrenne 2010). In the Shackleton Range sector, the main calcimicrobes are *Epiphyton*, *Angusticellularia* and subordinate *Tarthinia*, *Renalcis* and *Girvanella*, with rare occurrences of *Botomaella*.

In the Shackleton Range sector, the ajacicyathides proliferated in the open subtidal platform from muddy bottoms to calcimicrobe–archaeocyath patch reefs (see Appendix 1). They played different roles as minor framebuilders in the calcimicrobial boundstones with archaeocyaths or as main framebuilders in the archaeocyath cementstones. In Cambrian ecosystems, the mostly solitary ajacicyathides inhabited soft, muddy substrates with a high sedimentation rate (Debrenne 2007), as well as forming thickets and skeletal piles for the successive calcimicrobe–archaeocyath colonisation (Zhuravlev 2001).

The maximum diversity in the number of archaeocyath families (75 %) and the presence of rare calcimicrobe intergrowths (highest calcimicrobe diversity) occurs in the calcimicrobial boundstone with archaeocyaths (2 in Fig. 22; see Appendix 1). It could represent a transition zone between low-diversity calcimicrobe carpets and other calcimicrobe–archaeocyath patch reefs, where the volume of sessile archaeocyaths increases (from 15 % to 50 %) but the diversity of families decreases (30 % and 35 %, respectively; see 3 and 4 in Fig. 22). Furthermore, the small size of the growth framework cavities in the calcimicrobial boundstone with archaeocyaths indicates a homogeneous and dense colonisation of the substrate by calcimicrobes. In the Shackleton Range, *Epiphyton–Tarthinia–Girvanella* or *Epiphyton–Girvanella* intergrowths are not common (Fig. 8f–i). Examples of Cambrian *Series 2* intergrowths have been described in the *Tarthinia–Epiphyton–Gordonophyton–Renalcis* boundstone from Mongolia (Wood *et al*. 1993) and in dendritic thrombolites from North China (Lee *et al*. 2014). However, both examples lack *Girvanella* intergrowths and the latter lacks co-occurrence with archaeocyaths. Toyonian archaeocyathan-calcimicrobial reefs of South China display a diverse assemblage of calcimicrobes (Adachi *et al*. 2014), where *Girvanella* is found intergrowing with *Epiphyton* bushes and encrusting archaeocyaths. However, *Girvanella* crusts around archaeocyaths are very rare in the Shackleton Range sector.

The calcimicrobe–archaeocyath patch reefs with a lower diversity of archaeocyathan families (35 %) show larger growth cavities and an extensive development of early marine cement-supported fabrics, indicating that these patch reefs (calcimicrobe–archaeocyath boundstone and archaeocyath cementstone, respectively) developed wave-resistant frameworks under high-energy conditions.

The peloid–intraclastic–bioclastic packstones to grainstones with remains of archaeocyaths could represent storm sheets derived from areas close to the calcimicrobe–archaeocyath patch reefs and surrounding muddy bottoms and deposited above the fair-weather wave base (FWWB), whereas the archaeocyath floatstones were deposited below the FWWB.

The muddy bottoms were colonised by a diverse heterozoan assemblage. Trilobites, brachiopods, hyoliths and echinoderms are common in wackestone to packstone pockets, thus likely living in the vicinity of the calcimicrobe–archaeocyath patch reefs on muddy subtidal substrates. There is a high diversity of archaeocyath families (55 %) in wackestone to floatstone, the presence of Bronchocyathidae, Kymbecyathidae, Dictyocyathidae and Copleicyathidae being exclusive, with Bronchocyathidae being the dominant family together with the conspicuous Ajacicyathidae.

11. Comparison with neighbouring Cambrian inboard successions of the EAC

The Cambrian carbonate platform inboard successions are restricted to the central and southern Transantarctic Mountains and the PM (TAM and PM in Fig. 21) and they record the transition from passive to active margin deposition (Goodge 2020 and references therein).

The best-known Cambrian *Series 2* carbonate record corresponds to the lower Atdabanian to Botoman Shackleton Limestone (Byrd Group; Fig. 23 and references therein) in the central TAM (sector c-d in Fig. 21). The total thickness of the unit is unknown due to tectonic complication. The lower mixed siliciclastic–carbonate part is well recognised in the central Holyoake Range on the Errant Glacier side (~133 m thick; Myrow *et al*. 2002a, fig. 4). The upper carbonate-dominated succession, around 225–320 m thick, has been analysed in the N and centre of the Holyoake Range (Rees *et al*. 1989; Claybourn *et al*. 2019, respectively). The lower Shackleton Limestone consists of interbedded quartz sandstone with mud drapes and wave ripples and fine-grained dolomitic grainstone with hummocky cross-stratification (Myrow *et al*. 2002a).

The upper Shackleton Limestone comprises supratidal (Burgess & Lammerink 1979) to deep subtidal deposits on a carbonate ramp (Myrow *et al*. 2002a) where isolated bioherms (<2 m) and biohermal complexes (20–50 m thick) proliferated (Rees *et al*. 1989). Rees *et al*. (1989) recognised four depositional subenvironments whose lithofacies associations share some characteristics with those recognised in the Shackleton Range. The intertidal association corresponds to dolomitic limestones (fenestral cryptomicrobial laminites, fenestral mudstone, parallel- and ripple cross-laminated peloidal grainstone and dolomitic intraclastic flat pebble rudstone), while in the Shackleton Range they correspond to mixed sandy penecontemporaneous dolostones with a diverse allochem association. The carbonate sand shoal association shows varied allochems (ooids, coated grains, oncoids, bioclasts, grapestones) in thick, parallel-, planar cross- and bimodal cross-stratified grainstone sequences, which are interbedded with bioclastic, intraclastic and peloidal grainstones as well as oncolite rudstones. However, oncolite rudstones and bioclastic grainstones are not found in the Shackleton Range sector. In the Shackleton Limestone, the microstructures of ooids are diverse (radial, concentric or composite versus concentric cortices) as well as their nuclei (peloids, trilobites, echinoderms versus quartz grains or broken cortices). However, the presence of giant ooids or sandy oolitic compound intraclasts is not reported in the Shackleton Limestone. And, although early diagenetic processes are recorded (isopachous cement, micritisation, oomoldic and shelter porosity, equant spar), neither mimetic penecontemporaneous dolomitisation

https://doi.org/10.1017/S1755691022000111 Published online by Cambridge University Press

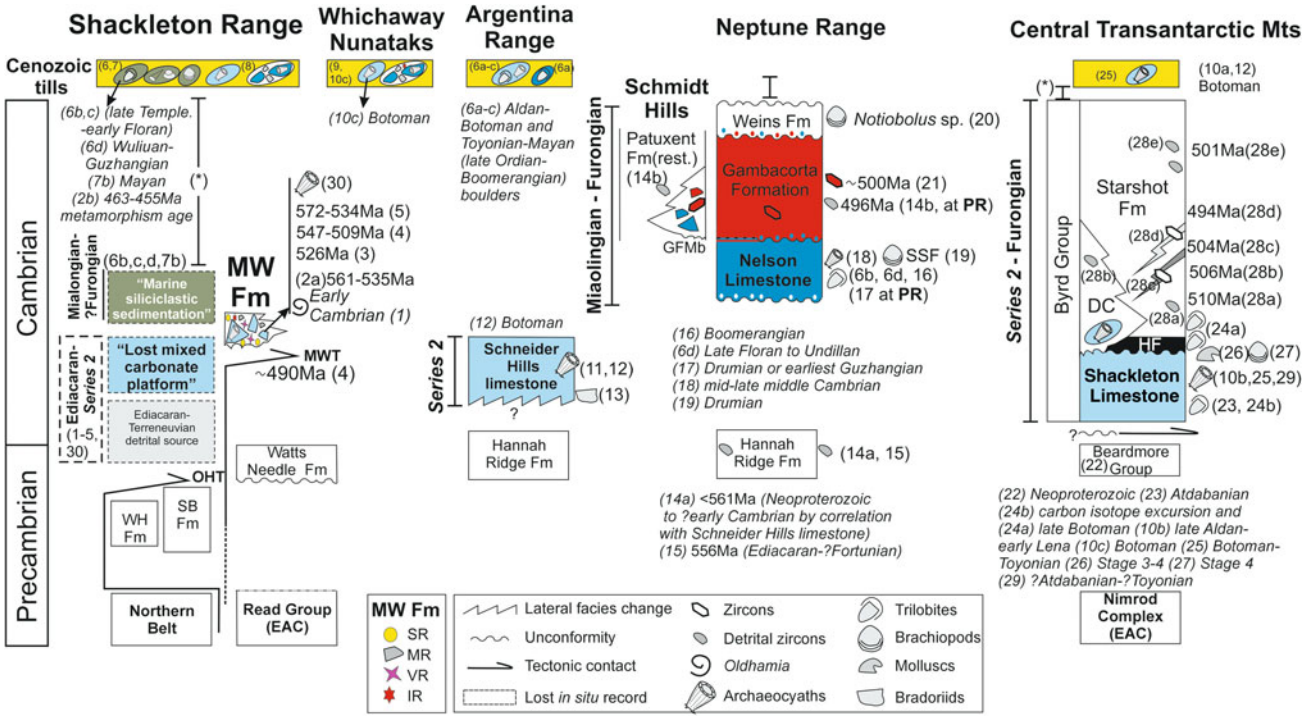

Figure 23 Reconstruction of the hidden Cambrian marine record in the Shackleton Range and possible equivalences to nearby Cambrian successions in the Whichaway Nunataks, the Pensacola Mountains (Argentina Range, Neptune Range) and the central Transantarctic Mountains. The most representative ages are given; for the Shackleton Range, see also Fig. 3. Key: 1 = *Oldhamia* cf. *radiata*, *Oldhamia* cf. *antiqua*, Buggisch *et al.* (1990). 2a = archaeocyath presence, Rb–Sr sedimentation? ages, and 2b = K–Ar metamorphism ages according to Buggisch *et al.* (1994a). 3 = Rb–Sr diagenesis? ages, Pankhurst *et al.* (1983). 4 = K–Ar mixtures? of inherited lower Cambrian ages of sedimentation/ diagenesis and Ross metamorphism, Buggisch *et al.* (1994b). 5 = K–Ar detrital muscovites ages with late Pan-African cooling history, Buggisch & Henjes-Kunst (1999). Trilobite-based ages: 6a = Palmer & Gatehouse (1972); 6b = Solov'ev & Grikurov (1979); 6c = Cooper & Shergold (1991); 6d = Lieberman (2004). Brachiopods: 7a = Thomson (1972); 7b = *Notiobulus tenuis*, Mayan stage, Popov & Solov'ev (1981). Archaeocyath presence: 8 = Höfle & Buggisch, (1995); 9 = Stephenson (1966). Archaeocyath-based age: 10a, b, c = Hill (1964a, 1964b, 1965); 11 = Konyushkov & Shulyatin (1980); 12 = Debrenne & Kruse (1989). 13 = Bradoriids, Rode *et al.* (2003). U–Pb detrital zircons ages: 14a = older limit for the depositional age; and 14b = maximum depositional age for the Patuxent Formation (rest.), in a restricted sense, according to Rowell *et al.* (2001); 15 = youngest zircon grains age and ?early Cambrian maximum depositional age inferred according to Goodge *et al.* (2004a). Trilobite-based ages: 16 = Evans *et al.* (1995); 17 = Evans *et al.* (2018). 18 = archaeocyath-based age, Wood *et al.* (1992). 19 = brachiopods, trilobites, Bassett-Butt (2016). 20 = *Notiobulus* sp., Storey *et al.* (1996). U–Pb zircon volcanism/magmatism ages: 21 = Millar & Storey, (1995), Van Schmus *et al.* (1997); 22 = Goodge *et al.* (2002). Trilobite-based ages: 23 = Rowell *et al.* (1988), Palmer & Rowell (1995); 24a = Myrow *et al.* (2002a). 24b = carbon isotope excursion IV (equivalent to CARE), Myrow *et al.* (2002a). 25 = archaeocyath-based ages, Debrenne & Kruse (1986). 26 = Mollusc-based ages, Claybourn *et al.* (2019). 27 = brachiopod-based ages, Claybourn *et al.* (2020). 28a, b, e = detrital youngest zircon grain ages, Goodge *et al.* (2004a, 2004b). 28c, d = U–Pb crystallisation ages, Goodge *et al.* (2004b). 29 = Kruse & Debrenne (2020). 30 = this study. Abbreviations: MW Fm = Mount Wegener Formation; EAC = East Antarctic craton; WH Fm = Wyeth Heights Formation; SB Fm = Stephenson Bastion Formation; OHT = Otter Highlands Thrust; MWT = Mount Wegener Thrust; GF Mb = Gorecki Felsite Member; PR = Patuxent Range; SSF = small shelly fossils; HF = Holyoake Formation; DC = Douglas Conglomerate; SR = Sedimentary rocks; MR = metamorphic rocks; VR = volcanic rocks; IR = igneous rocks; (*) = Rest of the record not represented. Stages used in each year of publication: Australian stages (Ordian, Templetonian, Floran, Undillan, Boomerangian); Siberian stages (Aldan, Lena, Botoman, Toyonian, Mayan). Precambrian and Cambrian subdivisions used in bold are according to the International Chronostratigraphic Chart (Cohen *et al.* 2013, available online at https://stratigraphy.org/chart).

nor early silicification processes are described in the Shackleton Limestone. In fact, dolomitisation of the carbonate sand shoal association is described as partial replacement of ooids by large dolomite crystals. The shallow-subtidal shelf association shows some common lithofacies such as peloid, intraclastic, bioclastic packstones to grainstones or oolitic grainstones derived from nearby sand shoals that are interpreted as storm deposits. However, bioturbated bioclastic wackestones and packstones or spongiostromata oncolite packstones are not recorded in the Shackleton Range sector. The archaeocyathan–microbial reef association is interbedded with burrow-mottled and oolitic limestones, and allochems from the carbonate sand shoals are also present in some of the reef complexes. This interdigitisation of facies and components is not observed in boundstone from the Shackleton Range sector. However, the diversity in calcimicrobes is much higher in the Shackleton Range, since only *Renalcis*, *Epiphyton* and *Girvanella* have been reported in the Shackleton Limestone.

Rees *et al.* (1989) described three types of reefs, formed by *Epiphyton*-bearing boundstone, *Renalcis* boundstone and stromatactis-bearing boundstone. Only the *Epiphyton*-bearing boundstone, developed in moderately high-energy areas, share some characteristics with the analysed boundstone microfacies. In fact, *Epiphyton* and *Angusticellularia* are the main calcimicrobes in calcimicrobe carpets, as well as in calcimicrobe–archaeocyath patch reefs in the Shackleton Range sector. In the Shackleton Limestone, the dominant reef type is *Epiphyton*-bearing boundstone with subordinate *Girvanella* and *Renalcis*. Archaeocyaths comprise one-third of its volume or are absent. This type of reef developed centimetre- to decimetre-scale, open growth-framework cavities colonised by calcimicrobes, lined by marine cement crusts with multi-episodic geopetal infills. However, boundstones of the Shackleton Range sector display millimetre- to centimetre-scale growth-framework cavities and lack multi-episodic geopetal infills (see mesostructure maps in Fig. 22).

In the central Holyoake Range, towards the upper part of the Shackleton Limestone, the biohermal complexes are capped by thick composite bored phosphatic hardgrounds that indicate the terminal drowning of the bioherms due to tectonic subsidence produced by the initiation of orogenesis in this region (Myrow *et al.* 2002a). The successive deep-water transgressive

https://doi.org/10.1017/S1755691022000111 Published online by Cambridge University Press

Holyoake Formation, with rare trilobites, grades into the shallowing- and coarsening upward Starshot Formation (Fig. 23 and references therein). The Starshot Formation contains late Botoman trilobites at the base (Myrow *et al*. 2002a) and clasts from the conglomeratic levels contain archaeocyathan limestone, metamorphic, igneous and volcanic rocks (Laird 1963). The overlying Douglas Conglomerate are alluvial fan, marine, braid deltas and associated lacustrine deposits (Rees & Rowell 1991), which contain sandstone and quartzite, eroded folded limestone from the Shackleton Limestone and rare granitoid, rhyolite, basalt, chert and dolomite clasts (Skinner 1964, 1965; Rees *et al*. 1987). Detrital zircons from the upper part of the Douglas Conglomerate indicate a maximum Miaolingian depositional age of around 506 Ma, and the Starshot Formation is cut by Miaolingian–Furongian intrusions with U–Pb crystallisation ages of 504 Ma and 495 Ma (Goodge *et al*. 2004b). Therefore, the Byrd Group (Shackleton Limestone, Holyoake and Starshot Formations and Douglas Conglomerate) reflects a shift from the passive carbonate ramp deposition to the onset of supracrustal deformation during the Botoman that produced the drowning of the carbonate ramp, tectonic deformation, uplift and deposition of a widespread clastic wedge (Myrow *et al*. 2002a).

In the central Transantarctic Mountains, Goodge (2020 and references therein) differentiated four main phases in the Cordilleran-type, active continental-margin Ross orogenic belt:

- Early Neoproterozoic passive-margin phase represented by the Beardmore Group;
- Ediacaran–Cambrian *Stage 3* (~580–515 Ma) passive to active margin phase: development of early continental-margin volcanism and Cambrian *Series 2* carbonate ramp (Shackleton Limestone);
- Cambrian *Stage 3*–Jiangshanian (~515–490 Ma) synorogenic phase: intra-arc deformation, magmatism, erosion and siliciclastic sedimentation (Holyoake and Starshot Formations) in a forearc setting (c-d in Fig. 21); and
- Jiangshanian–Tremadocian (~490–480 Ma) late orogenic phase: synorogenic succession intruded by post-tectonic magmas; sedimentation of alluvial fan and shallow marine deposits (Douglas Conglomerate and upper Starshot Formation, respectively).

The *in situ* Cambrian *Series 2* carbonate record closest to the Shackleton Range crops out in the Argentina Range, PM (Fig. 23). Rowell *et al*. (1992a) referred to this 200-m-thick formation informally as 'Schneider Hills limestone' and suggested that it may have been part of the same broad carbonate shelf that the Shackleton Limestone deposited on the western passive margin of the E Antarctica basement (Nimrod Group) (c-d in Figs 21, 23). However, infracrustal rocks do not crop at PM and its Cambrian *Series 2* deposits are not contiguous with those of the central TAM (Schneider Hills limestone is absent in the closest Neptune Range). In the PM the supracrustal rocks correspond to the Hannah Ridge Formation (Fig. 23). Detrital zircon data from this formation gave an age of latest Neoproterozoic or younger (Rowell *et al*. 2001; Goodge *et al*. 2004a). This formation underwent two phases of deformation prior to uplift, erosion and deposition of the Miaolingian Nelson Limestone, which contains supracrustal rock clasts with two cleavages in its basal conglomerate (Curtis & Storey 2003 and references therein). Evans *et al*. (2018) suggested that Cambrian *Series 2* (and older) limestones may be covered by snow and ice at the Patuxent Range or were even removed by uplift and erosion in the Neptune Range during an early phase of Ross orogeny. Alternatively, the lack of detrital inputs of this age in the succeeding record could also reflect a local palaeotopographic high that avoid the sedimentation during Cambrian *Series 2*.

Data on the Schneider Hills limestone are scarce and there is no published stratigraphic section. Konyushkov & Shulyatin (1980) described the presence of calcimicrobes (*Renalcis*, *Epiphyton*), stromatolites and gave a list of genera and species of archaeocyaths, but they did not figure them. Later, Debrenne & Kruse (1989) revised the Antarctic Cambrian archaeocyaths and gave the Konyushkov and Shulyatin's assemblage a Botoman age.

Rowell *et al*. (1992b) described a succession of several hundred meters, with a lower part containing bioclastic (archaeocyath-rich) and oolitic grainstones, bioturbated wackestones and packstones with scattered microbial reefs (0.5–10 m wide, up to 2 m thick). The top of the lower part is rich in camenellan tommotiids (*Dailyatia* Rowell *et al*. 1992b; *Dailyatia icari* sp. nov. Claybourn *et al*. 2021), and bradoriide *Bicarinella evansi* (Rode *et al*. 2003) and is overlaid by 200-m-thick Cambrian, massive boundstone with grainstone and burrowed flanking beds. Archaeocyaths are accessory components in the massive boundstone and flanking beds. The succession continues with 150–250-m-thick, thin-bedded bioturbated limestones with scattered small boundstone mounds and a second massive boundstone with small cavities (<1 cm) and flanking beds of alternating grainstone and burrowed packstone. Rowell *et al*. (1992b) compared the thick Schneider Hills limestone massive boundstones with those of similar size in Virginia, the shelf-margin skeletal algal reefs described by Barnaby & Read (1990).

Comparisons between the Shackleton Range and PM Cambrian *Series 2* carbonate platforms are limited due to existing data from the PM. The carbonate clast microfacies from the Shackleton Range sector do not exhibit bioclastic (archaeocyath-rich) grainstone, stromatolite or bioturbated wackestones or packstones. Burrowed dolomicrite with sandy infillings occur in the Shackleton Range sector (Fig. 7d) but we have interpreted them as part of the sandy-mixed carbonate tidal flat (7 in Fig. 22). Carbonate microfacies in common between the two regions are boundstone and oolitic grainstone, but they are widespread in the Cambrian *Series 2* carbonate platforms. The mesostructure of calcimicrobe–archaeocyath patch reefs from the Shackleton Range sector (Fig. 22) shows cavities larger than those of the Schneider Hills limestone. Therefore, only the comparisons between the archaeocyathan faunas in both sectors (see section 8) make paleobiogeographic sense.

In the PM, the Ross orogeny is characterised by three Miaolingian to ?Ordovician deformation events (Curtis *et al*. 2004 and references therein) constrained by radiometric and paleontological data (Fig. 23). The early contractional deformation event is around 505 Ma and produced folding, associated cleavages, emplacement of syntectonic granites (later Sherpan Peak phase) and exhumation of the Hanna Ridge Formation prior to deposition of the Miaolingian Nelson Limestone. It is followed by a middle Ross extensional event characterised by sedimentation of the Nelson Limestone that terminated by bimodal volcanism *ca*. 500 Ma (Gambacorta Formation). The Nelson Limestone is >400 m thick (Evans *et al*. 1995, 2018) and is Drumian or Drumian to early Guzhangian in age according to paleontological data (Fig. 23 and references therein), so the total thickness was deposited in a 4–5 Myr time interval.

The Weins Formation has an unconstrained post-Gambacorta Formation pre-Neptune Group age. The presence of *Notiobolus* sp. is recorded in the Weins Formation (Storey *et al*. 1996). This genus is of Wuliuan–Jiangshanian age, which is the combined range of its three extinct species (Popov & Solov'ev 1981; Holmer *et al*. 2001; Popov *et al*. 2015). Therefore, the Weins Formation has a ?Guzhangian–?Jiangshanian age. Finally, a late Ross contractional event, ?Furongian–?Ordovician (there are no fossils or

https://doi.org/10.1017/S1755691022000111 Published online by Cambridge University Press

radiometric dating), produced the moderate deformation and weak cleavage of the previous units and the syntectonic deformation of the basal part of the overlying Neptune Group (Storey *et al.* 1996).

In summary, the spatial and temporal tectonic variability along the palaeo-Pacific margin and the Mozambique seaway margin (sectors c-d and a-b, respectively, in Fig. 21) during the Ross orogeny controlled the development of carbonate platforms. Cambrian *Series 2* carbonate platforms, several hundred meters thick with calcimicrobe–archaeocyath bioconstructions, were developed on both margins during tectonic quiescent intervals from Atdabanian to Botoman (TAM) or at least during Botoman (PM and Shackleton Range). In the central TAM, the occurrence of shallow-water mixed siliciclastic–carbonate deposits is reported in the lower Shackleton Limestone, below the positive carbon excursion at the base of the Atdabanian or *Stage 3* (Myrow *et al.* 2002a); therefore, part of the mixed sedimentation could have started at the end of Terreneuvian in this sector. In the reconstructed lost Cambrian *Series 2* mixed carbonate platform of the Shackleton Range sector, the terrigenous influence is interpreted as part of the sandy mixed carbonate tidal flat deposits. Botoman is the age obtained from the assemblage of archaeocyaths in the Shackleton Range (see section 8). However, an older age cannot be ruled out for the development of a mixed siliciclastic–carbonate platform though, due to the existence of Ediacaran–Terreneuvian detrital ages recorded in the slope to basinal deposits of the Mount Wegener Formation (Fig. 24).

Some important differences observed in the Shackleton Range sector are the presence of early diagenetic phases such as pervasive mimetic dolomitisation (RD1) and authigenic and diagenetic silicification (Sch, RS1c-m), which are not described in other Cambrian inboard successions. The observed extensive penecontemporaneous dolomitisation can be related with more restrictive conditions in the Antarctic Mozambique seaway margin than in the Antarctic paleo-Pacific margin. The latitudinal differences (see ~520 Ma paleogeographic reconstruction by Merdith *et al.* 2017) and the character of the seaway margin itself could lead to more arid conditions that, along with microbial activity, favoured early dolomitisation. Likewise, in a back-arc setting, the weathering of the volcanic arc and/or its activity could provide large amounts of dissolved silica that would favour near-surface silicification processes in porous microfacies (e.g., diagenetic vadose fabrics of the oolitic shoal complex). In addition to silica-supersaturated pore fluids, near-surface silicification processes require unsaturated carbonate pore fluids and a pH below 9. There are different mechanisms that promote the replacement of carbonates by silica (see Hesse 1989), but it seems that the organic matter oxidation by sulphate-reducing bacteria would be a key reaction for the precipitation of silica in platform sediments (Noble & Van Stempvoort 1989).

In the Shackleton Range sector (Figs 21, 24), the synsedimentary brecciation of the mixed siliciclastic–carbonate platform took place during the terminal *Stage 3* (~515.5–514.3 Ma by correlation with the Australian data from Betts *et al.* 2018) or during the late Atdabanian to lowermost Botoman (~514.45 Ma considering the correlation age suggested by He *et al.* 2019) as indicated by the fauna recorded in the platform-derived clasts in the slope and basinal deposits of the Mount Wegener Formation. The first 700 m of thickness of the Mount Wegener Formation were deposited contemporaneously or shortly after platform breakup, as indicated by the successive diagenetic phases observed and their cross-cutting relationships recorded in the carbonate clasts and polymictic conglomerates (see section 6). At the same time, in central TAM, there was the synchronous development of an erosional unconformity, the drowning of the Shackleton carbonate ramp and its burial by siliciclastic sedimentation (Holyoake and lower Starshot Formations), which led to the cessation of carbonate production in this sector (Figs 21, 23).

It is unknown whether the synsedimentary platform brecciation led to the demise of the carbonate production in the Shackleton Range sector. Shallow marine siliciclastic sedimentation (trilobite shales) may have continued during the Wuliuan–? Guzhangian interval in a different tectonosedimentary setting (? African Mozambique seaway margin; a-b in Figs 21, 24). However, Cambrian carbonate production continued in the PM during Miaolingian (Nelson Limestone) and Furongian (subordinate oolitic limestones of the Weins Formation; see Storey *et al.* 1996; Fig. 23).

The lower Starshot Formation (central TAM, Fig. 23) has some similarities with the Mount Wegener Formation, regardless of their differing depositional environments (shoreline to deeper shelf versus slope to basinal deposits) and tectonosedimentary settings (forearc versus back-arc basin). The polymictic conglomerates from both formations reflect erosion of volcanic arcs and carbonate platforms, archaeocyath-bearing clasts included (Myrow *et al.* 2002a). The thickness of the Starshot Formation is unknown – up to 3000 m (Laird 1963) – and no depositional contacts have been described. It was deposited from shoreline to deep shelf (Laird 1963; Laird *et al.* 1971) and sandstone tempestite beds were deposited as wave-dominated turbidites (Myrow *et al.* 2002b). The basal part of the Starshot Formation is late Botoman in age (Myrow *et al.* 2002a). Therefore, the sedimentation of both units could be partially contemporaneous and under synorogenic conditions.

The total thickness of the Mount Wegener Formation is unknown but probably exceeds 1000 m (Buggisch & Henjes-Kunst 1999), especially considering its diagenetic evolution. The Mount Wegener Formation underwent various burial diagenetic processes (see section 6) such as dolomitisation (D2–D4) and hydrocarbon migration before undergoing the final tectonic deformation. The latest burial processes recorded correspond to late-fracture-related cementation (LVA and LVB systems), low-grade tectonically-induced plastic and cataclastic fabrics and very low-grade metamorphic overprinting. The late-fracture-related cementation produced the precipitation of very to extremely coarse non-ferroan to slightly ferroan poikilotopic calcite, ferroan saddle dolomite, coarse to very coarse ferroan calcite and varied silica phases such as megaquartz mosaics (Sqtz), quartz overgrowths and chert and microquartz replacements (RS2c-m). The cataclastic fabrics related to the nappe tectonism post-date all the observed cement and replacement phases. The low-grade metamorphic overprint and the southwards transport of the Mount Wegener Nappe occurred around 490 Ma as a result of the Ross (Pan-African) orogeny (Buggisch *et al.* 1994b; Fig. 24).

Finally, the Blaiklock Glacier Group (Shackleton Range), the Neptune Group (PM), the Douglas Conglomerate and the upper Starshot Formation (central TAM) represent late to post-orogenic siliciclastic sedimentation during the late Ross orogeny (Figs 23, 24).

12. Summary and conclusions

- In the Shackleton Range, carbonate clasts from the Cenozoic glacial erratics and the Cambrian Mount Wegener Formation exhibit up to 17 types of microfacies (ten dolostone and seven limestone).
- The Cenozoic glacial erratic archaeocyath-bearing clasts come from a local source at the Shackleton Range: the synorogenic upper slope to basinal deposits of the Cambrian Mount Wegener Formation.

https://doi.org/10.1017/S1755691022000111 Published online by Cambridge University Press

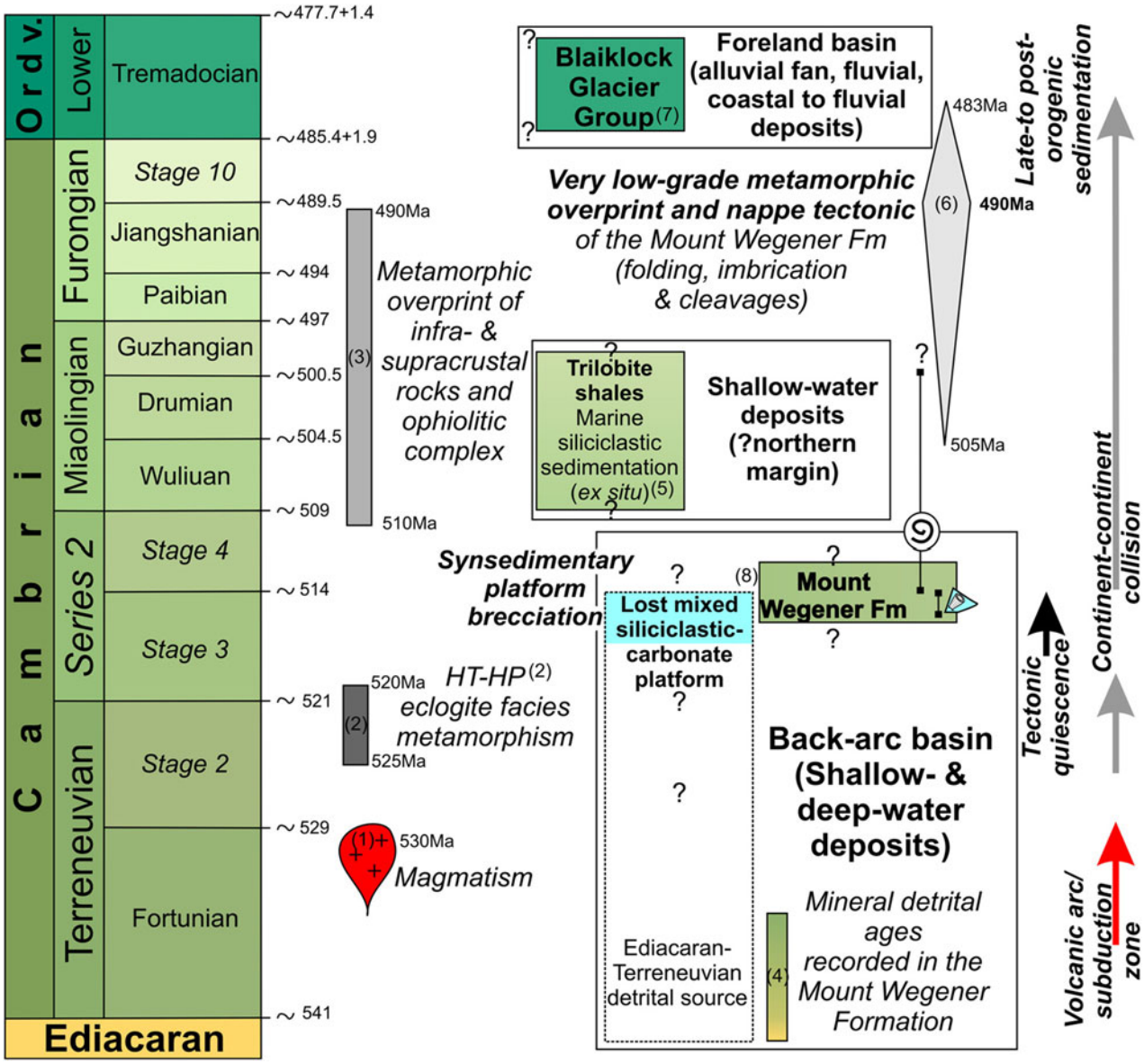

Figure 24 Chronostratigraphy of the Ediacaran to Ordovician sedimentary record of the 'Northern terrane' from the Shackleton Range sector and the main tectono-metamorphic and magmatic events recorded in the infra- and supracrustal rocks. Abbreviation: Ordv. = Ordovician. Ages are based on the following works: 1 = Zeh *et al.* (1999), Will *et al.* (2009). 2 = Romer *et al.* (2009). 3 = Tessensohn *et al.* (1999a). 4 = Pankhurst *et al.* (1983), Buggisch *et al.* (1994b), Buggisch & Henjes-Kunst (1999). 5 = Solov'ev & Grikurov (1979), Popov & Solov'ev (1981), Popov *et al.* (2015), Cooper & Shergold (1991), Lieberman (2004). 6 = Buggisch *et al.* (1994b). 7 = Pankhurst *et al.* (1983), Buggisch *et al.* (1999). 8 = this study.

- Specifically, the carbonate clasts come from a lost Cambrian *Series 2* mixed siliciclastic–carbonate platform that developed in a back-arc basin on the ?Mozambique seaway, related to the final amalgamation between E and W Gondwana during the Ross (Pan-African) orogeny.
- The Shackleton Range archaeocyathan and coralomorph assemblage consist of 34 taxa, it agrees with a terminal *Stage 3* for the lost mixed siliciclastic–carbonate platform. An older age cannot be ruled out due to the presence of Ediacaran–Terreneuvian detrital ages in the Mount Wegener Formation.
- Five new genera (*Buggischicyathus*, *Paragnaltacyathus*, *Shackletoncyathus*, *Santelmocyathus* and *Wegenercyathus*), six new species (*Rotundocyathus glacius*, *Buggischicyathus microporus*, *Paragnaltacyathus hoeflei*, *Shackletoncyathus buggischi*, *Santelmocyathus santelmoi* and *Wegenercyathus sexangulae*) and a new family Shackletoncyathidae are described.
- The first occurrence of *Kaltatocyathus*, *Rotundocyathus*, ?*Baikalocyathus*, ?*Ussuricyathellus*, ?*Fallocyathus*, ?*Antoniococsinus*, ?*Retecoscinus*, *Neoloculicyathus*, the coralomorph *T. kordae* and undoubtedly the presence of *Cadniacyathus* in Antarctica is reported in the Shackleton Range fauna.
- In the reconstructed lost platform, carbonate production was dominated by non-skeletal grains in platform-interior ?restricted and oolitic shoal complex settings, while the open subtidal platform was dominated by diverse calcimicrobes

https://doi.org/10.1017/S1755691022000111 Published online by Cambridge University Press

and a secondary to accessory heterozoan assemblage.

- In the platform-interior ?restricted setting, sandy mixed carbonate peritidal deposits were represented by non-skeletal grains such as mud peloids, bahamite peloids, superficial type 1 ooids and very well-rounded and sorted quartz grains. In the oolitic shoal complex, type 2 and type 3 ooids (giant ooids) were produced in high-turbulence conditions, while aggregate grains predominated in low-energy, depressed and protected backshoal settings.
- The main depositional sub-environments in the open subtidal platform were calcimicrobe carpets dominated by *Epiphyton* and/or *Angusticellularia*, calcimicrobe–archaeocyath patch reefs and open muddy bottoms. In the calcimicrobe–archaeocyath patch reefs, the archaeocyaths played an accessory (calcimicrobial boundstones with archaeocyaths) to a secondary/primary framebuilder role (calcimicrobe–archaeocyath boundstones and archaeocyath cementstones) and hyoliths and chancelloriids were the common associated fauna. The environs of the patch reefs and open muddy bottoms were colonised by a diverse heterozoan assemblage of solitary archaeocyaths and coralomorphs, echinoderms, brachiopods, trilobites and sponges (as evidenced by their megascleres).
- The diversity in calcimicrobes (*Epiphyton*, *Angusticellularia*, *Renalcis*, *Girvanella*, *Tarthina*, *Proaulopora*, *Subtifloria*, *Botomaella*) is the highest reported in the Antarctic Cambrian *Series 2* carbonate platforms so far. *Renalcis* and *Proaulopora* were able to colonise bottoms influenced by siliciclastic inputs. Only *Proaulopora* and *Subtifloria* do not form boundstones and are recorded as allochthonous calcimicrobe remains in grainstones and floatstones.
- The Ajacicyathidae archaeocyaths proliferated in the open subtidal platform from muddy bottoms to calcimicrobe–archaeocyath patch reefs. The greatest richness in archaeocyathan families (75 %) and calcimicrobe genera is recorded in calcimicrobial boundstones with archaeocyaths, where rare calcimicrobial intergrowths of *Epiphyton–Tarthinia–Girvanella* and/or *Epiphyton–Girvanella* occur. This study presents the first record of calcimicrobial intergrowths in Antarctic Cambrian *Series 2* carbonate platforms. The diversity in archaeocyath families in calcimicrobe–archaeocyath boundstones and archaeocyath cementstones is lower (30 and 35 %, respectively). Densocyathidae, Ajacicyathidae and Kaltatocyathidae (the latter with exclusive presence in calcimicrobe–archaeocyath boundstones) are the dominant families in the calcimicrobe–archaeocyath boundstones, whereas Ajacicyathidae is the only dominant family of the archaeocyath cementstones. The muddy bottoms display the highest richness in skeletal components and the second largest richness in number of archaeocyathan families (55 %). The archaeocyathan families that predominantly colonised muddy bottoms were Bronchocyathidae, Kymbecyathidae, Copleicyathidae and the conspicuous Ajacicyathidae.
- The Shackleton Range fauna shares 21 genera with the Botoman-equivalent Australian assemblages, but only nine species are shared: *Tumuliolynthus irregularis*, *Kaltatocyathus gregarius*, *Nochoroicyathus hystrix*, *Nochoroicyathus lawrencei*, *Thalamocyathus trachealis*, *Erismacoscinus bilateralis*, *Coscinoptycta convoluta*, *Paranacyathus sarmaticus* and *Archaeopharetra irregularis*. Within Antarctica autochthonous assemblages, only two Shackleton Range archaeocyaths are in common with the coeval carbonate platform faunas: *Kymbecyathus avius* (Shackleton Limestone, TAM) and *Thalamocyathus trachealis* (Schneider Hills limestone, Argentina Range).
- The affinity between Shackleton Range fauna and assemblages from Permo-Carboniferous tillites is greater. Shackleton Range fauna shares two species and three genera with the EW (Antarctica); two species and one genus with the Falkland Islands (South America); two species and two genera with the Dwyka Group, main Karoo Basin (South Africa); one species and two genera with the Dwyka Group, Aranos Basin (Namibia) and one genus with the Sierras Australes (Argentina).
- The affinity between the Shackleton Range fauna and assemblages from Antarctic Cenozoic deposits is greater, sharing four species and three genera with the King George Island; two species and five genera with the Wichaway Nunataks; and two species and two genera with the Weddel Sea faunas.
- The reconstructed deposits of the hidden/lost Shackleton Range platform are similar to others produced in coeval Cambrian platforms along the paleo-Pacific margin (TAM), but show clear differences (component richness/diversity, diagenetic and tectonically-induced processes) due to its latitudinal situation and tectonosedimentary evolution.
- The lost carbonate platform deposits underwent early marine phreatic and meteoric vadose diagenetic processes before the breakup and synsedimentary brecciation of the platform. Mimetic penecontemporaneous dolomitisation and early authigenic and diagenetic silicification are recorded only in platform-interior ?restricted and oolitic shoal complex deposits. The breakup and downslope transport

https://doi.org/10.1017/S1755691022000111 Published online by Cambridge University Press

of the carbonate clast are recorded as breccia fabrics, irregular vugs with crystal silt and angular quartz grain sedimentary infillings, and geopetal infills oriented inconsistently with the growth polarity of calcimicrobe microframeworks.

- At least the first 700 m of synorogenic upper slope to basinal deposits of the Mount Wegener Formation were deposited at the same time or shortly after the platform breakup around ~515.5–514.3 Ma as indicated by the presence of the terminal *Stage 3* archaeocyath- and *Tabulaconus*-bearing platform-derived clasts. The presence of Cambrian *Oldhamia* ichnospecies could suggest that sedimentation continued up to Wuliuan and even earliest Guzhangian.
- The Mount Wegener Formation underwent various burial processes such as dolomitisation (D2–D4) and hydrocarbon migration prior to late-fracture-related cementation (non-ferroan to slightly ferroan poikilotopic calcite, ferroan saddle dolomite, ferroan calcite, megaquartz mosaics), low-grade tectonically induced plastic fabrics (distorted archaeocyaths, flattened ooids, different types of twin lamellae in late-fracture-related cements) and, finally, cataclastic fabrics that post-dated all observed cementation and replacement phases.
- In Furongian times, very low-grade metamorphic conditions and tectonically induced features developed with the thrusting of the Mount Wegener Nappe over its foreland (EAC) around 490 Ma during the Ross (Pan-African) orogeny (Buggisch *et al.* 1994b).

13. Supplementary material

Supplementary material is available online at https://doi.org/10.1017/S1755691022000111.

14. Author contributions

Prof. Dr Werner Buggisch passed away on 6 April 2019 during the preparation of this manuscript. Dr Buggisch participated in four Antarctic expeditions between 1979 and 1995 and made important contributions to the geological knowledge of the Shackleton Range and the Ellsworth Mountains. We asked Dr Buggisch for the possibility of studying the carbonate and calcimicrobe–archaeocyath-bearing clasts from the Shackleton Range. Dr Buggisch responded enthusiastically and sent us all thin-sections and some samples. Unfortunately, although he was aware of our progress, he died before the manuscript was published. This work could not have been done without his help. Dr Buggisch reviewed and provided critical comments on sections 1, 2 and 3. M. R.-M. drafted sections 1–3, 5–6, 9–11 and designed the corresponding figures. A. P., S. M. and E. M.-E. drafted sections 7 and 8 and designed the corresponding figures and supplementary material. All authors discussed the results, wrote sections 4 and 12 and reviewed the final manuscript.

15. Acknowledgements

We want to thank the work done by Carlos Alonso Recio with the photography of archaeocyaths and montage of the plates (Photography Lab, Paleontology Area, Universidad Complutense de Madrid, UCM). We thank Fernando Cebrián for the graphic design of *Shackletoncyathus buggischi*. Assistance with the references provided by Pedro Martín Duque was greatly appreciated (Library, Faculty of Geology, UCM). We would like to extend our thanks to Aitor Antón, Juan Carlos Salamanca and Beatriz Moral for their work with the samples (Thin Section Lab, Stratigraphy Area, UCM). This paper is a contribution to the Spanish project CGL2017-87631-P. We especially want to thank all the reviewers for their thorough and accurate comments and recommendations. We would also like to acknowledge the corrections and comments made by Alistair John MacGowan and Iván Moreno González. Thanks to your help this work has improved substantially.

20. References

Adachi, N., Nakai, T., Ezaki, Y. & Liu, J. 2014. Late early Cambrian archaeocyath reefs in Hubei Province, South China: modes of construction during their period of demise. *Facies* **60**, 703–17.

Álvaro, J. J., Vennin, E., Moreno-Eiris, E., Perejón, A. & Bechstädt, T. 2000. Sedimentary patterns across the lower-middle Cambrian transition in the Esla nappe (Cantabrian Mountains, northern Spain). *Sedimentary Geology* **137**, 43–61.

Barnaby, R. J. & Read, J. F. 1990. Carbonate ramp to rimmed shelf evolution: lower to middle Cambrian Continental Margin, Virginia Appalachians. *Geological Society of America Bulletin* **102**, 391–404.

Bassett-Butt, L. 2016. Systematics, biostratigraphy and biogeography of brachiopods and other fossils from the middle Cambrian Nelson Limestone, Antarctica. *Geologiska Föreningen i Stockholm Förhandlingar (GFF)* **138**, 377–92.

Bedford, R. & Bedford, J. 1936. Further notes on Cyathospongia (Archaeocyathi) and other organisms from the lower Cambrian of Beltana, South Australia. *Kyancutta Museum, Memoirs* **3**, 21–26.

Bedford, R. & Bedford, J. 1937. Further notes on Archaeos (Pleospongia) from the lower Cambrian of south Australia. *Kyancutta Museum, Memoirs* **4**, 27–38.

Bedford, R. & Bedford, J. 1939. Development and classification of Archaeos (Pleospongia). *Kyancutta Museum, Memoirs* **6**, 67–82.

Bedford, R. & Bedford, W. R. 1934. New species of Archaeocyathinae and other organisms from the lower Cambrian of Beltana, South Australia. *Kyancutta Museum, Memoirs* **1**, 1–7.

Bedford, R. & Bedford, W. R. 1936. Further notes on Archaeocyathi (Cyathospongia) and other organisms from the lower Cambrian of Beltana, South Australia. *Kyancutta Museum, Memoirs* **2**, 9–20.

Bengtson, S., Conway Morris, S., Cooper, B. J., Jell, P. A. & Runnegar, B. N. 1990. Early Cambrian fossils from South Australia. *Memoirs of the Association of Australasian Palaeontologists* **9**, 1–364.

Betts, M. J., Paterson, J. R., Jacquet, S. M., Andrew, A. S., Hall, P. A., Jago, J. B., Jagodzinski, E. A., Preiss, W. V., Crowley, J. L., Brougham, T., Mathewson, C. P., García-Bellido, D. C., Topper, T. P., Skovsted, C. B. & Brock, G. A. 2018. Early Cambrian chronostratigraphy and geochronology of South Australia. *Earth-Science Reviews* **185**, 498–543.

Billings, E. 1861. New Species of lower Silurian fossils: on some new or little known species of lower Silurian fossils from the Potsdam Group (Primordial Zone). *Geological Survey of Canada* **1**, 1–24.

Boger, S. D. 2011. Antarctica – before and after Gondwana. *Gondwana Research* **19**, 335–71.

Boger, S. D. & Miller, J. M. 2004. Terminal suturing of Gondwana and the onset of the Ross-Delamerian orogeny: the cause and effect of an early Cambrian reconfiguration of plate motions. *Earth and Planetary Science Letters* **219**, 35–48.

Bornemann, J. G. 1884. Bericht über die fortsetzung seiner untersuchungen cambrischer archaeocyathus-formen und verwandter organismen von der insel sardinien. *Deutsche Geologische Gesellschaft, Zeitschrift* **36**, 702–06.

Brock, G. A., Engelbretsen, M. J., Jago, J. B., Kruse, P. D., Laurie, J. R., Shergold, J. H., Shi, G. R. & Sorauf, J. E.. 2000. Palaeobiogeographic affinities of Australian Cambrian faunas. In Wright, A. J., Young, G. C., Talent, J. A. & Laurie, J. R. (eds.) *Memoirs of the Association of Australasian Palaeontologists*, **23**, 1–61. Sydney.

Broili, F. 1915. Archaeocyathinae. *In* Von Zittel, K. (ed.) *Grundzüge der paläontologie*, 4th ed. München, Berlin: Oldenbourg. 121 pp.
Brommer, A. 1998. Strukturelle entwicklung und petrogenese des nördlichen kristallingürtels der shackleton range, antarktis: proterozoische und ross-orogene krustendynamik am rand des ostantarktischen kratons. *Berichte zur Polarforschung* **290**, 1–184.
Brommer, A., Millar, I. L. & Zeh, A. 1999. Geochronology, structural geology and petrology of the northern La Grange nunataks, Shackleton Range, Antarctica. *Terra Antarctica* **6**, 269–78.
Buggisch, W., Kleinschmidt, G., Kreuzer, H. & Krumm, S. 1990. Stratigraphy, metamorphism and nappe-tectonics in the Shackleton Range (Antarctica). *Geodätische und geophysikalische Veröffentlichungen. Reihe I* **15**, 64–86.
Buggisch, W., Kleinschmidt, G., Höhndorf, A. & Pohl, J. 1994a. Stratigraphy and facies of sediments and low-grade metasediments in; the Shackleton Range, Antarctica. *Porlarforschung* **63**, 9–32.
Buggisch, W., Kleinschmidt, G., Kreuzer, H. & Krumm, S. 1994b. Metamorphic and structural evolution of the southern Shackleton Range during the Ross orogeny. *Polarforschung* **63**, 133–56.
Buggisch, W., Höhndorf, A., Kreuzer, H., Paech, H.-J. & Weber, B. 1995a. Watts needle formation. *In* Thomson, J. W. & Thomson, M. R. A. (eds) *Geological map of Shackleton Range, Antarctica*. BAS GEOMAP Series, Sheet 4, 1:250.000, 29–34. Cambridge: British Antarctic Survey.
Buggisch, W., Höhndorf, A., Paech, H.-J., Kleinschmidt, G., Kreuzer, H. & Weber, B. 1995b. Stephenson bastion formation. *In* Thomson, J. W. & Thomson, M. R. A. (eds) *Geological map of Shackleton Range, Antarctica*. BAS GEOMAP Series, Sheet 4, 1:250.000, 35–37. Cambridge: British Antarctic Survey.
Buggisch, W., Bachtadse, V. & Henjes-Kunst, F. 1999. Lithostratigraphy, facies, geochronology and palaeomagnetic data from the Blaiklock Glacier Group, Shackleton Range, Antarctica. *Terra Antarctica* **6**, 229–39.
Buggisch, W. & Henjes-Kunst, F. 1999. Stratigraphy, facies, and provenance analyses of the lower Cambrian Mount Wegener Formation of the Shackleton Range, Antarctica. *Terra Antarctica* **6**, 211–28.
Buggisch, W. & Kleinschmidt, G. 1999. New evidence for nappe tectonics in the southern Shackleton Range, Antarctica. *Terra Antarctica* **6**, 203–10.
Buggisch, W. & Kleinschmidt, G. 2007. The Pan-African nappe tectonics in the Shackleton Range. *In* Cooper, A. K., Barrett, P. J., Storey, B., Stump, E. & Wise, W. and the 10th ISAES editorial team (eds) *Antarctica: a keystone in a changing world*. Proceedings of the 10th ISAES, USGS Open-File Report 2007–104, Short Research Paper 058.
Buggisch, W. & Webers, G. F. 1992. Facies of Cambrian carbonate rocks. Ellsworth Mountains, West Antarctica. *In* Webers, G. F., Craddock, C. and Splettstoesser. J. F., *Geology and paleontology of the Ellsworth Mountains, West Antarctica. Geological Society of America Memoire* **170**, 81–100.
Burgess, C. J. & Lammerink, W. 1979. Geology of the Shackleton Limestone (Cambrian) in the Byrd Glacier Area. *New Zealand Antarctic Record* **2**, 12–16.
Castillo, P., Fanning, C. M., Fernández, R., Poblete, F. & Hervé, F. 2017. Provenance and age constraints of Paleozoic siliciclastic rocks from the Ellsworth Mountains in West Antarctica, as determined by detrital zircon geochronology. *GSA Bulletin* **129**, 1568–84.
Choquette, P. W. & Pray, L. C. 1970. Geologic nomenclature and classification of porosity in sedimentary carbonates. *American Association of Petroleum Geologists, Bulletin* **54**, 207–50.
Clarkson, P. D. 1971. Shackleton Range geological survey 1970–1971. *Antarctic Journal of the United States* **6**, 121–22.
Clarkson, P. D. 1972. Geology of the Shackleton Range. *Bulletin British Antarctic Survey* **31**, 1–15.
Clarkson, P. D. 1982. Geology of the Shackleton Range: I. The Shackleton Range Metamorphic Complex. *Bulletin British Antarctic Survey* **51**, 257–83.
Clarkson, P. D. 1995. Introduction. *In* Thomson, J. W. & Thomson, M. R. A. (eds) *Geological map of Shackleton Range, Antarctica*. BAS GEOMAP Series, Sheet 4, 1:250.000, 1–7. Cambridge: British Antarctic Survey.
Clarkson, P. D., Tessensohn, F., Thomson, M. R. A., Belyatsky, B., Braun, H.-M., Buggisch, W., Grikurov, G. E., Hofmann, J., Höhndorf, A., Kamenev, E. N., Kameneva, G. J., Kleinschmidt G., Kreuzer, H., Leat P. T., Olesch, M., Paech, M.-J., Pankhurst, R. J., Peters, M., Roland, N. W., Schubert, W., Solov'ev, I. A., Spaeth, G., Techmer, K. S., Thomson, J. W., Weber, B., Weber, K. & King, S. 1995. *Geological map of Shackleton Range, Antarctica*. BAS GEOMAP Series, Sheet 4, 1:250.000, with supplementary text, 79 pp. Cambridge: British Antarctic Survey.
Clarkson, P. D. & Wyeth, R. 1983. Geology of the Shackleton Range: III. The Blaiklock Glacier Group. *Bulletin British Antarctic Survey* **53**, 233–44.
Claybourn, T. M., Jacquet, S. M., Skovsted, C., Topper, B., Holmer, T. P., & Brock, L. E. & A, G. 2019. Mollusks from the upper Shackleton Limestone (Cambrian Series 2) central Transantarctic Mountains, East Antarctica. *Journal of Palaeontology* **93**, 437–59.
Claybourn, T. M., Skovsted, Ch. B., Holmer, L. E., Pan, B., Myrow, P. M., Topper, T.P. & Brock, G. A. 2020. Brachiopods from the Byrd Group (Cambrian Series 2, Stage 4) central Transantarctic Mountains, East Antarctica: biostratigraphy, phylogeny and systematics. *Papers in Palaeontology* **6**, 349–83.
Claybourn, T. M., Skovsted, C. B., Betts, M. J., Holmer, L. E., Bassett-Butt, L. & Brock, G. A. 2021. Camenellan tommotiids from the Cambrian series 2 of East Antarctica: biostratigraphy, palaeobiogeography and systematics. *Acta Palaeontologica Polonica* **66**, 207–29.
Cohen, K. M., Finney, S. C., Gibbard, P. L. & Fan, J.-X. 2013. The ICS international chronostratigraphic chart. *Episodes* **36**, 199–204.
Cooper, R. A. & Shergold, J. H. 1991. Palaeozoic invertebrates of Antarctica. *In* Tingey, R. J. (ed.) *Geology of Antarctica*, 455–86. Oxford: Blackwell.
Cordie, D. R. & Dornbos, S. Q. 2019. Restricted morphospace occupancy of early Cambrian reef-building archaeocyaths. *Paleobiology* **45**, 331–46.
Curtis, M. L., Millar, I. L., Storey, B. C. & Fanning, M. 2004. Structural and geochronological constraints of early Ross orogenic deformation in the Pensacola Mountains. *Antarctica. GSA Bulletin* **116**, 619–36.
Curtis, M. L. & Storey, B. C. 2003. Early Palaeozoic near-surface deformation in the Neptune range, Antarctica: implications for the Ross and Gondwanian orogenies. *Journal of the Geological Society* **160**, 629–42.
Daily, B. 1973. Discovery and significance of basal Uratanna Formation, Mt Scott range, Flinders Ranges, South Australia. *Search* **4**, 202–05.
Dalziel, I. W. D. & Elliot, D. H. 1982. West Antarctica: problem child of Gondwanaland. *Tectonics* **1**, 3–19.
David, T. W. E. & Priestley, R. E. 1914. Glaciology, physiography, stratigraphy, and tectonic geology of south Victoria land, with short notes on paleontology by T. Griffith Taylor. *British Antarctic Expedition (1907–1909) Geology* **1**, 1–319.
Daye, M., Higgins, J. & Bosak, T. 2019. Formation of ordered dolomite in anaerobic photosynthetic biofilms. *Geology* **47**, 509–12.
Debrenne, F. 1958. Sur quelques archaeocyatha du jebel taïssa (Anti-Atlas occidental). *Service des Mines et de Carte Géologique du Maroc, Notes et Mémoires* **16**, 59–67.
Debrenne, F. 1969. Lower Cambrian Archaeocyatha from the Ajax mine, Beltana, south Australia. *Bulletin of the British Museum (Natural History), Geology Series* **17**, 295–376.
Debrenne, F. 1970. A revision of Australian genera of Archaeocyatha. *Royal Society of South Australia, Transactions* **94**, 21–48.
Debrenne, F. 1973. Modifications de la porosité primaire de la muraille externe chez les archéocyathes réguliers. *Annales de Paléontologie (Invertébrés)* **59**, 3–24.
Debrenne, F. 1974a (1973) Les archéocyathes irréguliers d'Ajax mine (Cambrien inférieur, Australie du Sud). *Bulletin du Muséum National d'Histoire Naturelle (Série 3)* **195**, 185–258.
Debrenne, F. 1974b. Anatomie et systématique des archéocyathes réguliers sans plancher d'Ajax mine (Cambrien inférieur, Australie du Sud). *Geobios* **7**, 91–138.
Debrenne, F. 1974c. K revizii roda *Paranacyathus* Bedford, R. et Bedford, W.R., 1937 [On the revision of the genus *Paranacyathus* Bedford, R. et Bedford, W.R., 1937]. *In* Zhuravleva, I. T. & Rozanov, A. Yu (eds) *Biostratigrafiya i paleontologiya nizhnego kembriya evropy i severnoy azii* [*Lower Cambrian biostratigraphy and paleontology of Europe and Northern Asia*], 167–78. Moscow: Nauka. [In Russian.]
Debrenne, F. 1975. Archaeocyatha provenant de blocs erratiques des tillites de dwyka (Afrique du Sud). *Annals of the South African Museum* **67**, 331–61.
Debrenne, F. 1992. The archaeocyathan fauna from the whiteout conglomerate, Ellsworth Mountains, west Antarctica. *Geological Society of America, Memoir* **170**, 279–84.
Debrenne, F. 2007. Lower Cambrian archaeocyathan bioconstructions. *Comptes Rendus Palevol* **6**, 5–19.
Debrenne, F., Lafuste, J. & Gangloff, R. 1981. Microstructure of *Tabulaconus* and its significance to the taxonomy of early Phanerozoic organisms. *In* Taylor, M. E. (ed.) *Short papers for the Second International Symposium on the Cambrian System.* Open-File Report 81–743, 64.
Debrenne, F., Rozanov, A. Y. & Webers, G. F. 1984. Upper Cambrian Archaeocyatha from Antarctica. *Geological Magazine* **121**, 291–99.
Debrenne, F., Gangloff, R. & Lafuste, J. 1987. *Tabulaconus* handfield: microstructure and its implications in the taxonomy of primitive corals. *Journal of Paleontology* **61**, 1–9.
Debrenne, F., Zhuravlev, A. Y. & Rozanov, A. Y. 1988. Novye rody pravil'nykh dnishchevykh i odnokamernykh arkheotsiat iz nizhnego

kembriya sibiri [New genera of regular tabulate and single-chambered archaeocyaths from the lower Cambrian of Siberia]. *Paleontologicheskiy Zhurnal* **4**, 97–99. [In Russian.]
Debrenne, F., Zhuravlev, A. Y. & Rozanov, A. Y. 1989. *Pravilnye arkheotsiaty* [*Regular archaeocyaths*], 198 pp. Moscow: Paleontologicheskiy Institut, Akademiya Nauk SSSR, Trudy 233. [In Russian.]
Debrenne, F., Zhuravlev, A. Y. & Kruse, P. D. 2002. Class archaeocyatha bornemann, 1884. *In* Hooper, J. N. A. & van Soest, R. W. M. (eds) *Systema Porifera. A Guide to the classification of Sponges* **2**, 1539–1699. New York: Kluver Academic/Plenum Publishers.
Debrenne, F., Zhuravlev, A. Y. & Kruse, P. D. 2012. Part E, revised, volume, chapter 19. *Systematic descriptions: Archaeocyatha. Treatise Online* **50**, 1–186. Lawrence, Kansas: The University of Kansas. Paleontological Institute.
Debrenne, F., Zhuravlev, A. Y. & Kruse, P. D. 2015. Systematic descriptions: Archaeocyatha. *In* Selden, P. A. (ed.) *Treatise on invertebrate paleontology. Part E (revised) Porifera* **5**, 923–1084. Lawrence, Kansas: The University of Kansas. Paleontological Institute.
Debrenne, F. & Debrenne, M. 1960. Révision de la collection T. H. Ting d'Archaeocyatha conservée au Musee de Marburg (Allemagne). *Société Géologique de France, Bulletin* **2**, 695–706.
Debrenne, F. & Gravestock, D. I. 1991. Archaeocyaths from the Sellick Hill Formation and Fork Tree Limestone on Fleurieu Peninsula, South Australia. *Geological Society of Australia Special Publication* **16**, 292–309.
Debrenne, F. & Kruse, P. D. 1986. Shackleton limestone archaeocyaths. *Alcheringa* **10**, 235–78.
Debrenne, F. & Kruse, P. D. 1989. Cambrian Antarctic archaeocyaths. *The Geological Society of London. Special Publication* **47**, 15–28.
Debrenne, F. & Zhuravlev, A. Y. 1990. New irregular archaeocyath taxa. *Geobios* **23**, 299–305.
Debrenne, F. & Zhuravlev, A. Y. 1992. *Irregular archaeocyaths.* Éditions du Centre National de la Recherche Scientifique, Cahiers de Paléontologie, Paris, 212 pp.
Debrenne, F. & Zhuravlev, A. Y. 1997. Cambrian food web: a brief review. *Geobios* **30**, 181–88.
Dickson, J. A. D. 1965. A modified staining technique for carbonates in thin section. *Nature* **205**, 587.
Dickson, J. A. D. 1966. Carbonate identification and genesis as revealed by staining. *Journal of Sedimentary Petrology* **36**, 491–505.
Dilliard, K. A., Pope, M. C., Coniglio, M., Hasiotis, S. T. & Lieberman, B. S. 2007. Stable isotope geochemistry of the lower Cambrian Sekwi formation, Northwest Territories, Canada: implications for ocean chemistry and secular curve generation. *Palaeogeography, Palaeoclimatology, Palaeoecology* **256**, 174–94.
DiLoreto, Z. A., Bontognali, T. R. R., Al Disi, Z. A., Al-Kuwari, H. A. S., Williford, K. H., Strohmenger, C. J., Sadooni, F., Palermo, C., Rivers, J. M., McKenzie, J. A., Tuite, M. & Dittrich, M. 2019. Microbial community composition and dolomite formation in the hypersaline microbial mats of the Khor Al-Adaid Sabkhas, Qatar. *Extremophiles* **23**, 201–18.
Duguid, S. M. A., Kurtis Kyser, T., James, N. P. & Rankey, E. C. 2010. Microbes and ooids. *Journal of Sedimentary Research* **80**, 236–51.
Dunham, R. J.. 1962. Classification of carbonate rocks according to their depositional texture. *American Association of Petroleum Geologists Memoir* **1**, 108–21.
Dunham, R. J. 1971. Meniscus cement. *In* Bricker, O. P. (ed.) *Carbonate cements studies in geology* **19**, 297–300. Baltimore: Johns Hopkins, University Press.
Ehrenberg, C. G. 1834. Dritter beitrag zur erkenntniss grosser organisation in der richtung des kleinsten raumes. *Abhandlungen der Königlichen Akademie der Wissenschaften zu Berlin* **1833**, 145–336.
Embry, A. F. & Klovan, J. E. 1971. A late Devonian reef tract on northeastern Banks Island, N.W.T. *Bulletin of Canadian Petroleum Geology* **19**, 730–81.
Etheridge, R. Jr. 1890. On some Australian species of the family Archaeocyathinae. *Royal Society of South Australia, Transactions* **13**, 10–22.
Evans, K. R., Rowell, A. J. & Rees, M. N. 1995. Sea-level changes and stratigraphy of the Nelson Limestone (Middle Cambrian), Neptune Range, Antarctica. *Journal of Sedimentary Research* **B65**, 32–43.
Evans, K. R., Mckenna III, L.W., Lieberman, B. S., Weichert, W. D. & Macleod, K. G. 2018. Geology of the Nelson Limestone, Postel Nunatak, Patuxent Range, Antarctica. *Antarctic Science* **30**, 29–43.
Ferrill, D. A., Morris, A. P., Evans, M. A., Burkhard, M., Groshong, R. H. & Onasch, C. M. 2004. Calcite twin morphology: a low-temperature deformation geothermometer. *Journal of Structural Geology* **26**, 1521–29.
Fitzsimons, I. C. W. 2000. Grenville-age basement provinces in East Antarctica: evidence for three separate collisional orogens. *Geology* **28**, 879–82.
Flügel, E. 2004. *Microfacies of carbonate rocks. Analysis, interpretation and application*. 976 pp. Berlin: Springer-Verlag.
Folk, R. L.. 1962. Spectral subdivision of limestone types. *American Association of Petroleum Geologists Memoir* **1**, 62–84.
Fritz, W. H. 1972. Lower Cambrian trilobites from the Sekwi Formation type section, Mackenzie Mountains, northwestern Canada. *Geological Survey of Canada Bulletin* **212**, 1–90.
Gandin, A. & Debrenne, F. 2010. Distribution of the archaeocyath-calcimicrobial bioconstructions on the early Cambrian shelves. *Paleoworld* **19**, 222–41.
Geyer, G. 2019. A comprehensive Cambrian correlation chart. *Episodes* **42**, 321–31.
Golovanov, N. P., Milstein, V. E., Mikhailov, V. M. & Shulyatin, O. G. 1979. Stromatolity i mikrofitolity khrebta shekltona (zapadnaya Antarktida) [Stromatolites and microphytolites of the Shackleton Range (West Antarctica)]. *Doklady Akademii Nauk SSSR* **249**, 977–79. [In Russian.]
Golovanov, N. P., Mikhailov, V. M. & Shulyatin, O. G. 1980. Pervie diagnostiruemie stromatoliti antarktidi i ich biostratigraficheskoe znachenie [First diagnostic stromatolites from Antarctica and their biostratigraphical significance]. *Antarktika* **19**, 152–59. [In Russian.]
Golynsky, A. V., Ferraccioli, F., Hong, J. K., Golynsky, D. A., von Frese, R. R. B., Young, D. A., Blankenship, D., Holt, J. W., Ivanov, S. V., Kiselev, A. V., Masolov, V. N., Eagles, G., Gohl, K., Jokat, W., Damaske, D., Finn, C., Aitken, A., Bell, R. E., Armadillo, E., Jordan, T. A., Greenbaum, J. S., Bozzo, E., Caneva, G., Forsberg, R., Ghidella, M., Galindo-Zaldivar, J., Bohoyo, F., Martos, Y. M., Nogi, Y., Quartini, E., Kim, H. R. & Roberts, J. L. 2018. New magnetic anomaly map of the Antarctic. *Geophysical Research Letters* **45**, 6437–49.
González, P. D., Tortello, M. F. & Damborenea, S. E. 2011. Early Cambrian archaeocyathan limestone blocks in low grade metaconglomerate from El Jagüelito Formation (Sierra Grande, Río Negro, Argentina). *Geologica Acta* **9**, 159–73.
González, P. D., Tortello, M. F., Damborenea, S. E., Naipauer, M., Sato, A. M. & Varela, R. 2013. Archaeocyaths from South America: review and a new record. In: *Lower Palaeozoic fossils, biostratigraphy and events from western Gondwana. Geological Journal, Special Issue* **48**, 114–25.
Goodge, J. W. 2020. Geological and tectonic evolution of the Transantarctic Mountains, from ancient craton to recent enigma. *Gondwana Research* **80**, 50–122.
Goodge, J. W., Myrow, P., Williams, I. S. & Bowring, S. 2002. Age and provenance of the Beardmore Group, Antarctica: constraints on Rodinia supercontinent breakup. *Journal of Geology* **110**, 393–406.
Goodge, J. W., Myrow, P., Phillips, D., Fanning, C. M. & Williams, I. S. 2004b. Siliciclastic record of rapid denudation in response to convergent-margin orogenesis, Ross orogen, Antarctica. *Geological Society of America, Special Paper* **378**, 105–26.
Goodge, J. W., Williams, I. S. & Myrow, P. 2004a. Provenance of Neoproterozoic and lower Paleozoic siliciclastic rocks of the central Ross Orogen, Antarctica: detrital record of rift-, passive-, and active-margin sedimentation. *GSA Bulletin* **116**, 1253–79.
Gordey, S. P. & Anderson, R. G. 1993. Evolution of the northern Cordillera and miogeocline, Nahanni map area (105–I), Yukon and northwest territories. *Geological Survey of Canada Memoir* **428**, 1–214.
Gordon, W. T. 1920. Scottish National Antarctic expedition 1902–1904: Cambrian organic remains from a dredging in the Weddell Sea. *Royal Society of Edinburgh, Transactions* **52**, 681–714.
Grant, R. E. 1836. Animal kingdom. *In* Todd, R. B. (ed.) *The cyclopaedia of anatomy and physiology* **1**, 107–18. London: Sherwood, Gilbert and Piper.
Gravestock, D. I. 1984. Archaeocyatha from lower parts of the lower Cambrian carbonate sequence in South Australia. *Memoirs of the Association of Australasian Palaeontologists* **2**, 1–139.
Gravestock, D. I., Alexander, E. M., Demidenko, Y., Esakova, E., Holmer, N. V., Jago, L. E., Lin, J. B., Melnikova, T., Parkhaev, L. M., Rozanov, P., Yu, A., Ushatinskaya, G. T., Zang, W.-L., Zhegallo, E. A. & Zhuravlev, A. Y. 2001. *The Cambrian biostratigraphy of the Stansbury Basin, South Australia. Transactions of the Palaeontological Institute* **282**, 1–344.
Grunow, A., Hanson, R. & Wilson, T. 1996. Were aspects of Pan-African deformation linked to Iapetus opening? *Geology* **24**, 1063–66.
Handfield, R. C. 1969. Early Cambrian coral-like fossils from the northern Cordillera of western Canada. *Canadian Journal of Earth Sciences* **6**, 782–85.
Handfield, R. C. 1971. Archaeocyatha from the Mackenzie and Cassiar mountains, Northwest Territories, Yukon Territory and British Columbia. *Geological Survey of Canada, Bulletin* **201**, 1–119.
Harvey, T. H. P., Williams, M., Condon, D. J., Wilby, P. R., Siveter, D. J., Rushton, A. W. A., Leng, M. J. & Gabbott, S. E. 2011. A refined chronology for the Cambrian succession of southern Britain. *Journal of the Geological Society* **168**, 705–16.

He, T., Zhu, M., Mills, B. J. W., Wyn, P. M., Zhuravlev, A. Y., Tostevin, R., Pogge von Strandmann, P. A. E., Yang, A., Poulton, S. W. & Shields, G. A. 2019. Possible links between extreme oxygen perturbations and the Cambrian radiation of animals. *Nature Geoscience* **12**, 468–74.

Henderson, R. A., Debrenne, F., Rowell, A. J. & Webers, G. F. 1992. Brachiopods, archaeocyathids and pelmatozoa from the Minaret Formation of the Ellsworth Mountains, West Antarctica. *In* Webers, G. F., Craddock, C. & Splettstoesser, J. F. (eds) *Geology and paleontology of the Ellsworth Mountains, West Antarctica*. Geological Society of America, Memoir **170**, 249–63. Boulder, Colorado: The Geological Society of America.

Herbosch, A. & Verniers, J. 2011. What is the biostratigraphic value of the ichnofossil *Oldhamia* for the Cambrian: a review. *Geologica Belgica* **14**, 229–48.

Hesse, R. 1989. Silica diagenesis: origin of inorganic and replacement cherts. *Earth-Science Reviews* **26**, 253–84.

Hill, D. 1964a. Archaeocyatha from loose material at Plunket Point at the head of Beardmore glacier. *In* Adie, R. J. (ed.) *Antarctic geology*, 609–22. Amsterdam: North Holland Publishing.

Hill, D. 1964b. Archaeocyatha from the Shackleton Limestone of the Ross System, Nimrod Glacier Area, Antarctica. *Transactions of the Royal Society of New Zealand, Geology* **2**, 137–46.

Hill, D. 1965. Archaeocyatha from Antarctica and a review of the phylum. *Trans-Antarctic Expedition 1955–1958, Scientific Reports* **10**, 1–151.

Hinde, G. J. 1889. On *Archaeocyathus*, billings, and on other genera, allied to or associated with it, from the Cambrian strata of North America, Spain, Sardinia, and Scotland. *Quarterly Journal of the Geological Society, London* **45**, 125–48.

Höfle, H.-C. & Buggisch, W. 1995. Glacial geology and petrography of erratics in the Shackleton Range. *Antarctica. Polarforschung* **63**, 183–201.

Hofmann, J., Kaiser, G., Klemm, W. & Paech, H.-J. 1980. K/Ar- Alter von doleriten und metamorphiten der shackleton range und der whichaway-nunataks, Ost- un südostumrandung des filchner-eisschelfs (Antarktis). *Zeitschrift für geologische Wissenschaften* **8**, 1227–32.

Holmer, L., Popov, L., Koneva, S. & Bassett, M. 2001. Cambrian–Early Ordovician brachiopods from Malyi Karatau, the western Balkhash region and Tien Shan, Central Asia. *Special Papers in Palaeontology* **65**, 1–180.

Hood, A. V. S. & Wallace, M. W. 2018. Neoproterozoic marine carbonates and their paleoceanographic significance. *Global and Planetary Change* **160**, 28–45.

Hotten, R. 1993. Die mafischen gange der Shackleton Range/Antarktika: petrographie, geochemie, isotopengeochemie und paläomagnetik. *Berichte zur Polarforschung* **118**, 1–225.

Hu, Y., Cai, C., Liu, D., Pederson, C. L., Jiang, L., Shen, A. & Immenhauser, A. 2020. Formation, diagenesis and palaeoenvironmental significance of upper Ediacaran fibrous dolomite cements. *Sedimentology* **67**, 1161–87.

Illing, L. V. 1954. Bahaman calcareous sands. *AAPG Bulletin* **38**, 1–95.

Jackson, I. S. C. & Claybourn, T. M. 2018. Morphometric analysis of inter- and intraspecific variation in the Cambrian series 2, stages 3–4 helcionelloid mollusc *Mackinnonia*. *Palaeontology* **61**, 761–73.

Jacobs, J., Fanning, C. M., Henjes-Kunst, F., Olesch, M. & Paech, H.-J. 1998. Continuation of the Mozambique belt into East Antarctica: Grenville-age metamorphism and polyphase Pan-African high-grade events in central Dronning Maud Land. *Journal of Geology* **106**, 385–406.

Jacobs, J., Fanning, C. M. & Bauer, W. 2003. Timing of Grenville-age vs. Pan-African medium- to high-grade metamorphism in western Dronning Maud Land (East Antarctica) and significance for correlations in Rodinia and Gondwana. *Precambrian Research* **125**, 1–20.

Jacobs, J., Opås, B., Elburg, M. A., Läufer, A., Estrada, S., Ksienzyk, A. K., Damaske, D. & Hofmann, M. 2017. Cryptic sub-ice geology revealed by a U-Pb zircon study of glacial till in Dronning Maud Land, East Antarctica. *Precambrian Research* **294**, 1–14.

Jago, J. B., Zang, W. L., Sun, X., Brock, G. A., Paterson, J. R. & Skovsted, C. B. 2006. A review of the Cambrian biostratigraphy of South Australia. *Palaeoworld* **15**, 406–23.

Jago, J. B., Gehling, J. G., Paterson, J. R., Brock, G. A. & Zang, W. 2012. Cambrian stratigraphy and biostratigraphy of the Flinders Ranges and the north coast of Kangaroo Island, South Australia. *Episodes* **35**, 247–55.

Jago, J. B., Gehling, J. G., Betts, M. J., Brock, G. A., Dalgarno, C. R., García-Bellido, D. C., Haslett, P. G., Jacquet, S. M., Kruse, P. D., Langsford, N. R., Mount, T. J. & Paterson, J. R. 2020. The Cambrian system in the Arrowie Basin, Flinders Ranges, South Australia. *Australian Journal of Earth Sciences* **67**, 923–48.

Jordan, T. A., Ferraccioli, F. & Leat, P. T. 2017. New geophysical compilations link crustal block motion to Jurassic extension and strike-slip faulting in the Weddell Sea rift system of West Antarctica. *Gondwana Research* **42**, 29–48.

Jordan, T. A., Riley, T. R. & Siddoway, C. S. 2020. The geological history and evolution of West Antarctica. *Nature Reviews Earth & Environment* **1**, 117–33.

Kerr, A. & Hermichen, W. D. 1999. Glacial modification of the Shackleton Range, Antarctica. *Terra Antarctica* **6**, 353–60.

Kleinschmidt, G. 2007. Shackleton Range. *In* Riffenburgh, B. (ed.) *Encyclopedia of the Antarctic* **1**, 890–91. New York and London: Taylor and Francis Group.

Kleinschmidt, G., Henjes-Kunst, F. & Tessensohn, F. 2001. Nappe tectonics in the central Shackleton Range, Antarctica. *Zeitschrift der Deutschen Geologischen Gesellschaft* **152**, 227–48.

Kleinschmidt, G., Buggisch, W., Läufer, A. L., Helferich, S. & Tessensohn, F. 2002. The 'Ross' orogenic structures in the Shackleton Range and their meaning for Antarctica. *In* Gamble, J. A., Skinner, D. N. B. & Henrys, S. (eds) *Antarctica at the close of a millennium*. Proceedings of 8th International Symposium on Antarctic Earth Sciences (ISAES) 35, 75–83. Wellington: The Royal Society of New Zealand.

Kleinschmidt, G. & Boger, S. D. 2009. The Bertrab, Littlewood and Moltke nunataks of Prinz-Regent-Luitpold-Land (Coats Land) enigma of East Antarctic geology. *Polarforschung* **78**, 95–104.

Kleinschmidt, G. & Buggisch, W. 1994. Plate tectonic implications of the structure of the Shackleton Range Antarctica. *Polarforschung* **63**, 57–62.

Konyushkov, K. N. & Shulyatin, O. G. 1980. Ob arkheotsiatakh antarktidy i ikh sopostavlenii s arkheotsiatami sibiri [On the archaeocyaths of Antarctica and their comparison with the archaeocyaths of siberia]. *In* Zhuravleva, I. T. (ed.) *Kembriy Altae–Sayanskoy skladchatoy, oblasti* [*Cambrian of the Altay-Sayan fold belt*], 143–50. Moscow: Nauka. [In Russian.]

Krohne, N., Lisker, F., Kleinschmidt, G., Klügel, A., Läufers, A., Estrada, S. & Spiegel, C. 2016. The Shackleton Range (East Antarctica): an alien block at the rim of Gondwana? *Geological Magazine* **155**, 841–64.

Kruse, P. D. 1978. New Archaeocyatha from the early Cambrian of the Mt Wright area, New South Wales. *Alcheringa* **2**, 27–47.

Kruse, P. D. 1982. Archaeocyathan biostratigraphy of the Gnalta Group at Mt. Wright, New South Wales. *Palaeontographica A* **177**, 129–212.

Kruse, P. D. & West, P. W. 1980. Archaeocyatha of the Amadeus and Georgina Basins. *BMR Journal of Australian Geology and Geophysics* **5**, 165–181.

Kruse, P. D., Zhuravlev, A. Y., Parkhaev, P. Y. & Zhu, M. 2017. Comment: a new lower Cambrian shelly fossil biostratigraphy for South Australia by Marissa J. Betts, John R. Paterson, James B. Jago, Sarah M. Jacquet, Christian B. Skovsted, Timothy P. Topper & Glenn A. Brock. *Gondwana Research* **44**, 258–61.

Kruse, P. D. & Debrenne, F. 2020. Ajax mine archaeocyaths: a provisional biozonation for the Upper Hawker Group (Cambrian stages 3–4), Flinders Ranges, South Australia. *Australasian Palaeontological Memoirs* **53**, 1–238.

Kruse P. D. & Jago, J. B. (eds) 2016. *Palaeo down under* 2. *Geological field excursion guide: Cryogenian-Ediacaran–Cambrian of the Adelaide Fold Belt*. Report Book 2016/00011. Department of State Development, South Australia, Adelaide.

Kruse, P. D. & Moreno-Eiris, E. 2013. Archaeocyaths of the White Point Conglomerate, Kangaroo Island, South Australia. *Alcheringa* **38**, 1–64.

Lafuste, J., Debrenne, F., Gandin, A. & Gravestock, D. 1991. The oldest tabulate coral and the associated Archaeocyatha, lower Cambrian, Flinders Ranges, South Australia. *Geobios* **24**, 697–718.

Laird, M. G. 1963. Geomorphology and stratigraphy of the Nimrod Glacier–Beaumont Bay region, southern Victoria land, Antarctica. *New Zealand Journal of Geology and Geophysics* **6**, 465–84.

Laird, M. G., Mansergh, G. D. & Chappell, J. M. A. 1971. Geology of the central Nimrod Glacier Area, Antarctica. *New Zealand Journal of Geology and Geophysics* **14**, 427–68.

Latif, K., Xiao, E., Riaz, M. & Hussein, A. A. A. 2019. Calcified cyanobacteria fossils from the Leiolitic bioherm in the Furongian Changshan Formation, Datong (North China Platform). *Carbonates and Evaporites* **34**, 825–43.

Lee, J.-H., Lee, H. S., Chen, J., Woo, J. & Chough, S. K. 2014. Calcified microbial reefs in Cambrian series 2, north China platform: implications for the evolution of Cambrian calcified microbes. *Palaeogeography, Palaeoclimatology, Palaeoecology* **403**, 30–42.

Lehrmann, D. J., Minzoni, M., Li, X., Yu, M., Payne, J. L., Schaal, B. M. K. & Enos, P. 2012. Lower Triassic oolites of the Nanpanjiang Basin, South China: facies architecture, giant ooids, and diagenesis – implications for hydrocarbon reservoirs. *AAPG Bulletin* **96**, 1389–414.

Lieberman, B. S. 2004. Revised biostratigraphy, systematics and paleobiogeography of the trilobites from the middle Cambrian Nelson Limestone, Antarctica. *The University of Kansas, Paleontological Contributions* **14**, 1–23.

Lisker, F., Schäfer, T. & Olesch, M. 1999. The uplift/denudation history of the Shackleton Range (Antarctica) based on fission-track analyses. *Terra Antarctica* **6**, 345–52.

Liu, L. J., Wu, Y. S., Jiang, H. X., Wu, N. Q. & Jia, L. Q. 2017. Paleoenvironmental distribution of Ordovician calcimicrobial associations in the Tarim Basin, northwest China. *Palaios* **32**, 462–89.

Liu, L., Liang, L., Wu, Y., Zhou, X., Jia, L. & Riding, R. 2020. Ordovician cyanobacterial calcification: a marine fossil proxy for atmospheric CO_2. *Earth and Planetary Science Letters* **530**, 115950.

Liu, W. & Zhang, X. 2012. *Girvanella*-coated grains from Cambrian oolitic limestone. *Facies* **58**, 779–87.

Loewy, S. L., Dalziel, I. W. D., Pisarevsky, S., Connelly, J. N., Tait, J., Hanson, R. E. & Bullen, D. 2011. Coats land crustal block, east Antarctica: a tectonic tracer for Laurentia?. *Geology* **39**, 859–62.

Longman, M. W. 1980. Carbonate diagenetic textures from near-surface diagenetic environments. *AAPG Bulletin* **64**, 461–87.

Luchinina, V. A. 2013. Cambrian algoflora: association of various microorganism groups. *Paleontological Journal* **47**, 989–96.

Machel, H. G. 2004. Concepts and models of dolomitization: a critical reappraisal. *Geological Society London Special Publications* **235**, 7–63.

MacNaughton, R. B., Moynihan, D. P., Roots, C. F. & Crowley, J. L. 2016. New occurrences of *Oldhamia* in eastern Yukon, Canada: stratigraphic context and implications for Cambrian deep-marine biostratigraphy. *Ichnos* **23**, 33–52.

Mángano, M. G. & Buatois, L. A. 2016. The Cambrian explosion. *In* Mángano, M. & Buatois, L. (eds) *The trace-fossil record of major evolutionary events. Topics in Geobiology* **39**, 73–126. Dordrecht: Springer-Verlag.

Mansy, J. L., Debrenne, F. & Zhuravlev, A. Y. 1993. Calcaires à archéocyathes du cambrien inférieur du nord de la colombie britannique (Canada). Implications paléogéographiques et précisions sur l'extension du continent américano-koryakien. *Geobios* **26**, 643–83.

Margolix, S. & Rex, R. 1971. Endolithic algae and micrite envelope formation in Bahamian oolites as revealed by scanning electron microscopy. *GSA Bulletin* **82**, 843–52.

Marsh, P. D. 1983. The late Precambrian and early Palaeozoic history of the Shackleton Range, Coats Land. *In* Oliver, R. L., James, P. R. & Jago, J. B. (eds) *Antarctic earth science*, 190–93. Canberra and Cambridge: Australian Academy of Science & Cambridge University Press.

Marsh, P. D. 1985. Ice surface and bedrock topography in coats land and part of Dronning Maud Land, Antarctica, from satellite imagery. *British Antarctic Survey Bulletin* **68**, 19–36.

Matsch, C. L. & Ojakangas, R. W. 1992. Stratigraphy and sedimentology of the Whiteout Conglomerate, an upper Paleozoic glacigenic unit, Ellsworth Mountains, West Antarctica. *In* Webers, G. F., Craddock, C. & Splettstoesser, J. F. (eds) *Geology and paleontology of the Ellsworth Mountains, West Antarctica. Geological Society of America Memoir* **170**, 37–62. Boulder, Colorado: The Geological Society of America.

Mazzullo, S. J. 2000. Organogenic dolomitization in peritidal to deep sea sediments. *Journal of Sedimentary Research* **70**, 10–23.

McMenamin, M. A. S., Debrenne, F. & Zhuravlev, A. Y. 2000. Early Cambrian Appalachian archaeocyaths: further age constraints from the fauna of New Jersey and Virginia, U.S.A. *Geobios* **33**, 693–708.

Medwedeff, D. A. & Wilkinson, B. H. 1983. Cortical fabric in calcite and aragonite ooids. *In* Peryt, T. (ed.) *Coated grains*, 109–15. Berlin: Springer-Verlag.

Merdith, A. S., Collins, A. S., Williams, S. E., Pisarevsky, S., Foden, J. D., Archibald, D. B., Blades, M. L., Alessio, B. L., Armistead, S., Plavsa, D., Clark, C. & Müller, R. D. 2017. A full-plate global reconstruction of the Neoproterozoic. *Gondwana Research* **50**, 84–134.

Millar, I. L. & Storey, B. C. 1995. Early Palaeozoic rather than Neoproterozoic volcanism and rifting within the Transantarctic Mountains. *Journal of the Geological Society* **152**, 417–20.

Morycowa, E., Rubinowski, Z. & Tokarski, A. K. 1982. Archaeocyathids from a moraine at Three Sisters Point, King George Island (South Shetland Islands, Antarctica). *Studia Geologica Polonica* **74**, 73–80.

Moyes, A. B., Groenewald, P. B. & Brown, R. W. 1993. Isotopic constraints on the age and origin of the Brattskarvet Intrusive Suite, Dronning Maud Land, Antarctica. *Chemical Geology* **106**, 453–66.

Myrow, P. M., Pope, M. C., Goodge, J. W., Fischer, W. & Palmer, A. R. 2002a. Depositional history of pre-Devonian strata and timing of ross Orogenic tectonism in the central Transantarctic Mountains, Antarctica. *Geological Society of America Bulletin* **114**, 1070–88.

Myrow, P. M., Fischer, W. & Goodge, J. W. 2002b. Wave-modified turbidites: combined-flow shoreline and shelf deposits, Cambrian, Antarctica. *Journal of Sedimentary Research* **72**, 641–56.

Noble, J. P. A. & Van Stempvoort, D. R. 1989. Early burial quartz authigenesis in Silurian platform carbonates, New Brunswick, Canada. *Journal of Sedimentary Research* **59**, 65–76.

Ogg, J. G., Ogg, G. M. & Gradstein, F. M. 2016. Cambrian. *In* Ogg, J. G., Ogg, G. M. & Gradstein, F. M. (eds) *A concise geologic time scale*, 41–55. Amsterdam: Elsevier.

Okulitch, V. J. 1935. Cyathospongia – a new class of Porifera to include the Archaeocyathinae. *Royal Society of Canada, Transactions (Series 3, Section 4)* **29**, 75–106.

Okulitch, V. J. 1937. Some changes in nomenclature of Archaeocyathi (Cyathospongia). *Journal of Paleontology* **11**, 251–52.

Olesch, M., Braun, H.-M., Kamenev, E. N., Kameneva, G. I. & Schubert, W. 1995. Read Group. *In* Thomson, J. W. & Thomson, M. R. A. (eds) *Geological map of Shackleton Range, Antarctica*, 8–13. BAS GEOMAP Series, Sheet 4, 1:250.000. Cambridge: British Antarctic Survey.

Paech, H. –J. 1982. Als geologe in den Read Mountains. In Lange, G. (ed.) *Bewährung in Antarktika, antarktisforschung der DDR*, 159–64. Leipzig: Brockhaus.

Palmer, A. R. & Gatehouse, C. G. 1972. Early and middle Cambrian trilobites from Antarctica. Contributions to the geology of Antarctica. *Geological Survey Professional Paper* **456–D**, 1–36.

Palmer, A. R. & Rowell, A. J. 1995. Early Cambrian trilobites from the Shackleton Limestone of the central Transantarctic Mountains. *Journal of Paleontology* **69**, 1–28.

Pankhurst, R. J., Marsh, P. D. & Clarkson, P. D. 1983. A geochronological investigation of the Shackleton Range. *In* Oliver, R. L., James, P. R. & Jago, J. B. (eds) *Antarctic earth sciences*, 176–82. Canberra and Cambridge: Australian Academy of Science & Cambridge University Press.

Pankhurst, R. J., Kreuzer, H., Höhndorf, A. & Belyatsky, B. 1985. Geochronology. *In* Thomson, J. W. & Thomson, M. R. A. (eds) *Geological map of Shackleton Range, Antarctica*, 53–56. BAS GEOMAP Series, Sheet 4, 1:250.000. Cambridge: British Antarctic Survey.

Paterson, J. R., Skovsted, C. B., Brock, G. A. & Jago, J. B. 2007. An early Cambrian faunule from the Koolywurtie Limestone Member (Parara Limestone), Yorke Peninsula, South Australia and its biostratigraphic significance. *Association of Australasian Palaeontologists, Memoir* **34**, 131–46.

Paxman, G. J. G., Jamieson, S. S. R., Ferraccioli, F., Bentley, M. J., Forsberg, R., Ross, N., Watts, A. B., Corr, H. F. J. & Jordan, T. A. 2017. Uplift and tilting of the Shackleton Range in east Antarctica driven by glacial erosion and normal faulting. *Journal of Geophysical Research Solid Earth* **122**, 2390–408.

Peng, S., Babcock, L. E. & Cooper, R. A. 2012. The Cambrian period. *In* Gradstein, F. M., Ogg, G. J., Schmitz, M. & Ogg, G. M. (eds) *The geologic time scale*, 437–88. Amsterdam: Elsevier.

Peng, S. & Robison, R. A. 2000. Agnostoid biostratigraphy across the middle-upper Cambrian boundary in Hunan, China. *Paleontological Society Memoir* **53**, 1–104.

Perejón, A., Moreno-Eiris, E. & Menéndez, S. 2008. Los arqueociatos del cámbrico Inferior de navalcastaño (Sierra Morena, Córdoba, España): sistemática y bioestratigrafía. *Boletín de la Real Sociedad Española de Historia Natural, Sección Geológica* **102**, 93–119.

Perejón, A., Rodríguez-Martínez, M., Moreno-Eiris, E., Menéndez, S. & Reitner, J. 2019. First microbial-archaeocyathan boundstone record from early Cambrian erratic cobbles in glacial diamictite deposits of Namibia (Dwyka Group, Carboniferous). *Journal of Systematic Palaeontology* **17**, 881–910.

Petrash, D. A., Bialik, O. M., Bontognali, T. R., Vasconcelos, C., Roberts, J. A., McKenzie, J. A. & Konhauser, K. O. 2017. Microbially catalyzed dolomite formation: from near-surface to burial. *Earth-Science Reviews* **171**, 558–82.

Pickering, K., Stow, D., Watson, M. & Hiscott, R. 1986. Deep-water facies, processes and models: a review and classification scheme for modern and ancient sediments. *Earth-Science Reviews* **23**, 75–175.

Pirie, J. H. H. 1913. Scottish National Antarctic expedition, 1902–04: deep-sea deposits. *Transactions of the Royal Society of Edinburgh*, **49**, 645–86.

Popov, L. E., Holmer, L. E., Hughes, N. C., Ghobadi Pour, M. & Myrow, P. M. 2015. Himalayan Cambrian brachiopods. *Papers in Palaeontology* **1**, 345–99.

Popov, L. E. & Solov'ev, I. A. 1981. Srednekembriyskie bezzamkovye brakhiopody, khantsellori, konikonkhii i trilobity zapadnoy antarktidy (khebty Sheklton i Ardzhentina) [Middle Cambrian inarticulate brachiopods, chancelloriids, hyolithids, and trilobites from West Antarctica (Shackleton and Argentina ranges)]. *Antarktika* **20**, 64–72. [In Russian.]

Pratt, B. 1984. *Epiphyton* and *Renalcis* – diagenetic microfossils from calcification of coccoid blue-green algae. *Journal of Sedimentary Petrology* **54**, 948–71.

Purdy, E. G. 1963a. Recent calcium carbonate facies of the Great Bahama Bank. 1. Petrography and reaction groups. *The Journal of Geology* **71**, 334–55.

Purdy, E. G. 1963b. Recent calcium carbonate facies of the Great Bahama Bank. 2. Sedimentary facies. *The Journal of Geology* **71**, 472–97.

Rees, M. N., Girty, G. H., Panttja, S. K. & Braddock, P. 1987. Multiple phases of early Paleozoic deformation in the central Transantarctic Mountains. *Antarctic Journal, Review* **22**, 33–35.

Rees, M. N., Pratt, B. R. & Rowell, A. J. 1989. Early Cambrian reefs, reef complexes, and associated lithofacies of the Shackleton Limestone, Transantarctic Mountains. *Sedimentology* **36**, 341–61.

Rees, M. N. & Rowell, A. J. 1991. The pre-Devonian Paleozoic clastics of the central Transantarctic Mountains: stratigraphy and depositional settings. *In* Thomson, M. R. A., Crame, J. A. & Thomson, J. W. (eds) *Geological evolution of Antarctica*, 187–92. Cambridge: Cambridge University Press.

Reid, R. P. & MacIntyre, I. G. 2000. Microboring versus recrystallization: further insight into the micritization process. *Journal of Sedimentary Research* **70**, 24–28.

Rex, D. C. 1972. K-Ar determinations on volcanics and associated rocks from the Antarctic Peninsula and Dronning Maud Land. *In* Adie, R. J. (ed.) *Antarctic geology and geophysics*, 133–36. Oslo: Universitetsforlaget.

Riding, R. 1991. Cambrian Calcareous cyanobacteria and algae. *In* Riding, R. (ed.) *Calcareous algae and stromatolites*, 305–34. Berlin: Springer-Verlag.

Riding, R. 2001. Calcified algae and bacteria. *In* Zhuravlev, A. Yu. & Riding, R. (eds) *Ecology of the Cambrian radiation*, 445–73. New York: Columbia University Press.

Rode, A., Lieberman, B. & Rowell, A. 2003. A new early Cambrian bradoriid (Arthropoda) from east Antarctica. *Journal of Paleontology* **77**, 691–97.

Roland, N. W., Braun, H. M., Hofman, J., Kamenev, E. N., Kamenenva, G. I., Kleischmidt, G., Olesch, M. & Paech, H.-J. 1995. Pioneers group. *In* Thomson, J. W. & Thomson, M. R. A. (eds) *Geological map of Shackleton Range, Antarctica*, 20–18. BAS GEOMAP Series, Sheet 4, 1:250.000. Cambridge: British Antarctic Survey.

Romer, T., Mezger, K. & Schmädicke, E. 2009. Pan-African eclogite facies metamorphism of ultramafic rocks in the Shackleton Range, Antarctica. *Journal of Metamorphic Geology* **27**, 335–47.

Rowell, A. J., Rees, M. N., Cooper, R. A. & Pratt, B. R. 1986. Early Paleozoic history of the central Transantarctic Mountains: evidence from the Holyoake Range, Antarctica. *Geological Society of America, Abstracts with Programs* **18**, 735.

Rowell, A. J., Rees, M. N., Cooper, R. A. & Pratt, B. R. 1988. Early Paleozoic history of the central Transantarctic Mountains: evidence from the Holyoake Range, Antarctica, New Zealand. *Journal of Geology and Geophysics* **31**, 397–404.

Rowell, A. J., Rees, M. N. & Evans, K. R. 1992a. Evidence of major middle Cambrian deformation in the ross orogen, Antarctica. *Geology* **20**, 31–34.

Rowell, A. J., Rees, M. N. & Evans, K. R. 1992b. Depositional setting of the lower and middle Cambrian in the Pensacola Mountains. *Antarctic Journal* **25**, 40–42.

Rowell, A. J., Van Schmus, W. R., Storey, B. C., Fetter, A. H. & Evans, K. R. 2001. Latest Neoproterozoic to Mid-Cambrian age for the main deformation phases of the Transantarctic Mountains: new stratigraphic and isotopic constraints from the Pensacola Mountains, Antarctica. *Journal of the Geological Society* **158**, 295–308.

Rowell, A. J. & Rees, M. N. 1989. Early Palaeozoic history of the Beardmore Glacier area: implications for a major Antarctic structural boundary within the Transantarctic Mountains. *Antarctic Science* **1**, 249–60.

Rowland, S. M. 2001. Archaeocyaths – a history of phylogenetic interpretation. *Journal of Paleontology* **75**, 1065–78.

Rozanov, A. Y. 1986. Problematica of the early Cambrian. *In* Hoffman, A. & Nitecki, M. H. (eds) *Problematic fossil taxa. Oxford Monographs on Geology and Geophysics* **5**, 87–96. New York: Oxford University Press.

Rozanov, A. Y. & Missarzhevskiy, V. V. 1966. Biostratigrafiya i fauna nizhnikh gorizontov kembriya [Biostratigraphy and fauna of the lower horizons of the Cambrian]. *Geologicheskiy Institut, Akademiya Nauk SSSR, Trudy* **148**, 1–126. [In Russian.]

Schmädicke, E. & Will, T. M. 2006. First evidence of eclogite facies metamorphism in the Shackleton Range, Antarctica: trace of a suture between east and west Gondwana. *Geology* **34**, 133–36.

Scholle, P. A. & Ulmer-Scholle, D. S. 2003. *A color guide to the petrography of carbonate rocks: grains, textures, porosity, diagenesis. AAPG Memoir* 77, 474 pp. Tulsa: American Association of Petroleum Geologists.

Schubert, W., Braun, H.-M., Kamenec, E. N. & Olesch, M. 1995. Stratton group. *In* Thomson, J. W. & Thomson, M. R. A. (eds) *Geological map of Shackleton Range, Antarctica*, 14–19. BAS GEOMAP Series, Sheet 4, 1:250.000. Cambridge: British Antarctic Survey.

Scrutton, C. T. 1979. Early fossil cnidarian. *In* House, M. R. (ed.) *The origin of major invertebrate groups. Systematics Association Special Publication* **12**, 161–207. London: Academic Press.

Shackleton, R. M. 1996. Precambrian collision tectonics in Africa. *Geological Society of London Special Publication* **76**, 345–62.

Sharp, W. E. 1965. The deposition of hydrothermal quartz and calcite. *Economic Geology* **60**, 1635–44.

Sibley, D. F. & Gregg, J. M. 1987. Classification of dolomite rocks textures. *Journal of Sedimentary Petrology* **57**, 967–75.

Skidmore, M. J. & Clarkson, P. D. 1972. Physiography and glacial geomorphology of the Shackleton Range. *British Antarctic Survey Bulletin* **30**, 69–80.

Skinner, D. N. B. 1964. A summary of the geology of the region between Byrd and Starshot glaciers, South Victoria Land. *In* Adie, R. J. (ed.) *Antartic geology*, 284–92. Amsterdam: North-Holland.

Skinner, D. N. B. 1965. Petrographic criteria of the rock units between the Byrd and Starshot glaciers, South Victoria Land, Antarctica. *New Zealand Journal of Geology and Geophysics* **8**, 292–303.

Solov'ev, I. A. & Grikurov, G. E. 1979. Novye dannye o rasprostanenii kembriyskikh trilobitov v khrebtakh ardzhentina i shekIton [New data on the distribution of Cambrian trilobites in the Argentina and Shackleton ranges]. *Antarktika, Doklady Komissii* **18**, 54–73.

Spaeth, G., Hotten, R., Peters, M. & Techmer, K. 1995. Mafic dikes in the Shackleton Range, Antarctica. *Polarforschung* **63**, 101–21.

Steinhoff, I. & Strohmenger, C. 1996. Zechstein 2 carbonate platform subfacies and grain-type distribution (upper Permian, Northwest Germany). *Facies* **35**, 105–32.

Stephens, N. & Sumner, D. Y. 2002. *Renalcis* as fossilized biofilm clusters. *Palaios* **17**, 225–36.

Stephenson, P. J. 1966. Geology. 1. Theron mountains, Shackleton Range and Wichaway nunataks. *Trans-Antarctic Expedition 1955–1958 Scientific Reports* **8**, 1–78.

Stone, P., Thomson, M. R. A. & Rushton, W. A. 2012. An early Cambrian archaeocyath-trilobite fauna in limestone erratics from the upper carboniferous Fitzroy Tillite Formation, Falkland Islands. *Earth and Environmental Science Transactions of the Royal Society of Edinburgh* **102**, 201–25.

Storey, B. C., Macdonald, D. I. M., Dalziel, I. W. D., Isbell, J. L. & Millar, I. L. 1996. Early Paleozoic sedimentation, magmatism, and deformation in the Pensacola Mountains, Antarctica: the significance of the ross orogeny. *GSA Bulletin* **108**, 685–707.

Sugden, D. E., Fogwill, C. J., Hein, A. S., Stuart, F. M., Kerr, A. R. & Kubik, P. W. 2014. Emergence of the Shackleton Range from beneath the Antarctic ice sheet due to glacial erosion. *Geomorphology* **208**, 190–99.

Sumner, D. Y. & Grotzinger, J. P. 1993. Numerical modeling of ooid size and the problem of Neoproterozoic giant ooids. *Journal of Sedimentary Petrology* **63**, 974–82.

Talarico, F., Kleinschmidt, G. & Henjes-Kunst, F. 1999. An ophiolitic complex in the northern Shackleton Range, Antarctica. *Terra Antarctica* **6**, 293–315.

Tan, Q., Shi, Z.-J., Tian, Y.-M., Wang, Y. & Wang, C.-C. 2018. Origin of ooids in ooidal-muddy laminites: a case study of the lower Cambrian Qingxudong Formation in the Sichuan Basin, South China. *Geological Journal* **53**, 1716–27.

Taylor, T. G. 1910. The Archaeocyathinae from the Cambrian of South Australia with an account of the morphology and affinities of the whole class. *Royal Society of South Australia, Memoirs* **2**, 55–188.

Tessensohn, F. 1997. Shackleton range, ross orogen and SWEAT hypothesis. *In* Ricci, C. A. (ed.) *The Antarctic region: geological evolution and processes*, 5–12. Siena: Terra Antarctica Publication.

Tessensohn, F., Kleinschmidt, G., Talarico, F., Buggisch, W., Brommer, A., Henjes-Kunst, F., Kroner, U., Millar, I. L. & Zeh, A. 1999a. Ross-age amalgamation of east and west Gondwana: evidence from the Shackleton Range, Antarctica. *Terra Antarctica* **6**, 317–25.

Tessensohn, F., Kleinschmidt, G. & Buggisch, W. 1999b. Permo-Carboniferous glacial beds in the Shackleton Range. *Terra Antarctica* **6**, 337–44.

Tessensohn, F. & Thomson, M. R. A. 1990. European Geological initiative for the Shackleton Range. *Antarctic Science* **2**, 265–66.

Thomson, M. R. A. 1972. Inarticulate Brachiopoda from the Shackleton Range and their stratigraphical significance. *British Antarctic Survey Bulletin* **31**, 17–20.

Thomson, M. R. A., Solov'ev, I. A. & Buggisch, W. 1995. Trilobite shales. *In* Thomson, J. W. & Thomson, M. R. A. (eds) *Geological map of Shackleton Range, Antarctica*, 42–44. BAS GEOMAP Series, Sheet 4, 1:250.000. Cambridge: British Antarctic Survey.

Thomson, M. R. A. & Weber, B. 1999. Discovery of an Ordovician invertebrate fauna in the Blaiklock Glacier Group, Shackleton Range, Antarctica. *Terra Antarctica* **6**, 241–48.

Ting, T. H. 1937. Revision der Archaeocyathinen. *Neues Jahrbuch für Geologie, Mineralogie und Paläontologie (Abteilung B)* **78**, 327–79.

Tingey, R. J. (ed.) 1991. *The geology of Antarctica*. Oxford Monographs on Geology and Geophysics 17, 680 pp. Oxford University Press.

Trower, E. J., Lamb, M. P. & Fischer, W. W. 2017. Experimental evidence that ooid size reflects a dynamic equilibrium between rapid precipitation and abrasion rates. *Earth and Planetary Science Letters* **468**, 112–18.

Tucker, M. E. 1992. The Precambrian–Cambrian boundary: seawater chemistry, ocean circulation and nutrient supply in metazoan evolution, extinction and biomineralization. *Journal of the Geological Society* **149**, 655–68.

Tucker, M. E. & Wright, V. P. 1990. *Carbonate sedimentology*. 482 pp. London: Blackwell Scientific Publications.

Van Schmus, W. R., McKenna, L. W., Gonzales, D. A. & Rowell, A. J. 1997. U/Pb geochronology of parts of the Pensacola, Harold Byrd, and Queen Maud Mountains, Antarctica. *In* Ricci, C. A. (ed.) *The Antarctic region: geological evolution and processes*, 187–200. Siena: Terra Antarctica Publication.

Vasconcelos, C., McKenzie, J. A., Bernasconi, S., Grujic, D. & Tiens, A. J. 1995. Microbial mediation as a possible mechanism for natural dolomite formation at low temperatures. *Nature* **377**, 220–22.

Verrill, A. E. 1865. Classification of polyps (extract condensed from Synopsis of the Polyps and Corals of the North Pacific Exploring Expedition under Commodore C. Ringgold and Captain John Rodgers, U.S.N.). *Communications of the Essex Institute* **4**, 145–52.

Vologdin, A. G. 1937. Arkheotsiaty i rezul'taty ikh izucheniya v SSSR [Archaeocyaths and the results of their study in the USSR]. *Problemy Paleontologii* **2–3**, 453–500. [In Russian.]

Vologdin, A. G. 1956. K klassifikatsii tipa archaeocyatha [On the classification on the phylum archaeocyatha]. *Akademiya Nauk SSSR, Doklady* **111**, 877–80. [In Russian.]

Vologdin, A. G. 1957. Arkheotsiaty i ikh stratigraficheskoe znachenie [Archaeocyaths and their stratigraphic significance]. *Acta Palaeontologica Sinica* **5**, 173–222. [In Russian.]

Vologdin, A. G. 1960. O rode *Ajacicyathus* Bedford et Bedford, 1939 i sem. Ajacicyathidae bedford et bedford, 1939 [On the genus *Ajacicyathus* Bedford et Bedford, 1939 and the fam. Ajacicyathidae Bedford et Bedford, 1939]. *Akademiya Nauk SSSR, Doklady* **130**, 421–24. [In Russian.]

Vologdin, A. G. 1961. Arkheotsiaty i ikh stratigraficheskoe znachenie [Archaeocyaths and their stratigraphic significance]. *Mezhdunarodnyy Geologicheskiy Kongress. XX Sessiya, Meksika. Kembriyskaya Sistema, ee Paleogeografiya i Problema Nizhney Granitsy. Tom* 3. *Zapadnaya Evropa, Afrika, SSSR, Aziya, Amerika.* [*International Geological Congress. XX Session, Mexico. The Cambrian System, its Paleogeography and Lower Boundary Problem. Volume* 3. *Western Europe, Africa, USSR, Asia, America*], 173–99. [In Russian].

Voronin, Y. I. 1974. Sistematika semeystva Ajacicyathidae Bedford R. et J., 1939 [Systematics of the family Ajacicyathidae Bedford R. et J., 1939]. *In* Zhuravleva, I. T. & Rozanov, A. Yu. (eds) *Biostratigrafiya i paleontologiya nizhnego kembriya evropy i severnoy azii* [*Lower Cambrian biostratigraphy and paleontology of Europe and Northern Asia*], 124–37. Moscow: Nauka. [In Russian.]

Voronin, Y. I. 1988. Novye septal'nye arkheotsiaty [New septate archaeocyaths]. *Sovmestnaya Sovetsko-Mongol'skaya Paleontologicheskaya Ekspeditsiya, Trudy* **33**, 5–10. [In Russian.]

Voronova, L. G., Drozdova, N. A., Esakova, N. V., Zhegallo, E. A., Zhuravlev, A. Y., Rozanov, A. Y., Sayutina, T. A. & Ushatinskaya, G. T. 1987. Iskopaemye nizhnego kembriya Gor makkenzi (Kanada) [Lower Cambrian fossils of the Mackenzie Mountains (Canada)]. *Paleontologicheskiy Institut, Akademiya Nauk SSSR, Trudy* **224**, 1–88. [In Russian.]

Wang, C.-C., Jacobs, J., Elburg, M. A., Läufer, A., Thomas, R. J. & Elvevold, S. 2020. Grenville-age continental arc magmatism and crustal evolution in central Dronning Maud Land (East Antarctica): zircon geochronological and Hf-O isotopic evidence. *Gondwana Research* **82**, 108–27.

Weber, B. 1991. Microfossils in Proterozoic sediments from the southern Shackleton Range, Antarctica: a preliminary report. *Zeitschrift für geologische Wissenschaften* **19**, 185–97.

Weber, B. & Brady, S. J. 2004. A marginal marine ichnofauna from the Blaiklock Glacier Group (?Lower Ordovician) of the Shackleton Range, Antarctica. *Earth and Environmental Science Transactions of the Royal Society of Edinburgh* **94**, 1–20.

Webers, G. F., Craddock, C. & Splettstoesser, J. F. 1992. *Geology and paleontology of the Ellsworth Mountains, West Antarctica*. Geological Society of America, Memoir **170**, 1–445. Boulder, Colorado: The Geological Society of America.

Wentworth, C. K. 1922. A scale of grade and class terms for clastic sediments. *The Journal of Geology* **30**, 377–92.

Wherry, E. T. 1916. A peculiar oolite from Bethlehem, Pennsylvania. *Proceedings of the United States National Museum* **49**, 153–56.

Wilkinson, B. H., Buczynski, C. & Owen, R. M. 1984. Chemical control of carbonate phases; implications from upper Pennsylvanian calcite-aragonite ooids of southeastern Kansas. *Journal of Sedimentary Research* **54**, 932–47.

Will, T. M., Zeh, A., Gerdes, A., Frimmel, H. E., Millar, I. L. & Schmädicke, E. 2009. Palaeoproterozoic to palaeozoic magmatic and metamorphic events in the Shackleton Range, east Antarctica: constraints from zircon and monazite dating, and implications for the amalgamation of Gondwana. *Precambrian Research* **17**, 25–45.

Will, T. M., Frimmel, H. E., Zeh, A., Le Roux, P. & Schmädicke, E. 2010. Geochemical and isotopic constraints on the tectonic and crustal evolution of the Shackleton Range, East Antarctica, and correlation with other Gondwana crustal segments. *Precambrian Research* **180**, 85–112.

Winland, H. D. & Matthews, R. K. 1974. Origin and significance of Grapestone, Bahama Islands. *Journal of Sedimentary Research* **44**, 921–27.

Woo, J. & Chough, S. K. 2010. Growth patterns of the Cambrian microbialite: phototropism and speciation of *Epiphyton*. *Sedimentary Geology* **229**, 1–8.

Wood, R., Evans, K. R. & Zhuravlev, A. Y. 1992. A new post-early Cambrian archaeocyath from Antarctica. *Geological Magazine* **129**, 491–95.

Wood, R., Zhuravlev, A. Y. & Chimed Tseren, A. 1993. The ecology of lower Cambrian buildups from Zuune Arts, Mongolia: implications for early metazoan reef evolution. *Sedimentology* **40**, 829–58.

Wright, V. P. 1992. A revised classification of limestones. *Sedimentary Geology* **76**, 177–85.

Wrona, R. 1989. Cambrian Limestone erratics in the tertiary glaciomarine sediments of King George Island. West Antarctica. *Polish Polar Research* **10**, 533–53.

Wrona, R. & Zhuravlev, A. Y. 1996. Early Cambrian archaeocyaths from glacial erratics of King George Island (South Shetland Islands), Antarctica. *Palaeontologia Polonica* **55**, 9–36.

Yoshida, M., Jacobs, J., Santosh, M. & Rajesh, H. M. 2003. Role of Pan-African events in the circum-east Antarctic orogen of east Gondwana: a critical overview. *Geological Society of London, Special Publications* **206**, 57–75.

Zeh, A., Millar, I. L., Kroner, U. & Görz, I. 1999. The structural and metamorphic evolution of the northern Haskard Highlands, Shackleton Range, Antarctica. *Terra Antarctica* **6**, 249–68.

Zeh, A., Millar, I. L. & Horstwood, M. S. A. 2004. Polymetamorphism in the NE Shackleton Range, Antarctica: constraints from petrology and U-Pb, Sm-Nd, Rb-Sr TIMS and in situ U-Pb LA-PIMMS dating. *Journal of Petrology* **45**, 949–73.

Zempolich, W. C. & Baker, P. A. 1993. Experimental and natural mimetic dolomitization of aragonite ooids. *Journal of Sedimentary Research* **63**, 596–606.

Zhang, X., Dai, M., Wang, M. & Qi, Y. 2019. Calcified coccoid from Cambrian Miaolingian: revealing the potential cellular structure of *Epiphyton*. *PLoS ONE* **14**, e0213695.

Zhuravlev, A. Y. 1988. Arkheotsiaty nizhnego kembriya kraynego severo-vostoka SSSR [Lower Cambrian archaeocyaths of the extreme northeast of the USSR]. *Institut Geologii i Geofiziki, Sibirskoe Otdelenie, Akademiya Nauk SSSR, Trudy* **720**, 97–110. [In Russian.]

Zhuravlev, A. Y. 1996. Reef ecosystem recovery after the early Cambrian extinction. *Geological Society of London Special Publications* **102**, 79–96.

Zhuravlev, A. Y. 2001. Paleoecology of Cambrian reef ecosystems. *In* Stanley Jr. G. D. (ed.) *The history and sedimentology of ancient reef systems*, 121–57. New York: Kluwer Academic/Plenum Publishers.

Zhuravlev, A. Y. & Gravestock, D. I. 1994. Archaeocyaths from Yorke Peninsula, South Australia and archaeocyathan early Cambrian zonation. *Alcheringa* **18**, 1–54.

Zhuravlev, A. Y. & Wood, R. 1995. Lower Cambrian reefal cryptic communities. *Palaeontology* **38**, 443–70.

Zhuravleva, I. T. 1951. O novom rode arkheotsiat s grebenchatymi dnishchami v kembriyskikh izvestnyakakh sibiri [On a new archaeocyathan genus with pectinate tabulae from the Cambrian limestones of Siberia]. *Akademiya Nauk SSSR, Doklady* **81**, 77–80. [In Russian.]

Zhuravleva, I. T. 1954. Nastavlenie po sboru i izucheniyu arkheotsiat [Manual for the collection and study of archaeocyaths]. *Paleontologicheskiy Institut, Akademiya Nauk SSSR* **V**, 1–46.

Zhuravleva, I. T. 1955. Arkheotsiaty kembriya vostochnogo sklona kuznetskogo Ala-Tau [Cambrian archaeocyaths of the eastern flank of the Kuznetsk Ala-Tau]. *Paleontologicheskiy Institut, Akademiya Nauk SSSR, Moscow* **56**, 5–56. [In Russian.]

Zhuravleva, I. T. 1960a. Novye dannye ob arkheotsiatakh sanashtykgol'skogo gorizonta [New data on the archaeocyaths of the Sanashtykgol horizon]. *Geologiya i Geofizika* **2**, 42–46. [In Russian.]

Zhuravleva, I. T.. 1960b. *Arkheotsiaty Sibirskoy platformy [Archaeocyaths of the Siberian platform]* Akademiya Nauk SSSR. [In Russian].

Zhuravleva, I. T.. 1963. *Arkheotsiaty sibiri. Odnostennye arkheotsiaty (Otryady Monocyathida i Rhizacyathida) [Archaeocyaths of Siberia. One-walled Archaeocyaths (orders Monocyathida and Rhizacyathida)]*. Moscow: Akademiya Nauk SSSR.

Zhuravleva, I. T. 1974. *Katalog rodov arkheotsiat. Chast'* 1 [*Catalogue of archaeocyath genera. Part* 1]. 228 pp. Novosibirsk: Nauka. [In Russian.]

Zhuravleva, I. T., Konyushkov, K. N. & Rozanov, A. Y. 1964. Arkheotsiaty Sibiri. *Dvustennye Arkheotsiaty* [*Archaeocyaths of Siberia. Two-walled Archaeocyaths*]. 132 pp. Moscow: Nauka. [In Russian.]

Zhuravleva, I. T., Korshunov, V. I. & Rozanov, A. Y. 1969. Atdabanskiy yarus i ego obosnovanie po arkheotsiatam v stratotipicheskom razreze [The Atdabanian stage and its justification based on the archaeocyaths of the Stratotype section]. *In* Zhuravleva, I. T. (ed.) *Biostratigrafiya i paleontologiya nizhnego kembriya sibiri i dal'nego vostoka [Lower Cambrian biostratigraphy and paleontology of Siberia and the Far east]*, 5–59. Moscow: Nauka. [In Russian.]

Zhuravleva, I. T., Konyaeva, I. A., Osadchaya, D. V. & Boyarinov, A. S. 1997. Biostratigraphy of the Kiya River section. Early Cambrian archaeocyaths and spicular sponges from the Kiya River section (Kuznetsk Alatau). *Annales de Paléontologie (Vertébrés-Invertébrés)* **83**, 3–92.

MS received 20 October 2021. Accepted for publication 12 June 2022. First published online 28 July 2022